Safety and Performance Indicators for Repositories in Salt and Clay Formations

GRS - 240

Gesellschaft für Anlagen-
und Reaktorsicherheit
(GRS) mbH

Safety and Performance Indicators for Repositories in Salt and Clay Formations

Jens Wolf
André Rübel
Ulrich Noseck
Dirk Becker

July 2008

Acknowledgement:

The underlying work of this report was supported by the federal Ministry of Economics and Technology (BMWi) under the identification number 02 E 9954 titled „Wissenschaftliche Grundlagen zum Nachweis der Langzeitsicherheit von Endlagern (WiGru)“.

The work was carried out under the auspices of the Gesellschaft für Anlagen- und Reaktorsicherheit (GRS) mbH.

Responsibility for the content of this publication lies solely with the authors.

GRS - 240
ISBN 978-3-939355-14-4

Keywords:
Assessment, Clay, High Level Waste, Host Rock, Indicator, Long-term Safety, Reference Values, Repository, Salt

Preface

The assessment of the long-term safety of a repository for radioactive or hazardous waste requires a comprehensive system understanding and capable and qualified numerical tools. All relevant processes which contribute to mobilisation and release of contaminants from the repository, transport through the host rock and adjacent rock formations as well as exposition in the biosphere have to be implemented in the programme package. The objective of the project “Scientific basis for the assessment of the long-term safety of repositories”, identification number 02 E 9954, was to follow national and international developments in this area, to evaluate research projects, which contribute to knowledge, model approaches and data, and to perform specific investigations to improve the methodologies of the long-term safety assessment.

This project, founded by the German Federal Ministry of Economics and Technology (BMWi), was performed in the period from 01. November 2004 to 31. July 2008. The results of the key topics investigated within the project are published in the following reports.

GRS report 222: About the role of vapour transport during bentonite re-saturation

GRS report 238: Elemente eines Safety Case zur Realisierung eines Endlagers in Deutschland

GRS report 239: Chemical effects in the near field of a HLW repository in rock salt

GRS report 240: Safety and Performance indicators for repositories in clay and salt formations

GRS report 241: Impact of climate change on far-field and biosphere processes for HLW repositories in rock salt

GRS report 242: Gase im Endlager im Salz

The results of the whole project are summarised in the overall final report.

GRS report 237: Scientific basis for the assessment of the long-term safety of repositories

Contents

1 Introduction

According to NEA a safety case is the synthesis of evidence, analyses and arguments that quantify and substantiate a claim that the repository will be safe after closure and beyond the time when active control of the facility can be relied on /NEA 04/. Most national regulations give safety criteria in terms of dose and/or risk, and these indicators are evaluated for a range of evolution scenarios for the disposal system using mathematical analyses. Robustness of the safety case is, however, strengthened by the use of multiple lines of evidence leading to complementary safety arguments, also qualitative ones that can compensate for shortcomings in any single argument. One type of evidence and arguments in support of a safety case is the use of safety indicators complementary to dose and risk.

Such complementary indicators can avoid to some extent the difficulties faced in evaluating and interpreting doses and risks. In particular the individual human behaviour as well as near-surface processes, which are the basis for calculation of dose and risk, are difficult to predict over long time scales. In contrast the possible evolutions of a well-chosen host rock can be bounded with reasonable confidence over much longer time scales, i.e. about one million years into the future. Hence, there is a trend in some recent safety cases towards evaluating, safety indicators in addition to dose and risk, like radiotoxicity fluxes from the geosphere, which do not rely on description of human behaviour and which can support the statement of low consequences of any radionuclide release to the surface environment and increase the robustness of the safety case, e. g. /NAG 02/.

The use of complementary safety indicators has been widely discussed in international fora and projects, e. g. /IAE 94/, /IAE 03/, /BEC 03/. In the frame of the SPIN project /BEC 03/ safety and performance indicators for radioactive waste repositories in crystalline formations were identified and their applicability tested by calculations for recent safety assessments of different countries. Recommendations for the use of different safety and performance indicators in different time frames were given.

Safety indicators provide conclusions about the safety of the total repository system, while performance indicators contribute to analysis of the performance of single barriers or sub-systems. The suitability of single safety and performance indicators is to some extent host-rock specific. For salt and clay formations other indicators might be

usable than those identified for granite. The work presented here aims at the identification of suitable indicators for repositories in salt and clay formations. It is not intended to compare the two formations with regard to the safe disposal of radioactive waste. A first set of safety and performance indicators for both host rocks has been derived on the basis of results of the SPIN project. Reference values for the safety indicators have been determined. The suitability of the indicators and their significance for different time frames is demonstrated by means of deterministic model calculations and exemplary parameter variations of previous studies /RUE 07/, /BUH 08a/.

2 Safety and performance indicators

Within this work a first set of safety and performance indicators is proposed and tested. In this chapter the different indicators proposed and how they are calculated are briefly described. More details especially about the performance indicators can be found in chapters 4 and 5 about the respective host-rock formations.

2.1 Safety indicators

The terminology used by different organisations is rather inhomogeneous i.e. there is no internationally uniform definition for a safety indicator. In this study a safety indicator is defined as follows:

A safety indicator is a quantity, calculable by means of suitable models, that provides a measure for the total system performance with respect to a specific safety aspect, in comparison with a reference value quantifying a global or local level that can be proven, or is at least commonly considered, to be safe.

A safety indicator always requires a reference value, which is important for the safety statement. These reference values are derived in chapter 3. The objective of the use of other safety indicators than dose or risk is to achieve additional independent safety statements. In this way they contribute to confidence building by illustrating robustness of the safety assessment in particular for longer time frames, for which the uncertainty of dose strongly increases.

Effective dose rate [Sv/a]

The effective dose rate represents the annual effective dose to an average member of the group of the most exposed individuals. It takes into account dilution and accumulation in the biosphere, different exposure pathways as well as living and nutrition habits. It is calculated using

$$\sum_{\text{all nuclides } n} c_n B_n \qquad (2.1)$$

with the activity concentration c_n [Bq/m^3] of radionuclide *n* in the biosphere water, which is used by man for drinking, feeding livestock or irrigation and into which radionuclides are released from the geosphere. The biosphere dose conversion factor B_n, is the annual dose to the most exposed members of the public (so-called critical group) caused by a unit concentration of radionuclide n in the biosphere water. It is measured in [(Sv/a)/(Bq/m^3)]. This indicator takes into account several exposition pathways (cf. section 0). The safety statement of the indicator has a clear relevance for human health (and allows an assessment of the individual health risk). In this study biosphere water is assumed to be taken from a well in a near-surface aquifer.

Radiotoxicity concentration in biosphere water [Sv/m^3]

This indicator represents the radiotoxicity of the radionuclides in 1 m^3 of biosphere water. It also can be understood as the dose which is received by drinking 1 m^3 of biosphere water. It is calculated with

$$\sum_{\text{all nuclides } n} c_n D_n \qquad (2.2)$$

with the ingestion dose coefficient D_n which represents the dose caused by ingestion of radionuclide *n* (Sv per ingested Bq). The ingestion dose coefficients for adults, which correspond to the committed effective dose integrated over 50 years, are used /ICR 96/. The effects of daughters produced in vivo are accounted for in the ingestion dose coefficients.

For the computation of the radiotoxicity concentration in the biosphere water no exposure pathways need to be defined and thus the calculated radiotoxicity concentration is independent of a specific biosphere model, and can therefore be regarded as a more robust indicator for longer time frames. In comparison to the individual dose rate the safety statement of this indicator is restricted in a way that it assesses only the impact of the drinking water from the considered aquifer with respect to human health.

Radiotoxicity flux from geosphere [Sv/a]

The indicator represents the radiotoxicity of the radionuclides released from the geosphere to the biosphere in a year. It can also be understood as the annual dose to a

single human being who would ingest all radionuclides released from the geosphere to the biosphere. It is calculated with

$$\sum_{\text{all nuclides } n} s_n D_n \tag{2.3}$$

with the activity flux s_n [Bq/a] of radionuclide n from the geosphere to the biosphere. The radiotoxicity flux eliminates the uncertainty associated with the dilution in the aquifer, but it has only a weak relation to human health. It is preferably applicable to long time frames. The safety statement of this indicator shows, whether there is a significant influence of the repository on the groundwater in the aquifer or not.

2.2 Performance indicators

In this study a performance indicator is defined as follows:

A performance indicator is a quantity, calculable by means of appropriate models, that provides a measure for the performance of a system component, several components or the whole system.

Performance indicators are usually applied to subsystems of the repository. Performance indicators are useful for optimisation of the disposal system, for improving the understanding of the role played by different system components and for communicating these issues, both to experts and the general public. A performance indicator does not need reference values or technical criteria.

Compartments for performance indicators are different for repositories in clay and salt formations due to the different repository structure and design. A detailed description and definitions for the compartments in salt and clay host-rock formations are given in chapters 4 and 5, respectively. The following performance indicators are applied.

Radiotoxicity in compartments [Sv]

The indicator represents nuclide-specific radiotoxicities as well as the total radiotoxicities in different compartments

$$a_{n,i} D_n \quad \text{and} \quad \sum_{\text{nuclides } n} a_{n,i} D_n \tag{2.4}$$

with the activity $a_{n,i}$ [Bq] of radionuclide n in compartment i. In this study the radionuclides Tc-99 and I-129 representing radionuclides with different half-lives and different sorption properties are exemplarily considered beside the total radiotoxicity of all radionuclides.

Radiotoxicity flux from compartments [Sv/a]

This indicator represents the radiotoxicity flux from compartment i for single radionuclides as well as summed over all radionuclides

$$s_{n,i} D_n \quad \text{and} \quad \sum_{\text{nuclides } n} s_{n,i} D_n \tag{2.5}$$

with the activity flux $s_{n,i}$ (Bq/a) of radionuclide n from compartment i. The radiotoxicity fluxes for all radionuclides as well as for Tc-99 and I-129 are considered.

Time-integrated radiotoxicity flux from compartments [Sv]

This indicator represents the cumulated radiotoxicity flux from a compartment for single radionuclides as well as summed over all radionuclides and is calculated with

$$\int_0^t D_n s_{n,i}(\tau)\, d\tau \quad \text{and} \quad \sum_{\text{nuclides } n} \left(\int_0^t D_n s_{n,i}(\tau)\, d\tau \right) \tag{2.6}$$

The radiotoxicity fluxes for all radionuclides as well as for Tc-99 and I-129 are considered.

3 Reference values

The following chapter explains how the reference values for the safety indicators were derived. For the effective dose rate and the radiotoxicity concentration in biosphere water global reference values were derived. For the radiotoxicity flux from the geosphere a local reference value was derived since this indicator is mainly based on site-specific assumptions (e. g. the natural groundwater flow). Moreover, it is useful to rely on a set of both local and global reference values in order to substantiate a safety conclusion.

The first step in deriving an appropriate reference value is the determination of a natural background value. In a second step a safety margin to this natural background value is defined. The general philosophy of this procedure is to keep the reference values comparatively low in order to enhance the confidence in the safety statement given by the corresponding safety indicator. Therefore the reference value is set to one third of the natural background value in this report.

3.1 Effective dose rate

The effective dose rate to exposed individuals is the main indicator internationally accepted for assessing the safety of a repository system. In many countries the regulatory authorities have established regulatory limits for this indicator. For example, in the German regulation § 47 StrlSchV the limit for the effective dose rate is 0.3 mSv/a. This limit was chosen since it represents a small proportion relative to the natural background radiation doses. The average natural background radiation in Germany is in the range of 2 to 3 mSv/a /BMU 07/. This radiation originates from

- Cosmic radiation: 0.3 to 0.5 mSv/a (depending on altitude, 0.3 mSv/a at sea level)
- Terrestrial radiation: 0.4 mSv/a
- Inhalation (mainly from inhalation of radon): 1.4 mSv/a
- Ingestion: 0.3 mSv/a

The derivation of a reference value for the effective dose rate used here differs from this approach. Since a release of radionuclides from a repository would mainly cause an exposition by ingestion, the given value of 0.3 mSv/a is the natural background value considered here.

With the proposed safety margin **the suggested reference value for the dose rate is 0.1 mSv/a.** This value meets the legal limit valid in several countries in Europe.

3.2 Radiotoxicity concentration in biosphere water

For the derivation of the reference value for the radiotoxicity in biosphere water only radionuclide concentrations in drinking water are evaluated. These values are used since it can be assumed that observed concentrations in drinking water are harmless for human health. Thus characteristic drinking water qualities in Germany provide a safe reference value for the radiotoxicity concentration in biosphere water.

Tab. 3.1 Ingestion dose coefficients /ICR 96/, activity and radiotoxicity concentrations of drinking water in Germany /BMU 03/

Nuclide	Ingestion dose coefficient [Sv/Bq]	Activity concentration	Radiotoxicity concentration
		[Bq/m^3]	[Sv/m^3]
U-238	$4.50 \cdot 10^{-8}$	5.0	$2.25 \cdot 10^{-7}$
U-234	$4.90 \cdot 10^{-8}$	6.0	$2.94 \cdot 10^{-7}$
Ra-226	$2.80 \cdot 10^{-7}$	5.0	$1.40 \cdot 10^{-6}$
Rn-222	$3.50 \cdot 10^{-10}$	5 900	$2.07 \cdot 10^{-6}$
Pb-210	$6.90 \cdot 10^{-7}$	1.5	$1.04 \cdot 10^{-6}$
Po-210	$1.20 \cdot 10^{-6}$	0.5	$6.00 \cdot 10^{-7}$
Th-232	$2.30 \cdot 10^{-7}$	0.1	$2.30 \cdot 10^{-8}$
Ra-228	$6.90 \cdot 10^{-7}$	3.0	$2.07 \cdot 10^{-6}$
Th-228	$7.20 \cdot 10^{-8}$	0.2	$1.44 \cdot 10^{-8}$
U-235	$4.70 \cdot 10^{-8}$	0.3	$1.41 \cdot 10^{-8}$
Total			$7.74 \cdot 10^{-6}$

Table 3.1 contains characteristic mean values of radionuclide concentrations in drinking water according to /BMU 03/. K-40 is not considered, since it does not accumulate in the human body. The largest contributions to the radiotoxicity concentrations are by Rn-222, Ra-228, Ra-226 and Pb-210. Ingestion dose coefficients of short-lived daughter nuclides are added to those of their mother nuclides. This is important for the relevance of Rn-222: in contrast to its daughter nuclides radon is gaseous at room temperature and is not chemically reactive. Therefore the ingestion dose coefficients of radioactive radon isotopes are assumed to be zero (Tables 3.3 to 3.5). But its short-

lived daughters Po-218, Pb-214 and Bi-214 have a radiological importance (Tables 3.3 to 3.5) and can not be neglected. The ingestion dose coefficient of Rn-222 is considered here as the sum of the ingestion dose coefficients of the three daughter nuclides yielding a value of $3.50 \cdot 10^{-10}$ Sv/Bq. In some publications /KEN 02/, /SSK 95/ a higher value for the ingestion dose coefficient of Rn-222 is considered ($3.50 \cdot 10^{-9}$ Sv/Bq), but according to the philosophy mentioned above the lower value was used here in order to avoid a high reference value. The resulting background value for the radiotoxicity concentration in biosphere water is $7.7 \cdot 10^{-6}$ Sv/m^3 (Table 3.1).

With the proposed safety margin **the suggested reference value for the radiotoxicity concentration in biosphere water is $2 \cdot 10^{-6}$ Sv/m^3.**

3.3 Radiotoxicity flux from the geosphere

The derivation of the reference value for the safety indicator radiotoxicity flux from the geosphere is more problematic than the previously described approaches. A reference value for this indicator is usually site-specific since it is based on the natural groundwater flux, which cannot be determined on very large scales. But even on local scales the determination of a natural groundwater flux in the vicinity of a repository is difficult and implies a lot of uncertainties.

Here the reference value is determined for the area at Gorleben, since a lot of data from an extensive drilling, exploration and monitoring programme for the overlying rock of the Gorleben salt dome are available, e. g. /KLI 07/. The basic assumption is that the corresponding natural background value is represented by the product of the radionuclide concentrations and the groundwater flow in the near surface aquifer.

For the natural groundwater flow in the near surface aquifer the parameter used in the PA model for calculating the indicators is applied /PAG 88/: The overlying rock formation along the migration pathway is modelled as homogeneous sandy aquifer with an average width of 820 m, a thickness of 45 m, and a porosity of 0.2. With a pore velocity of about 6.5 m/a, the resulting natural groundwater flow amounts to 48 000 m^3/a.

In order to calculate the reference values all radioactive isotopes of the three natural decay chains are considered. However, only concentrations for uranium and thorium are available from different wells of the near surface aquifer at Gorleben. The concen-

trations of all other radionuclides are calculated from the concentration of the mother nuclides of the three natural decay chains U-238, U-235 and Th-232. It is assumed that all radionuclides in a decay chain are in secular equilibrium, i.e. the total activity concentration of each radionuclide in the decay chain corresponds to that of the mother nuclide. This is not necessarily correct as analyses in many natural systems, e. g. /GEL 97/, have shown.

Only the mobile fraction of the total activity concentration contributes to the radiotoxicity flux. The mobile fraction of each radionuclide is determined by its sorption properties. These are different for the different elements and geomatrices, respectively. Three approaches were considered, since different data for sorption coefficients of individual radionuclides are available.

In the first approach, the total concentration of all radionuclides in a single decay chain is calculated as the product of the concentration of the respective mother nuclide in the groundwater $c_{l,m}$ and the retardation factor of the mother nuclide $R_{f,m}$. The mobile concentration of radionuclide i is then derived from

$$c_{l,i} = \frac{c_{l,m} \cdot R_{f,m}}{R_{f,i}} \tag{3.1}$$

with the retardation factor

$$R_f = 1 + \frac{(1-n)}{n} \rho_s K_d \tag{3.2}$$

with the porosity n, the rock density ρ_s, and the element specific distribution coefficient K_d. The mother nuclide is denoted by the index m and the respective radionuclide from the same decay chain with index i.

Therefore, the concentration of each radionuclide in the groundwater is determined by the ratio of the retardation factors of the mother nuclide and the respective radionuclide.

The mean groundwater concentrations for uranium and thorium are derived from data of 14 and 19 samples, respectively, which are available for the near surface aquifer in the Gorleben area. The resulting mean concentrations are 0.72 nmol/l ($1.7 \cdot 10^{-7}$ kg/m^3)

for uranium and 1.43 nmol/l ($3.3 \cdot 10^{-7}$ kg/m^3) for thorium. The activity concentration of the three radionuclides in the groundwater is calculated with a nuclide-specific activity-to-mass conversion factor regarding the natural abundance of the uranium isotopes. The resulting average activity concentrations are listed in Table 3.2.

Tab. 3.2 Mother isotopes of the three natural decay chains and their average concentration in the groundwater in the near-surface aquifer at Gorleben site

Radionuclide	Half-life [a]	Natural abundance in element [wt. %]	Conversion factor [Bq/kg]	Average conc. [Bq/m^3]
U-238	$4.468 \cdot 10^9$	99.2742	$1.245 \cdot 10^7$	2.12
U-235	$7.038 \cdot 10^8$	0.7204	$8.000 \cdot 10^7$	$9.88 \cdot 10^{-2}$
Th-232	$1.405 \cdot 10^{10}$	100.00	$4.065 \cdot 10^6$	1.35

The R_f-values for each radionuclide are calculated with the same data used in the performance assessment calculations presented in the chapters 4 and 5. The data for the porosity and the rock density are listed in Table 4.8 and the K_d-values stem from /BUH 91/ and are listed in Table 4.9. The radiotoxicity concentration is derived as the product of activity concentration and ingestion dose coefficient. The ingestion dose coefficients /ICR 96/, retardation factors activity and radiotoxicity concentrations for the radionuclides from the three decay chains are listed in Tables 3.3 to 3.5.

For radon, thallium and bismuth no sorption data are available, but since their ingestion dose coefficients are quite small, they do not significantly contribute to the radiotoxicity concentrations.

The total radiotoxicity concentration in the groundwater is calculated as the sum of the radiotoxicity concentrations of all three decay chains. The total radiotoxicity concentration is then $3.08 \cdot 10^{-4}$ Sv/m^3 and the resulting natural radiotoxicity flux from the geosphere is 14.8 Sv/a.

The results show that by far the highest contribution to the natural radiotoxicity flux stems from the thorium decay chain. The total radiotoxicity concentration of this decay chain is dominated by the two radium isotopes Ra-224 and Ra-228.

Tab. 3.3 Calculated activity and radiotoxicity concentration of the thorium series

Nuclide	Ingestion dose coefficient [Sv/Bq]	R_f [-]	Concentration c_l	
			[Bq/m^3]	[Sv/m^3]
Th-232	$2.30 \cdot 10^{-7}$	$3.0 \cdot 10^{3}$	1.35	$3.10 \cdot 10^{-7}$
Ra-228	$6.90 \cdot 10^{-7}$	$1.0 \cdot 10^{1}$	405.10	$2.80 \cdot 10^{-4}$
Ac-228	$4.30 \cdot 10^{-10}$	$4.0 \cdot 10^{2}$	10.13	$4.35 \cdot 10^{-9}$
Th-228	$7.20 \cdot 10^{-8}$	$3.0 \cdot 10^{3}$	1.35	$9.72 \cdot 10^{-8}$
Ra-224	$6.50 \cdot 10^{-8}$	$1.0 \cdot 10^{1}$	405.10	$2.63 \cdot 10^{-5}$
Rn-220	0	n/a	n/a	0
Po-216	0	$1.0 \cdot 10^{4}$	0.41	0
Pb-212	$6.00 \cdot 10^{-9}$	$4.0 \cdot 10^{2}$	10.13	$6.08 \cdot 10^{-8}$
Bi-212	$2.60 \cdot 10^{-10}$	n/a	n/a	n/a
Tl-208	0	n/a	n/a	0
Po-212	0	$1.0 \cdot 10^{4}$	0.41	0
Total	$1.06 \cdot 10^{-6}$		$8.34 \cdot 10^{2}$	$3.06 \cdot 10^{-4}$

Tab. 3.4 Calculated activity and radiotoxicity concentration of the uranium series

Nuclide	Ingestion dose coefficient [Sv/Bq]	Rf [-]	Concentration c_l	
			[Bq/m^3]	[Sv/m^3]
U-238	$4.50 \cdot 10^{-8}$	$2.1 \cdot 10^{1}$	2.12	$9.54 \cdot 10^{-8}$
Th-234	$3.40 \cdot 10^{-9}$	$3.0 \cdot 10^{3}$	0.02	$5.04 \cdot 10^{-11}$
Pa-234	$5.10 \cdot 10^{-10}$	$1.0 \cdot 10^{4}$	0.0045	$2.27 \cdot 10^{-12}$
U-234	$4.90 \cdot 10^{-8}$	$2.1 \cdot 10^{1}$	2.12	$1.04 \cdot 10^{-7}$
Th-230	$2.10 \cdot 10^{-7}$	$3.0 \cdot 10^{3}$	0.02	$3.12 \cdot 10^{-9}$
Ra-226	$2.80 \cdot 10^{-7}$	$1.0 \cdot 10^{1}$	4.45	$1.25 \cdot 10^{-6}$
Rn-222	0	n/a	n/a	n/a
Po-218	$1.00 \cdot 10^{-10}$	$1.0 \cdot 10^{4}$	0.0045	$4.45 \cdot 10^{-13}$
Pb-214	$1.40 \cdot 10^{-10}$	$4.0 \cdot 10^{2}$	0.11	$1.56 \cdot 10^{-11}$
Bi-214	$1.10 \cdot 10^{-10}$	n/a	n/a	n/a
Po-214	0	$1.0 \cdot 10^{4}$	0.0045	0
Pb-210	$6.90 \cdot 10^{-7}$	$4.0 \cdot 10^{2}$	0.11	$7.68 \cdot 10^{-8}$
Bi-210	$1.30 \cdot 10^{-9}$	n/a	n/a	n/a
Po-210	$1.20 \cdot 10^{-6}$	$1.0 \cdot 10^{4}$	0.0045	$5.34 \cdot 10^{-9}$
Total	$2.48 \cdot 10^{-6}$		$8.96 \cdot 10^{0}$	$1.53 \cdot 10^{-6}$

Tab. 3.5 Calculated activity and radiotoxicity concentration of the actinium series

Nuclide	Ingestion dose coefficient [Sv/Bq]	Rf [-]	Concentration c_l	
			[Bq/m^3]	[Sv/m^3]
U-235	$4.70 \cdot 10^{-8}$		0.10	$4.64 \cdot 10^{-9}$
Th-231	$3.40 \cdot 10^{-10}$	$3.0 \cdot 10^{3}$	0.0007	$2.35 \cdot 10^{-13}$
Pa-231	$7.10 \cdot 10^{-7}$	$1.0 \cdot 10^{4}$	0.0002	$1.47 \cdot 10^{-10}$
Ac-227	$1.10 \cdot 10^{-6}$	$4.0 \cdot 10^{2}$	0.0052	$5.71 \cdot 10^{-9}$
Th-227	$8.80 \cdot 10^{-9}$	$3.0 \cdot 10^{3}$	0.0007	$6.08 \cdot 10^{-12}$
Ra-223	$1.00 \cdot 10^{-7}$	$1.0 \cdot 10^{1}$	0.21	$2.08 \cdot 10^{-8}$
Rn-219	0	n/a	n/a	0
Po-215	0	$1.0 \cdot 10^{4}$	0.0002	0
Pb-211	$1.80 \cdot 10^{-10}$	$4.0 \cdot 10^{2}$	0.0052	$9.34 \cdot 10^{-13}$
Bi-211	0	n/a	n/a	0
Tl-207	0	n/a	n/a	0
Total	$1.97 \cdot 10^{-6}$		$3.18 \cdot 10^{-1}$	$3.13 \cdot 10^{-8}$

In order to check the calculation results all calculated activity concentrations are compared to annually documented concentration values in German groundwaters /BMU 03/. The comparison shows that the concentrations for most of the radionuclides are in a similar range. However, important exceptions are the concentrations for the radionuclides Ra-228 and Ra-224 from the thorium series. For both radionuclides the calculated concentrations are more than ten times higher than normal background concentrations in Germany, indicating that the calculated values and therewith the total radiotoxicity concentration of the thorium decay chain is much too high. The reason for these high concentrations is the high ratio of the retardation factors (i.e. K_d-values) applied for thorium and radium.

By comparing the K_d-values for radium used here (0.0009 m^3/kg) with results from other investigations (for instance 0.04 m^3/kg for freshwater and 0.002 m^3/kg for saltwater in sandy Gorleben aquifers /SUT 98/), it becomes obvious that the coefficients for radium are disputable. Since all measured thorium concentrations belong to a freshwater aquifer (TDS < 10 g/l), the discrepancy between calculated and observed radium concentrations might be explained by the sorption coefficient.

The resulting consequences are:

1. A discussion of a suitable set of retardation factors for future calculations is necessary.

2. The calculated reference value is probably too high and should be replaced by a lower value.

Therefore a second approach is used. As long as the first item is not clarified sorption is neglected here. A secular equilibrium only for the activity concentrations in the mobile phase is considered. In this case the total ingestion dose coefficient of each decay chain can be used to calculate a radiotoxicity concentration in the geosphere by multiplication with the observed concentrations for the three mother nuclides. The resulting total radiotoxicity concentration is $6.88 \cdot 10^{-6}$ Sv/m^3 and the corresponding flux is 0.33 Sv/a. This value is consistent with the result of a third approach using sorption values from newer investigations /SUT 98/ for freshwater in a sandy aquifer. The results for all three approaches are shown in Table 3.6.

Tab. 3.6 Reference values determined by different sorption approaches

Approach	Applied sorption coefficients	Radiotoxicity flux [Sv/a]
1	K_d-values of the model /PAG 88/	14.78
2	No sorption	0.33
3	K_d-values by /SUT 98/	0.27

With the proposed safety margin **the suggested reference value for the radiotoxicity flux from the geosphere is 0.1 Sv/a**.

As discussed this reference value is associated with high uncertainties. In particular the following issues contribute to uncertainty and need to be improved:

- Derivation of an appropriate natural groundwater flow in the near surface aquifer: This parameter is highly site-specific and needs to be determined during characterisation of a potential site.

  A number of simplifications are adopted to determine adequate radiotoxicity concentrations in this aquifer. The uncertainty of this value can be reduced by direct analyses of radionuclides from the three decay chains in groundwater wells in the aquifer. Of particular interest are the Ra-isotopes, which are the radionuclides

dominating radiotoxicity fluxes in all three decay chains. If such data are not available the determination of the mobile concentration needs to be improved, more actual data need to be used and different geochemical conditions and therefore different K_d-values for different groundwater type wells should be regarded.

4 Salt formations

In this chapter the use of safety and performance indicators for nuclear waste repositories in salt formations is examined. A salt rock formation provides a dry environment and has a low porosity and permeability, which results in negligible water flow. Due to the rheological behaviour of salt under the conditions given in a repository faults and fractures are sealed, which might otherwise provide a path for the release of radionuclides. Under these conditions there is no water movement in the waste environment in the normal evolution of a repository system in salt and no radionuclide release is expected[1]. This means that the indicators considered in this report can not be calculated for the normal evolution. Therefore altered evolution scenarios have to be defined in order to be able to test different indicators.

4.1 Considered test cases and parameter variations

For the discussion on safety and performance indicators two altered evolution test cases were chosen, which possibly represent altered evolution scenarios. However, a complete derivation of scenarios has not been performed yet. These test cases are based on the results of a German joint R & D project /BUH 08a/ for evaluating and assessing safety concepts for HLW repositories in rock salt and for identifying the major needs for future research projects in this field.

Test case 1 "Failure of shaft and drift seals": It is assumed that both the shaft seal and the two drift seals (Figure 4.5) do not meet the technical requirements and that their permeability is considerably higher than expected. This test case represents a continuous path from the overlying rock to the disposed waste and only occurs if several (geo)technical barriers fail at the same time.

Test case 2 "Fluid reservoir": In this test case two fluid reservoirs of 100 m^3, which were not detected during the exploration and the operational period, are assumed to open at the beginning of the post operational period and fill two connected boreholes in the middle of the repository. Fluid reservoirs with a volume of 100 m^3 have been detected in salt domes in Northern Germany, though restricted to layers (for example an-

[1] Possible small releases of gaseous radionuclides are not considered in this report.

hydrite layers) to which a sufficient safety distance will be kept during the construction of a repository.

Both test cases are based on very pessimistic assumptions and are expected to have very low probabilities at a real repository system. For both test cases a parameter variation was carried out, exemplarily for one important parameter: for the first test case the length of the time period between the end of the operational period and the failure of the shaft seal and for the second test case the reference convergence rate.

4.2 Concept, model and data

In this section the concept of the repository in a salt dome and the input data used for the PA calculations are summarised. The concept for the repository is based on a conceptual design proposed within /BUH 08b/.

4.2.1 Repository concept

The host rock formation is assumed to be a salt dome with a sedimentary coverage of about 200 m to 300 m thickness. The repository is located in a depth of 870 m below surface (disposal level) in a very homogeneous rock salt layer within the salt dome. The repository consists of two access shafts, a central field (CF) and two access (or flank) drifts, which connect the central field with a horizontal network of transfer drifts (Figure 4.1). From the inner transfer drifts boreholes are drilled to a depth of 300 m, 290 m are intended for the waste canister and 10 m for a plug for closing the boreholes. The distance between the central field and the waste sections of the repository is about 450 m. A borehole concept is used in order to minimize the required amount of backfill material and thus the time of backfill compaction. In the reference concept crushed salt is applied for backfilling and for the borehole plug.

The philosophy of the safety concept is the isolation of the emplaced waste by the tight and long-term stable salt formation. The waste canisters are not considered to represent a long-term barrier.

The function of the engineered barriers is to reseal the disturbed salt rock formation after the construction of the repository. The main engineered barriers are the shaft seal

and the drift seals. The drift seals are located between the central field and the access drifts.

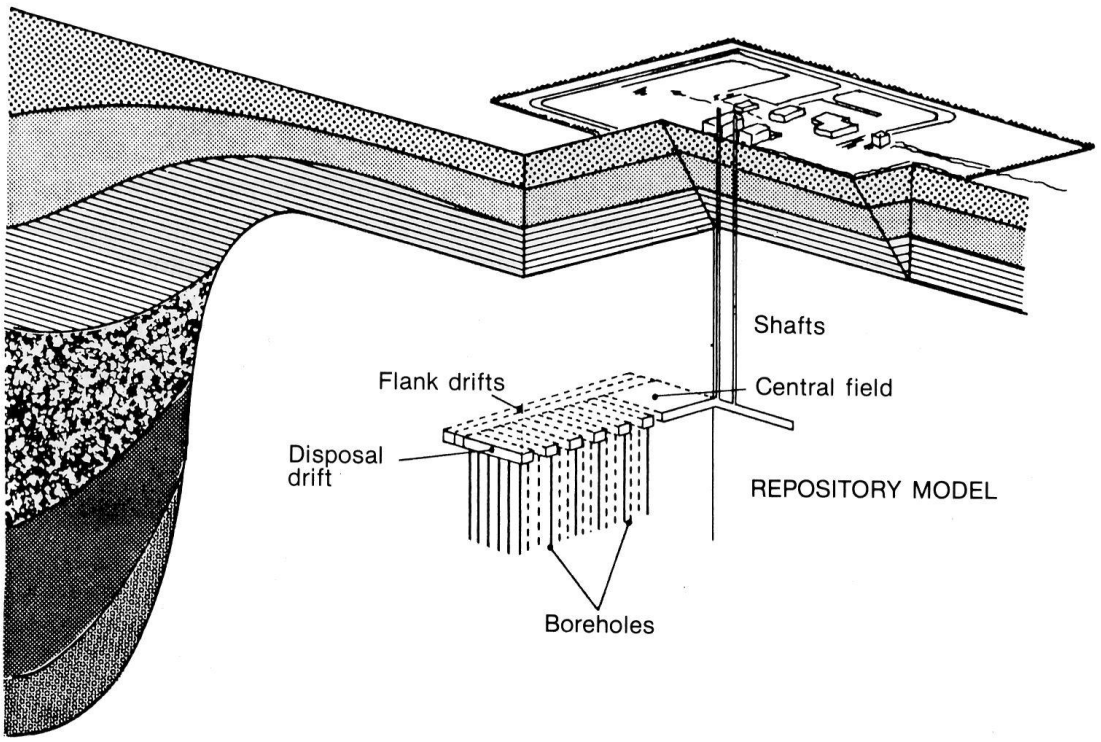

Fig. 4.1 Schematic view of a waste repository in a salt dome (from /PAG 88/)

4.2.2 Model and compartments

Figure 4.2 shows a general scheme of the relevant barriers for a repository in salt formations. They can be classified into geotechnical (man made) barriers and geological (natural) barriers.

Based on this scheme the repository system has been divided into several compartments for the calculation of the performance indicators. In accordance to the SPIN project the term “barrier” is replaced by “compartment” in the context of performance indicators in order to avoid the discussion which part of the repository system can be addressed as a barrier.

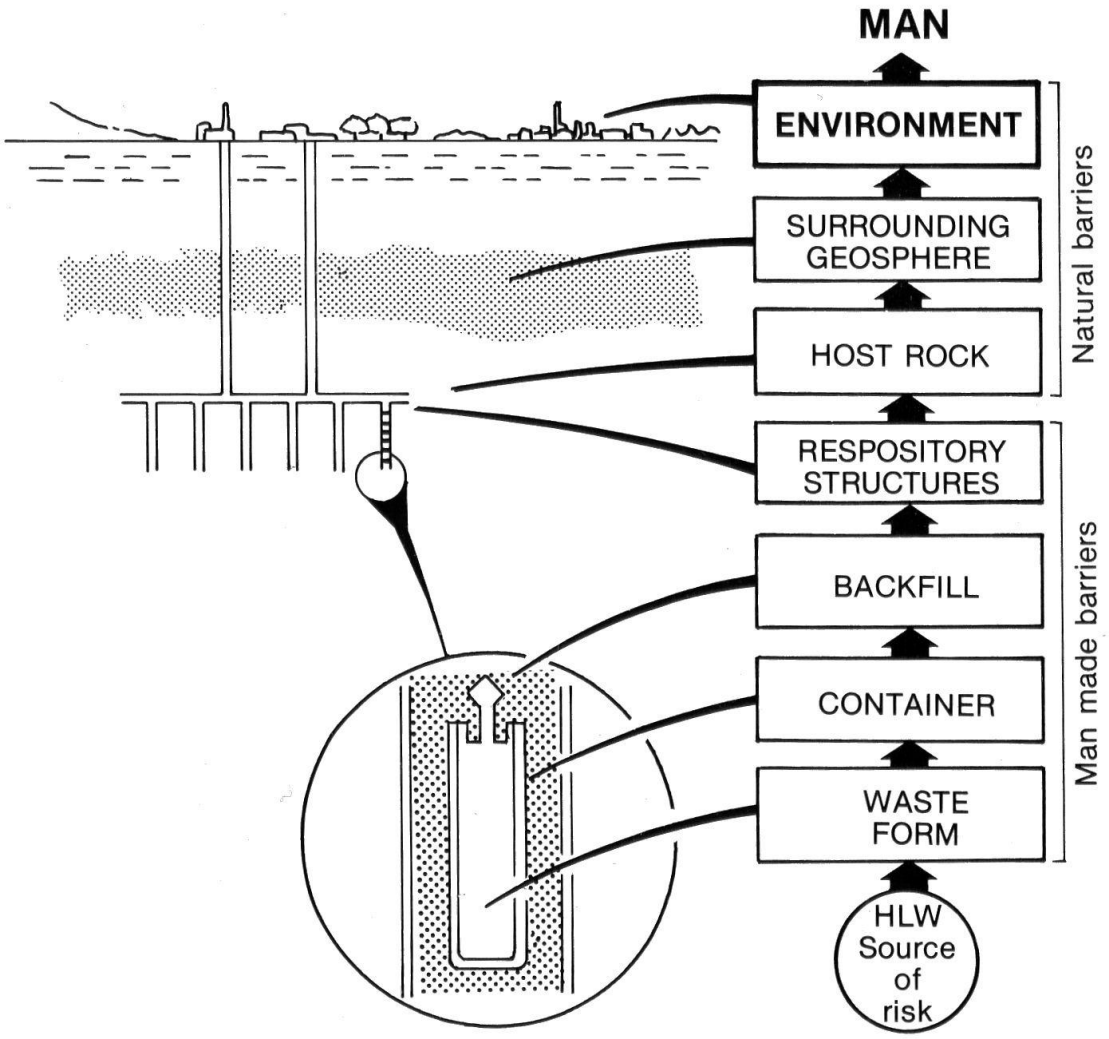

Fig. 4.2 Compartments considered for the repository in a salt formation (from /PAG 88/)

Figure 4.3 presents the different compartments that are considered for the calculation of the performance indicator “Radiotoxicity in compartments”. The radiotoxicity in these compartments represents the total mobilised (solved and precipitated) radiotoxicity. The remaining radiotoxicity inventory in the waste segments (SF1, SF2, HLW and ILW) is not covered by this indicator. The different compartments are:

- **Spent Fuel:** Due to the large area of the repository that is required to dispose the spent fuel (SF) waste, the fields with emplaced SF canisters are divided in two compartments (SF1 and SF2). Each compartment comprises 60 boreholes with 58 SF canisters in each borehole. The compartments contain the waste forms, the canisters with SF rods, and the backfill material in the boreholes (Figure 4.2).
  Both fluid reservoirs regarded in the second test case are located in SF2.

- **High Level Waste:** The HLW compartment (HLW) includes 15 boreholes with 215 canisters in each borehole. This compartment contains the waste forms of high-level vitrified waste from reprocessing of spent fuel, the canisters, and the backfill material in the boreholes.
- **Intermediate Level Waste:** The ILW compartment (ILW) includes 35 boreholes with 213 ILW canisters in each borehole. This compartment contains the waste forms of ILW, the ILW canisters, and the backfill material in the boreholes.
- **Repository Galleries:** For the calculation of the radiotoxicity inventories this compartment is divided into the central field (CF) and the transfer and access drifts of the different waste compartments (SF1-S, SF2-S, HLW-S and ILW-S, see Figure 4.3). For example SF1-S represents all segments of access and transfer drifts above the compartment SF1.
- **Overlying Rock:** The overlying rock comprises all geological units above the salt dome.
- **Total:** This compartment includes all compartments given above plus the not mobilised inventory in the waste compartments (SF1, SF2, HLW and ILW) and the radiotoxicity emitted from the overlying rock to the biosphere. It represents the decay-corrected initial inventory.

The biosphere is not considered as a compartment for this performance indicator.

Figure 4.4 presents the different compartments that are considered for the calculation of the performance indicators “Radiotoxicity flux from compartments” and “Time-integrated radiotoxicity flux”. The arrows represent those compartment boundaries where radionuclide fluxes are calculated. The biosphere receives the release of radionuclides from the upper part of the overlying rock.

The flux from the waste compartments represents the sum of several fluxes (from every borehole considered in the compartment). That means that positive and negative fluxes of different boreholes (inflow in one borehole and outflow in another borehole at the same time) can compensate each other in the calculations. This fact can complicate the interpretation of the calculated indicators. An example is given in chapter 4.4.2.

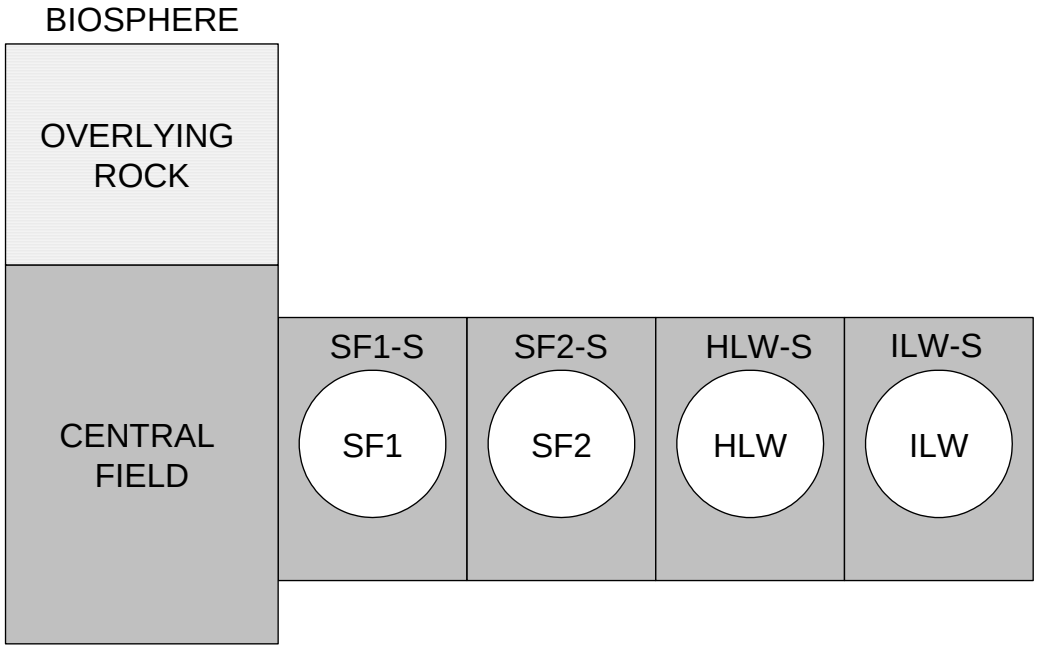

Fig. 4.3 Compartments considered for the performance indicator “Radiotoxicity in compartments”.

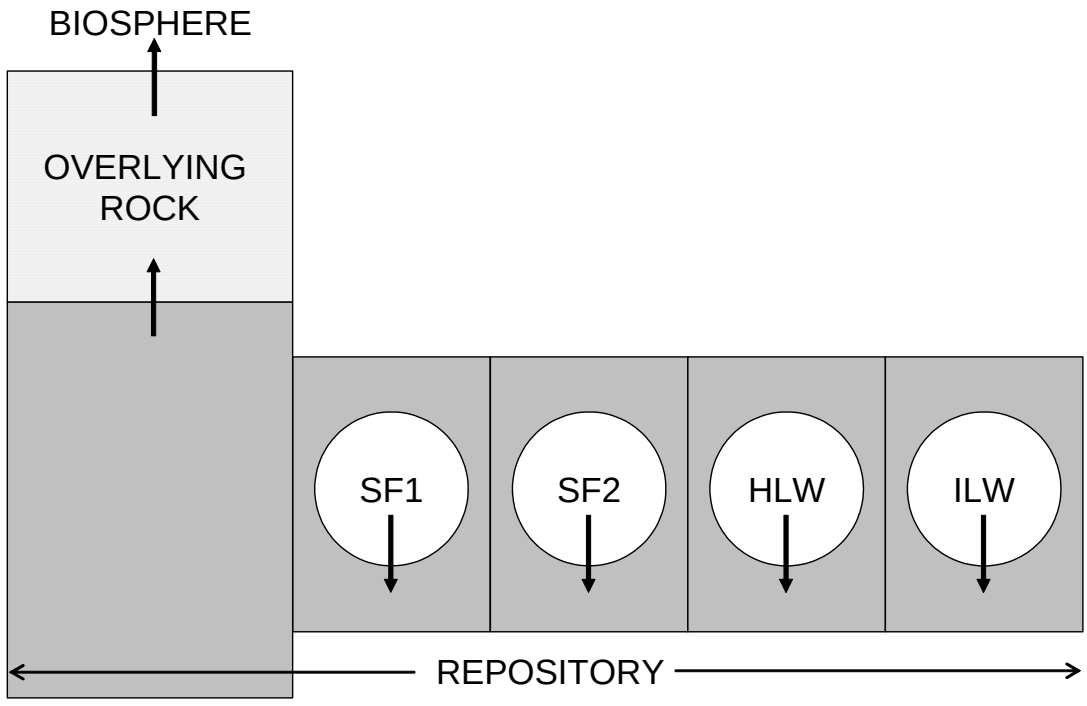

Fig. 4.4 Compartments considered for the performance indicator “Radiotoxicity flux from compartments” and “Time-integrated radiotoxicity flux”

For the modelling of the radionuclide transport in the different compartments the EMOS modules LOPOS, CHETLIN and EXCON/EXMAS were used /HIS 99, KUE 96, BUH 99/:

- **LOPOS**: This program models the mobilisation of radionuclides from the waste and the transport through a repository with looped structures under the influence of the convergence. Considered transport processes are advection, convection, dispersion and diffusion taking into account sorption, solubility and radioactive decay.
- **CHETLIN**: This program models the 1D-transport of the radionuclides through the porous media of the overlying rock. It calculates the advective, dispersive and diffusive radionuclide transport in the far-field with consideration of linear sorption and radioactive decay.
- **EXCON/EXMAS**: Both programs model the transport of radionuclides through the biosphere. EXCON uses the calculated radionuclide activity concentration in the overlying rock to calculate radiation exposures (the effective dose rate and the radiotoxicity concentration) and EXMAS uses the radionuclide activity flux (for the calculation of the radiotoxicity flux). The exposition pathways are described in chapter 0.

4.2.3 Input data

This section describes the input data used for the calculation of the selected indicators. The input data are mainly based on data of the project SAM /BUH 91/ and new data provided by the ISIBEL project /BUH 08a/. The input data are arranged in five different categories:

- geometry,
- source-term,
- repository,
- overlying rock and
- biosphere.

4.2.3.1 Geometry

The geometry is described in detail in /BUH 08b/. The main difference to the repository concept in ISIBEL is the extension of the SF section in order to be able to emplace the total waste volumes of heat-generating waste (HGW) that are expected to accumulate in Germany until 2080.

Considered types of waste packages are steel canisters (type BSK 3) for spent fuel rods, HLW canisters (vitrified waste, type CSD-V) and ILW canisters (compacted ILW constituents of spent fuel elements, type CSD-C). The canister data are given in Table 4.1.

Tab. 4.1 Canister data

Canister Name	Canister Type	Length [m]	Radius [m]	Mass [kg]
SF	BSK-3	4.98	0.22	5 300
HLW	CSD-V	1.34	0.22	700
ILW	CSD-C	1.34	0.22	490

The chosen geometric configuration of the boreholes guarantees that the maximum temperature near the waste is less than 200°C. The minimum distances between the boreholes is about 60 m for SF canisters and HLW canisters and 20 m for ILW canisters. The repository consists of ten waste sections, eight sections for SF (120 boreholes), one section for HLW (15 boreholes), and one section for ILW (35 boreholes).

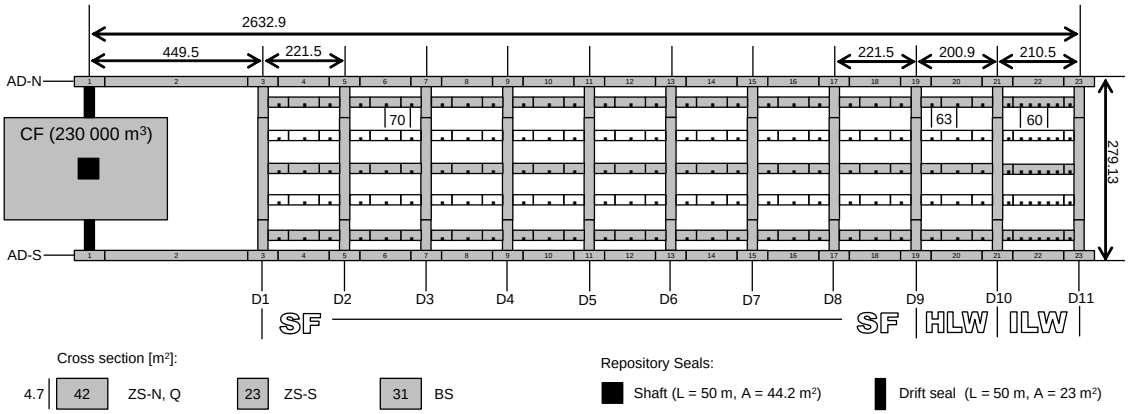

Fig. 4.5 Plane view of the repository model. Black dots represent the vertical boreholes

Altogether

- 6960 (120 × 58) SF canisters,
- 3225 (15 × 215) HLW canisters and
- 7455 (35 × 213) ILW canisters

are assumed to be emplaced in the repository. As shown in Figure 4.5 the SF section comprises the largest part of the repository. It is assumed in this concept that the SF are emplaced nearest to the central field followed by the HLW and the ILW.

The fluid reservoirs considered in the second test case are located in the fifth section (SF2 at the transfer drift D5).

4.2.3.2 Source term

The inventories of the different waste canister types are based on data from /BUH 08b/. These data and the resulting total amounts are listed in Tables 4.2 and 4.3.

After a cooling time of 30 years the waste canisters are emplaced in the repository. No time delay by the operational period is considered for this study.

The failure of the canisters starts as soon as a brine flows into a borehole with emplaced waste. For all canister types a uniformly distributed canister lifetime is assumed with a minimum lifetime of 0 years and a maximum lifetime of 100 years. A barrier effect of the canister or the cladding is not taken into account. The release from the waste matrix starts immediately after failure of the canister. The radionuclides become dissolved in the water volume inside the void volume of the borehole. Some radionuclides may precipitate if they reach their solubility limits within this volume. Neither temporal change nor spatial differences in chemical conditions are taken into account.

Different mobilisation rates are used for the three waste types. Only SF mobilisation will be described here. It will be seen later that all relevant processes occur in the SF section of the emplacement area.

Tab. 4.2 Radionuclide inventory (activation and fission products)

Nuclide	Half-life [a]	SF [Bq/can.]	HLW [Bq/can.]	ILW [Bq/can.]	Total [Bq]	Total [Sv]
C-14	$5.730 \cdot 10^{3}$	$7.37 \cdot 10^{10}$	-	$1.4 \cdot 10^{10}$	$6.17 \cdot 10^{14}$	$3.58 \cdot 10^{05}$
Co-60	$5.272 \cdot 10^{0}$	$1.63 \cdot 10^{15}$	$3.32 \cdot 10^{13}$	$7.71 \cdot 10^{13}$	$1.21 \cdot 10^{19}$	$4.10 \cdot 10^{10}$
Ni-59	$7.500 \cdot 10^{4}$	$8.14 \cdot 10^{11}$	$7.00 \cdot 10^{07}$	-	$5.66 \cdot 10^{15}$	$3.57 \cdot 10^{05}$
Ni-63	$1.000 \cdot 10^{2}$	$1.16 \cdot 10^{14}$	$9.50 \cdot 10^{09}$	$2.71 \cdot 10^{13}$	$1.01 \cdot 10^{18}$	$1.51 \cdot 10^{08}$
Se-79	$1.100 \cdot 10^{6}$	$2.98 \cdot 10^{10}$	$1.72 \cdot 10^{10}$	$5.51 \cdot 10^{07}$	$2.63 \cdot 10^{14}$	$7.63 \cdot 10^{05}$
Sr-90	$2.864 \cdot 10^{1}$	$5.99 \cdot 10^{15}$	$3.23 \cdot 10^{15}$	$1.40 \cdot 10^{13}$	$5.22 \cdot 10^{19}$	$1.60 \cdot 10^{12}$
Zr-93	$1.500 \cdot 10^{6}$	$1.58 \cdot 10^{11}$	$8.92 \cdot 10^{10}$	$8.60 \cdot 10^{09}$	$1.45 \cdot 10^{15}$	$1.77 \cdot 10^{06}$
Nb-94	$2.000 \cdot 10^{4}$	$1.36 \cdot 10^{11}$	$8.18 \cdot 10^{06}$	-	$9.47 \cdot 10^{14}$	$1.61 \cdot 10^{06}$
Mo-93	$3.500 \cdot 10^{3}$	$6.95 \cdot 10^{09}$	$6.47 \cdot 10^{06}$	-	$4.84 \cdot 10^{13}$	$1.56 \cdot 10^{05}$
Tc-99	$2.100 \cdot 10^{5}$	$1.04 \cdot 10^{12}$	$6.19 \cdot 10^{11}$	$2.31 \cdot 10^{09}$	$9.22 \cdot 10^{15}$	$5.90 \cdot 10^{06}$
Pd-107	$6.500 \cdot 10^{6}$	$8.33 \cdot 10^{09}$	$4.65 \cdot 10^{09}$	-	$7.30 \cdot 10^{13}$	$2.70 \cdot 10^{03}$
Sn-126	$2.345 \cdot 10^{5}$	$4.47 \cdot 10^{10}$	$2.43 \cdot 10^{10}$	$1.51 \cdot 10^{06}$	$3.89 \cdot 10^{14}$	$1.97 \cdot 10^{06}$
I-129	$1.570 \cdot 10^{7}$	$2.44 \cdot 10^{09}$	$1.65 \cdot 10^{04}$	$5.31 \cdot 10^{06}$	$1.70 \cdot 10^{13}$	$1.87 \cdot 10^{06}$
Cs-135	$2.000 \cdot 10^{6}$	$2.45 \cdot 10^{10}$	$1.62 \cdot 10^{10}$	$7.11 \cdot 10^{07}$	$2.23 \cdot 10^{14}$	$4.46 \cdot 10^{05}$
Cs-137	$3.017 \cdot 10^{1}$	$8.60 \cdot 10^{15}$	$4.67 \cdot 10^{15}$	$1.51 \cdot 10^{13}$	$7.50 \cdot 10^{19}$	$9.75 \cdot 10^{11}$
Sm-151	$9.300 \cdot 10^{1}$	$2.00 \cdot 10^{13}$	$1.53 \cdot 10^{13}$	$6.00 \cdot 10^{10}$	$1.89 \cdot 10^{17}$	$1.85 \cdot 10^{07}$

Tab. 4.3 Radionuclide inventory (actinide elements)

Nuclide	Half-life [a]	SF [Bq/can.]	HLW [Bq/can.]	ILW [Bq/can.]	Total [Bq]	Total [Sv]
Th-series						
Pu-244	$8.000 \cdot 10^{7}$	$6.95 \cdot 10^{04}$	$1.12 \cdot 10^{02}$	-	$4.84 \cdot 10^{08}$	$1.17 \cdot 10^{02}$
Cm-244	$1.810 \cdot 10^{1}$	$3.46 \cdot 10^{14}$	$1.13 \cdot 10^{14}$	$9.51 \cdot 10^{10}$	$2.77 \cdot 10^{18}$	$3.33 \cdot 10^{11}$
Pu-240	$6.563 \cdot 10^{3}$	$3.83 \cdot 10^{13}$	$7.61 \cdot 10^{10}$	$5.20 \cdot 10^{10}$	$2.67 \cdot 10^{17}$	$6.68 \cdot 10^{10}$
U-236	$2.342 \cdot 10^{7}$	$1.91 \cdot 10^{10}$	$6.63 \cdot 10^{07}$	-	$1.33 \cdot 10^{14}$	$6.25 \cdot 10^{06}$
Th-232	$1.405 \cdot 10^{10}$	$2.10 \cdot 10^{00}$	$5.65 \cdot 10^{00}$	-	$3.28 \cdot 10^{04}$	$7.55 \cdot 10^{-3}$
U-232	$6.890 \cdot 10^{1}$	$1.24 \cdot 10^{09}$	$1.11 \cdot 10^{07}$	-	$8.65 \cdot 10^{12}$	$2.85 \cdot 10^{-06}$
Np-series						
Cm-245	$8.500 \cdot 10^{3}$	$2.72 \cdot 10^{10}$	$1.11 \cdot 10^{10}$	-	$2.25 \cdot 10^{14}$	$4.73 \cdot 10^{07}$
Pu-241	$1.435 \cdot 10^{1}$	$9.27 \cdot 10^{15}$	$1.27 \cdot 10^{13}$	$1.00 \cdot 10^{13}$	$6.47 \cdot 10^{19}$	$3.10 \cdot 10^{11}$
Am-241	$4.322 \cdot 10^{2}$	$1.03 \cdot 10^{13}$	$6.20 \cdot 10^{13}$	$3.51 \cdot 10^{10}$	$2.72 \cdot 10^{17}$	$5.44 \cdot 10^{10}$
Np-237	$2.144 \cdot 10^{6}$	$2.63 \cdot 10^{10}$	$1.66 \cdot 10^{10}$	$7.20 \cdot 10^{06}$	$2.37 \cdot 10^{14}$	$2.60 \cdot 10^{07}$
U-233	$1.592 \cdot 10^{5}$	$4.12 \cdot 10^{06}$	$1.83 \cdot 10^{04}$	-	$2.87 \cdot 10^{10}$	$1.46 \cdot 10^{03}$
Th-229	$7.880 \cdot 10^{3}$	$1.27 \cdot 10^{04}$	$6.63 \cdot 10^{03}$	-	$9.08 \cdot 10^{08}$	$4.45 \cdot 10^{02}$
U-series						
Cm-246	$4.730 \cdot 10^{3}$	$6.81 \cdot 10^{10}$	$2.27 \cdot 10^{10}$	-	$5.47 \cdot 10^{14}$	$1.15 \cdot 10^{08}$
Pu-242	$3.750 \cdot 10^{5}$	$1.84 \cdot 10^{11}$	$3.08 \cdot 10^{08}$	$2.80 \cdot 10^{08}$	$1.29 \cdot 10^{15}$	$3.08 \cdot 10^{08}$
Am-242	$1.410 \cdot 10^{2}$	$3.06 \cdot 10^{11}$	$1.55 \cdot 10^{11}$	-	$2.63 \cdot 10^{15}$	$4.99 \cdot 10^{08}$
U-238	$4.468 \cdot 10^{9}$	$1.86 \cdot 10^{10}$	$6.67 \cdot 10^{07}$	-	$1.30 \cdot 10^{14}$	$5.83 \cdot 10^{06}$
Pu-238	$8.774 \cdot 10^{1}$	$2.61 \cdot 10^{14}$	$4.28 \cdot 10^{11}$	$4.71 \cdot 10^{11}$	$1.82 \cdot 10^{18}$	$4.19 \cdot 10^{11}$
U-234	$2.455 \cdot 10^{5}$	$4.97 \cdot 10^{10}$	$2.10 \cdot 10^{08}$	-	$3.46 \cdot 10^{14}$	$1.70 \cdot 10^{07}$
Th-230	$7.540 \cdot 10^{4}$	$9.61 \cdot 10^{05}$	$3.17 \cdot 10^{06}$	-	$1.69 \cdot 10^{10}$	$3.55 \cdot 10^{03}$
Ra-226	$1.600 \cdot 10^{3}$	$1.27 \cdot 10^{03}$	$6.25 \cdot 10^{03}$	-	$2.90 \cdot 10^{07}$	$8.11 \cdot 10^{00}$
Ac -series						
Am-243	$7.370 \cdot 10^{3}$	$2.13 \cdot 10^{12}$	$1.05 \cdot 10^{12}$	$3.51 \cdot 10^{08}$	$1.82 \cdot 10^{16}$	$3.67 \cdot 10^{09}$
Pu-239	$2.411 \cdot 10^{4}$	$2.10 \cdot 10^{13}$	$4.54 \cdot 10^{10}$	$3.00 \cdot 10^{10}$	$1.47 \cdot 10^{17}$	$3.66 \cdot 10^{10}$
U-235	$7.038 \cdot 10^{8}$	$7.77 \cdot 10^{08}$	$3.51 \cdot 10^{06}$	-	$5.42 \cdot 10^{12}$	$2.56 \cdot 10^{05}$
Pa-231	$3.276 \cdot 10^{4}$	$1.98 \cdot 10^{06}$	$1.22 \cdot 10^{06}$	-	$1.78 \cdot 10^{10}$	$1.26 \cdot 10^{04}$

Tab. 4.4 Mobilisation rates for different fractions of spent fuel elements /KES 05/

	Metal parts	Fuel Matrix	IRF[2]
Mobilisation rate [a^{-1}]	$3.6 \cdot 10^{-3}$	$1.0 \cdot 10^{-6}$	instantaneous

For the different fractions of spent fuel elements different mobilisation rates are taken into account (Table 4.4). The corresponding percentages of the different fractions for every radionuclide are listed in Table 4.5.

Tab. 4.5 Relative inventory in the different fractions of spent fuel elements in per cent /KES 05/

Element	Metal parts	Fuel Matrix	IRF
C	72.20	26.41	1.39
Ni, Mo, Nb	99.50	0.47	0.03
Sn	0.00	98.00	2.00
I, Se	0.00	97.00	3.00
Cs	0.00	96.00	4.00
Sr	0.00	99.90	0.10
Pd, Sm	0.00	99.00	1.00
Zr	9.40	86.07	4.53
Tc	0.10	99.89	0.01
Pb, Cm, Am, Pu, Pa, U, Th, Ac, Np, Ra	0.00	99.99	0.01

4.2.3.3 Repository

In the repository conservative solubility limits (Table 4.6) are used, sorption is not considered. The calculation of the temperature increase due to the heat production of the waste in the repository is based on data of the SAM project. Since the repository concept used there differs from the concept here, the temperature data are not well adapted for the chosen concept.

[2] Instantaneous Release Fraction

Tab. 4.6 Solubility limits

Element	Solubility limits [mol·l^{-1}]	Element	Solubility limits [mol·l^{-1}]
C	$1.0 \cdot 10^{-2}$	Cs	$1.0 \cdot 10^{0}$
Co	$1.0 \cdot 10^{0}$	Sm	$1.0 \cdot 10^{-4}$
Ni	$1.0 \cdot 10^{-4}$	Pb	$1.0 \cdot 10^{0}$
Se	$1.0 \cdot 10^{-4}$	Ra	$1.0 \cdot 10^{-6}$
Sr	$1.0 \cdot 10^{-3}$	Th	$1.0 \cdot 10^{-6}$
Zr	$1.0 \cdot 10^{-6}$	Pa	$1.0 \cdot 10^{-6}$
Nb	$1.0 \cdot 10^{-4}$	U	$1.0 \cdot 10^{-4}$
Mo	$1.0 \cdot 10^{-4}$	Np	$1.0 \cdot 10^{-5}$
Tc	$1.0 \cdot 10^{-4}$	Pu	$1.0 \cdot 10^{-6}$
Pd	$1.0 \cdot 10^{-4}$	Am	$1.0 \cdot 10^{-5}$
Sn	$1.0 \cdot 10^{-4}$	Cm	$1.0 \cdot 10^{-5}$
I	$1.0 \cdot 10^{0}$		

Tab. 4.7 General data

Parameter	Dimension	Value
Average rock density	kg/m^3	2 300
Average fluid density	kg/m^3	1 200
Depth of repository (= reference level)	m b. s.	870
Rock temperature (reference level)	K	310
Geothermal gradient	K/m	0.03
Rock pressure (reference level)	MPa	18
Hydrostatic pressure (reference level)	MPa	10
Reference convergence rate	1/a	0.01
Permeability of the shaft seal	m^2	10^{-17}
Permeability of the drift seals	m^2	10^{-17}
Initial plug porosity	-	0.3
Initial backfill porostiy	-	0.3

All further project relevant input data related to the modelling of the near field are given in Table 4.7. The technically achievable permeability of the shaft and drift seals is assumed to be 10^{-17} m^2. These values are changed for the test case “Failure of shaft and drift seals”. The permeability of the shaft seal is set to 10^{-14} m^2 after a time period of 50 years after repository closure, the permeability of the drift seal is set to 10^{-15} m^2 for the whole test case.

4.2.3.4 Overlying rock

For the radionuclide transport outside the repository advection, dispersion and dilution (Table 4.8), sorption (Table 4.9) and radioactive decay are taken into account.

Tab. 4.8 Transport parameter values for the overlying rock

Parameter	Dimension	Value
Total length (modelled area)	m	9 394
Cross sectional area (modelled area)	m^2	36 900
Natural groundwater flow	m^3/a	48 000
Dispersion length	m	65
Molecular diffusion coefficient	m^2/a	$3 \cdot 10^{-2}$
Porosity	-	0.2
Rock density	kg/m^3	2 500

Tab. 4.9 Sorption coefficients for the overlying rock

Element	Sorption coefficient [m^3/kg]	Element	Sorption coefficient [m^3/kg]
C	$5.0 \cdot 10^{-3}$	Sm	1.0
Ni	$1.0 \cdot 10^{-2}$	Pb	$4.0 \cdot 10^{-2}$
Se	$3.0 \cdot 10^{-4}$	Po	1.0
Sr	$5.0 \cdot 10^{-4}$	Ra	$9.0 \cdot 10^{-4}$
Zr	$1.0 \cdot 10^{-1}$	Ac	$4.0 \cdot 10^{-2}$
Nb	$1.0 \cdot 10^{-1}$	Th	$3.0 \cdot 10^{-1}$
Mo	$1.0 \cdot 10^{-3}$	Pa	1.0
Tc	$7.0 \cdot 10^{-3}$	U	$2.0 \cdot 10^{-3}$
Pd	$1.0 \cdot 10^{-2}$	Np	$3.0 \cdot 10^{-2}$
Sn	$2.0 \cdot 10^{-1}$	Pu	1.0
I	$5.0 \cdot 10^{-4}$	Am	1.0
Cs	$1.0 \cdot 10^{-3}$	Cm	1.0

The parameter values for the aquifer are based on investigations of overlying rocks of salt domes in Northern Germany /BUE 85/. The geological formation along the migration pathway is modelled as a homogeneous medium (porosity 0.2) with an average width of 820 m and a thickness of 45 m /PAG 88/. With a pore velocity of about 6.5 m/a, the resulting natural groundwater flow is 48 000 m^3/a.

4.2.3.5 Biosphere

The application of the biosphere model is in compliance with German regulations /AVV 90/. The following exposition pathways are included for the calculation of the dose conversion factors (Table 4.10):

- consumption of contaminated drinking water,
- consumption of fish from contaminated ponds,
- consumption of plants irrigated with contaminated water,
- consumption of milk and meat from cattle, which were watered and fed with contaminated fodder and
- exposure due to habitation on the contaminated land.

In Table 4.11 the dose coefficients for ingestion used to calculate the radiotoxicity from the radionuclide activity are listed. Dose coefficients of short-lived daughter nuclides not explicitly included in the calculation are added to their mother nuclides under the assumption of radioactive equilibrium in the contaminated water before ingestion.

Tab. 4.10 Dose conversion factors of relevant nuclides for age class > 17 a

Nuclide	Dose conversion factor [(Sv/a)/(Bq/m^3)]	Nuclide	Dose conversion factor [(Sv/a)/(Bq/m^3)]
C-14	$4.6 \cdot 10^{-8}$	Am-241	$8.0 \cdot 10^{-7}$
Co-60	$3.9 \cdot 10^{-6}$	Np-237	$4.7 \cdot 10^{-6}$
Ni-59	$4.9 \cdot 10^{-9}$	U-233	$3.9 \cdot 10^{-6}$
Ni-63	$1.1 \cdot 10^{-9}$	Pa-233	$8.8 \cdot 10^{-9}$
Se-79	$3.4 \cdot 10^{-7}$	Th-229	$1.7 \cdot 10^{-5}$
Sr-90	$1.8 \cdot 10^{-7}$	Ra-225	$1.1 \cdot 10^{-7}$
Zr-93	$3.7 \cdot 10^{-8}$	Ac-225	$3.7 \cdot 10^{-8}$
Nb-94	$3.1 \cdot 10^{-6}$	Pu-242	$9.4 \cdot 10^{-7}$
Mo-93	$3.2 \cdot 10^{-7}$	Am-242m	$7.6 \cdot 10^{-7}$
Tc-99	$8.8 \cdot 10^{-9}$	Pu-238	$7.5 \cdot 10^{-7}$
Sn-126	$1.6 \cdot 10^{-5}$	U-238	$7.1 \cdot 10^{-7}$
I-129	$5.6 \cdot 10^{-7}$	Th-234	$4.8 \cdot 10^{-9}$
Cs-135	$5.7 \cdot 10^{-8}$	U-234	$1.4 \cdot 10^{-6}$
Cs-137	$9.5 \cdot 10^{-7}$	Th-230	$3.7 \cdot 10^{-5}$
Sm-151	$3.2 \cdot 10^{-10}$	Ra-226	$3.0 \cdot 10^{-5}$
Cm-244	$3.8 \cdot 10^{-7}$	Pb-210	$2.3 \cdot 10^{-6}$
Pu-240	$9.6 \cdot 10^{-7}$	Po-210	$4.9 \cdot 10^{-6}$
U-236	$5.6 \cdot 10^{-7}$	Am-243	$2.0 \cdot 10^{-6}$
Th-232	$1.1 \cdot 10^{-4}$	Pu-239	$9.8 \cdot 10^{-7}$
Ra-228	$2.4 \cdot 10^{-6}$	U-235	$3.3 \cdot 10^{-6}$
U-232	$5.4 \cdot 10^{-6}$	Pa-231	$4.0 \cdot 10^{-5}$
Th-228	$1.3 \cdot 10^{-6}$	Ac-227	$1.0 \cdot 10^{-5}$
Cm-245	$1.4 \cdot 10^{-6}$	Th-227	$1.9 \cdot 10^{-8}$
Pu-241	$1.8 \cdot 10^{-8}$	Ra-223	$1.1 \cdot 10^{-7}$

Tab. 4.11 Dose coefficients for ingestion to calculate the radiotoxicity

Nuclide[3]	Ingestion dose coefficient [Sv/Bq]	Nuclide	Ingestion dose coefficient [Sv/Bq]
C-14	$5.80 \cdot 10^{-10}$	Am-241	$2.00 \cdot 10^{-7}$
Co-60	$3.40 \cdot 10^{-9}$	Np-237	$1.10 \cdot 10^{-7}$
Ni-59	$6.30 \cdot 10^{-11}$	U-233	$5.10 \cdot 10^{-8}$
Ni-63	$1.50 \cdot 10^{-10}$	Pa-233	$8.70 \cdot 10^{-10}$
Se-79	$2.90 \cdot 10^{-9}$	Th-229	$4.90 \cdot 10^{-7}$
Sr-90 +	$3.07 \cdot 10^{-8}$	Ra-225	$9.90 \cdot 10^{-8}$
Zr-93 +	$1.22 \cdot 10^{-9}$	Ac-225 +	$2.43 \cdot 10^{-8}$
Nb-94	$1.70 \cdot 10^{-9}$	Pu-242	$2.40 \cdot 10^{-7}$
Mo-93 +	$3.22 \cdot 10^{-9}$	Am-242m +	$1.90 \cdot 10^{-7}$
Tc-99	$6.40 \cdot 10^{-10}$	Pu-238	$2.30 \cdot 10^{-7}$
Sn-126 +	$5.07 \cdot 10^{-9}$	U-238	$4.50 \cdot 10^{-8}$
I-129	$1.10 \cdot 10^{-7}$	Th-234 +	$3.91 \cdot 10^{-9}$
Cs-135	$2.00 \cdot 10^{-9}$	U-234	$4.90 \cdot 10^{-8}$
Cs-137	$1.30 \cdot 10^{-8}$	Th-230	$2.10 \cdot 10^{-7}$
Sm-151	$9.80 \cdot 10^{-11}$	Ra-226 +	$2.80 \cdot 10^{-7}$
Cm-244	$1.20 \cdot 10^{-7}$	Pb-210 +	$6.91 \cdot 10^{-7}$
Pu-240	$2.50 \cdot 10^{-7}$	Po-210	$1.20 \cdot 10^{-6}$
U-236	$4.70 \cdot 10^{-8}$	Am-243 +	$2.01 \cdot 10^{-7}$
U-232	$3.30 \cdot 10^{-7}$	Pu-239	$2.50 \cdot 10^{-7}$
Th-232	$2.30 \cdot 10^{-7}$	U-235 +	$4.73 \cdot 10^{-8}$
Ra-228 +	$6.90 \cdot 10^{-7}$	Pa-231	$7.10 \cdot 10^{-7}$
Th-228 +	$1.43 \cdot 10^{-7}$	Ac-227	$1.10 \cdot 10^{-6}$
Cm-245	$2.10 \cdot 10^{-7}$	Th-227	$8.80 \cdot 10^{-9}$
Pu-241	$4.80 \cdot 10^{-9}$	Ra-223 +	$1.00 \cdot 10^{-7}$

[3] A plus sign after the radionuclide name indicates that the dose coefficient for this nuclide includes the dose coefficient for all daughter nuclides up to the next one given in the table.

4.3 Safety indicators

All three safety indicators described in chapter 2 are calculated for the repository in salt for both test cases; namely the

- effective dose rate [Sv/a],
- radiotoxicity concentration in the biosphere water [Sv/m^3] and
- radiotoxicity flux from the geosphere (overlying rock) [Sv/a].

These three safety indicators are normalised by division by their according reference value described in chapter 3.

In the context of a safety case for a repository system it is important to conclude how the three safety indicators demonstrate the long-term safety with regard to the three different safety aspects (chapter 2) using independently derived reference values. This will be demonstrated here for the two selected test cases.

4.3.1 Test case: Failure of shaft and drift seals

In general, the temporal evolution of the safety indicators is quite similar (Figure 4.6). The effective dose rate and the radiotoxicity concentration in biosphere water only differ in the factor each radionuclide is multiplied with (the dose conversion factor in case of the effective dose and the ingestion dose coefficient in case of radiotoxicity). Since only a few radionuclides (I-129 and Cs-135, see Table 4.12) dominate the release of radionuclides to the biosphere, the curves' shape is quite similar.

The normalised radiotoxicity concentration in biosphere water and the normalised radiotoxicity flux from the geosphere show almost the same progression. Although the reference values are derived independently, the curves are virtually identical: If the radiotoxicity flux from the geosphere is divided by the natural groundwater flow the reference value for the radiotoxicity concentration in the geosphere is $2.1 \cdot 10^{-6}$ Sv/m^3 (0.1 Sv/a divided by 48 000 m^3), the reference value for the radiotoxicity concentration in drinking water is $2.0 \cdot 10^{-6}$ Sv/m^3. Since the natural groundwater flux is assumed to be constant the resulting indicators give almost the same safety margin to the reference value.

All three normalised indicators remain below the reference value for the calculated period of one million years. For the radiotoxicity indicators the safety margin to this limit is very small in the time period between 7 000 to 40 000 years. The normalised effective dose rate is about one order of magnitude below this limit.

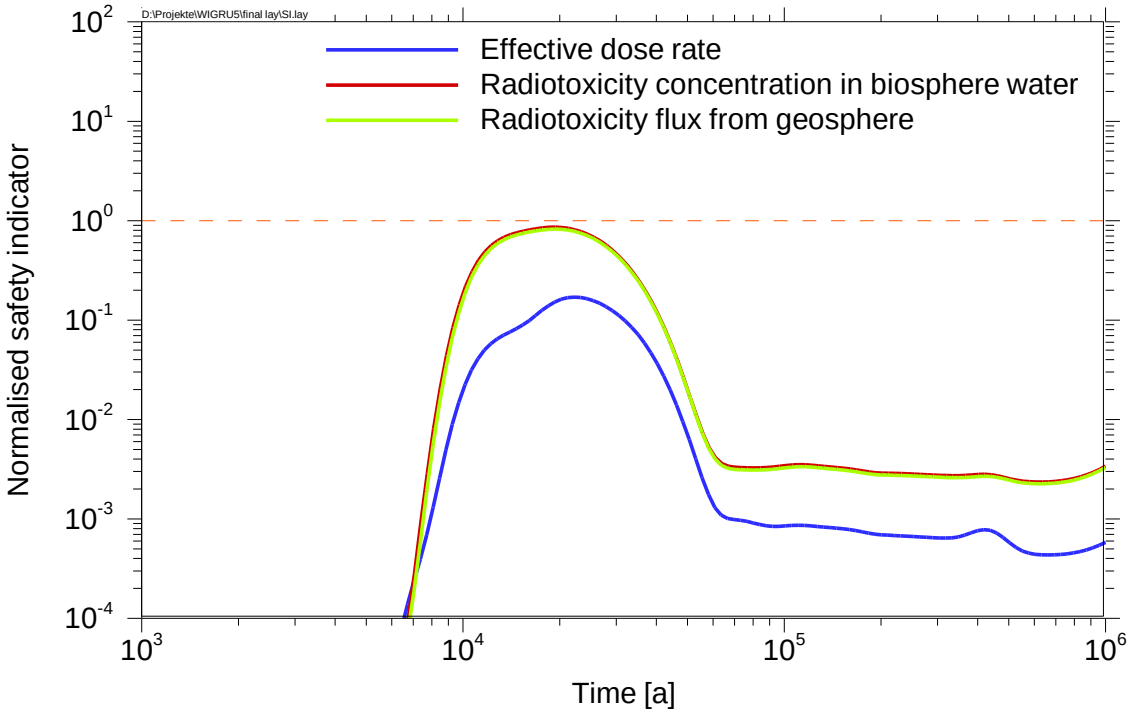

Fig. 4.6 Normalised safety indicators

All three safety indicators are dominated by the radionuclides I-129 and Cs-135, at early times also by Se-79. Since all three indicators show the similar temporal evolution the discussion on the dominating radionuclides is restricted here to the effective dose rate. The conclusions drawn can be easily transferred to the two other indicators[4].

The maximum value of the effective dose rate is $1.7 \cdot 10^{-5}$ Sv/a at 2 200 years. The maximum is dominated by I-129 and Cs-135. Table 4.12 lists the radionuclides that cause the highest maximum dose exposures. The radionuclides that are important contributors to the dose rate are characterised by a high solubility and a weak sorption in the overlying rock.

[4] There are only small differences, for example the relatively high dose conversion factor of Np-237 leads to a small peak after $4.38 \cdot 10^5$ years for the effective dose rate. This peak is hardly visible for the other two indicators due to the comparably low ingestion dose coefficient.

Tab. 4.12 List of the dominating radionuclides for the test case “Failure of shaft and drift seals”

Nuclide	Maximum Dose Exposure [Sv/a]	Point in Time of Appearance [a]
Cs-135	$1.04 \cdot 10^{-5}$	24 300
I-129	$7.91 \cdot 10^{-6}$	16 800
Mo-93	$5.74 \cdot 10^{-7}$	19 300
Se-79	$1.27 \cdot 10^{-7}$	14 000
Np-237	$2.38 \cdot 10^{-8}$	438 000
Ra-226	$1.86 \cdot 10^{-8}$	50 600
U-233	$1.39 \cdot 10^{-8}$	50 300

In Figure 4.7 the results from a parameter variation of the time period between repository closure and the failure of the shaft and drift seals is shown for all three indicators.

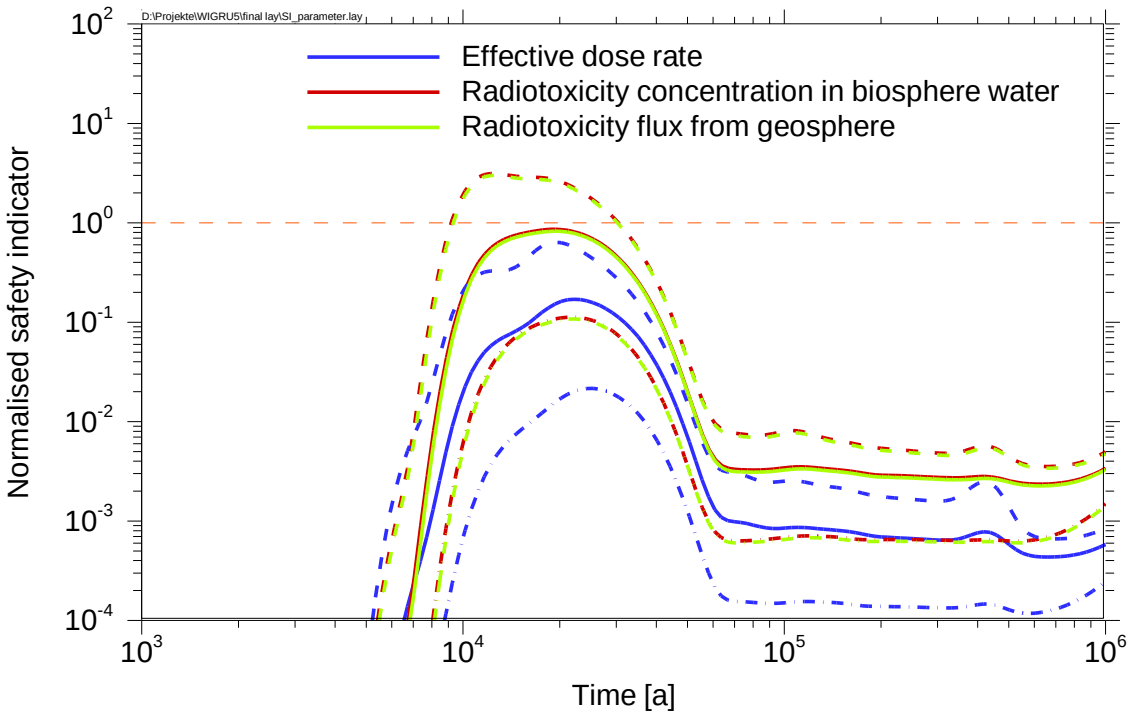

Fig. 4.7 Normalised safety indicators for variations of the time period before failure of shaft and drift seals (solid lines: reference; dashed lines: time period of 25 years dash, dot lines: a time period of 75 years)

It can be seen, that the reduction of this time period from 50 to 25 years causes an exceedance of the reference values of the two indicators between about 9 000 and 30 000 years. The effective dose rate remains below the reference value. An extension

of the period from 50 to 75 years yields a reduction of all safety indicators. The safety margin is then one order of magnitude for the radiotoxicity concentration in the biosphere and the radiotoxicity flux in the geosphere and two orders of magnitude for the effective dose rate.

4.3.2 Test case: Fluid reservoir

All three indicators are more than four orders of magnitude below their reference values (Figure 4.8). They give a strong argument for the safety of the repository system for this type of evolution.

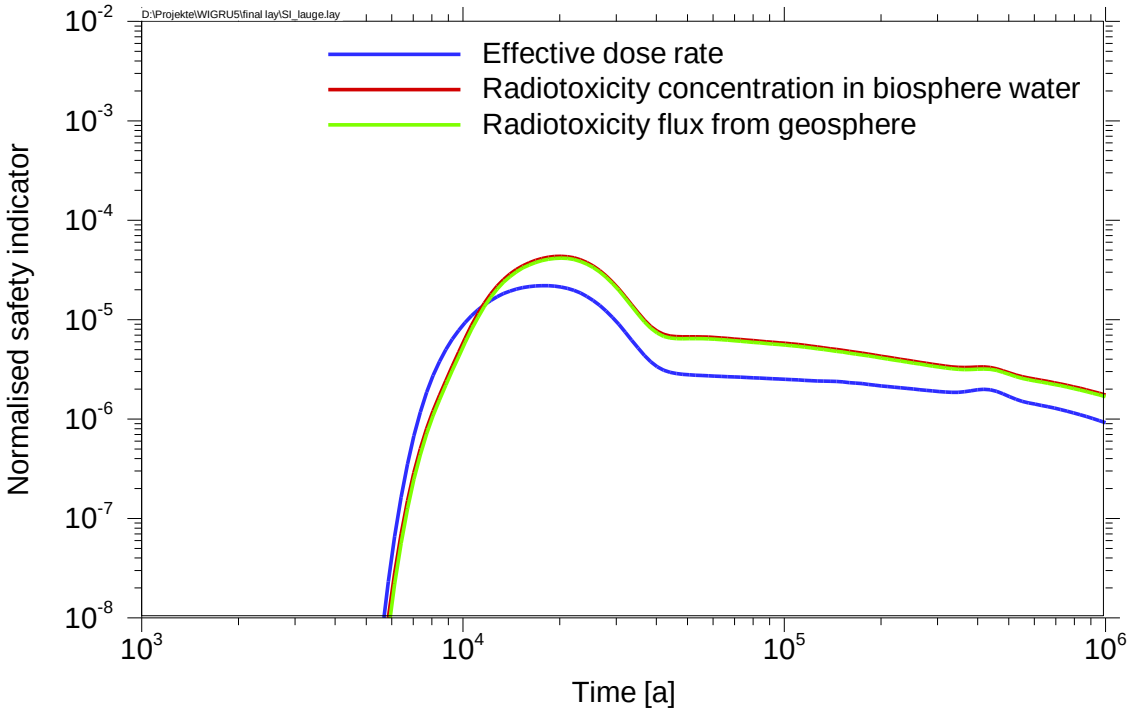

Fig. 4.8 Normalised safety indicators

The total maxima of the curves are about four orders of magnitude lower than in the first test case. Due to the lower permeability of the geotechnical barriers the brine inflow into and out of the repository is much smaller than in the first test case. The total brine inflow in one million years is 1 385 m^3, about 5 % of the inflow of the first test case (27 868 m^3), and the outflow out of the repository is 1 057 m^3, about 4 % of the outflow of the first test case (26 248 m^3).

Tab. 4.13 List of the dominating radionuclides for the test case “Fluid reservoir”

Nuclide	Maximum Dose Exposure [Sv/a]	Point in Time of Appearance [a]
Se-79	$1.83 \cdot 10^{-9}$	16 100
Cs-135	$4.43 \cdot 10^{-10}$	26 600
I-129	$3.37 \cdot 10^{-10}$	19 300
Ra-226	$1.39 \cdot 10^{-10}$	55 500
U-233	$4.30 \cdot 10^{-11}$	381 000
Np-237	$3.88 \cdot 10^{-11}$	483 000

The maximum value of the effective dose rate of $2.2 \cdot 10^{-9}$ Sv/a is mainly caused by Se-79 (80 %) at $1.76 \cdot 10^{4}$ years. At later times other radionuclides contribute more significantly, especially Cs-135, I-129, Ra-226 and U-233 (see Table 4.13). Table 4.12 and Table 4.13 contain the same radionuclides with the exception of Mo-93, which does not contribute at all to the effective dose rate in the second test case. Due to its short half live (3 500 a) and its larger retention within the repository structure with intact seal constructions no release from the repository of this radionuclide is calculated.

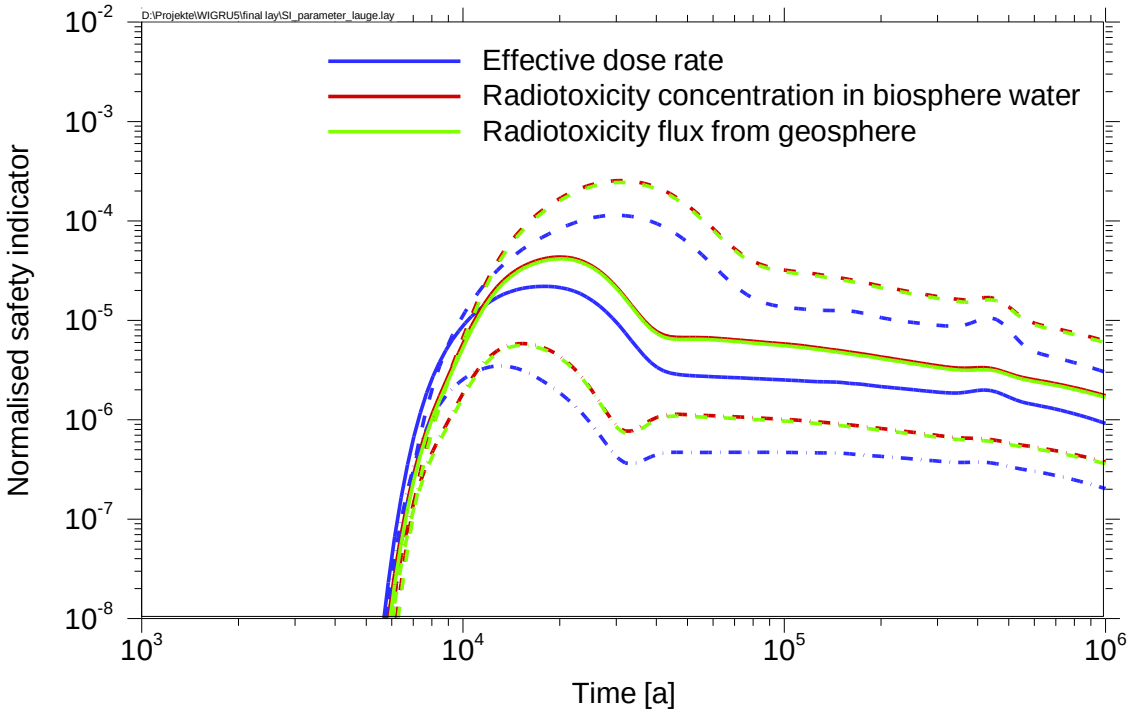

Fig. 4.9 Normalised safety indicators for variations of the reference convergence rate (solid lines: reference, dashed lines: convergence rate of 0.005 a^{-1}, the dash and dot lines: convergence rate of 0.015 a^{-1})

Figure 4.9 shows a variation of the reference convergence rate, an important and sensitive parameter for PA calculations in rock salt. Since all three indicators are still more than three orders of magnitude below the reference value, this variation is not relevant with regard to the overall safety of the repository system.

Altogether one can summarise that for the integrated PA calculations performed in this study all safety indicators show similar safety margins to the reference values derived in chapter 3. The margins of the second test case are about four orders of magnitude higher than in the first case. Despite the uncertainties in the derivation of the reference values, the additional calculations of the two radiotoxicity safety indicators substantiate thus the statement of safety of the repository system obtained from the effective dose rate.

4.4 Performance indicators

In contrast to safety indicators that provide a measure on the safety of the whole repository system, performance indicators are primarily used to describe the behaviour of the radionuclides in individual compartments of the repository system. The selection of the compartments mainly depends on the concept. Therefore the following results are strongly related to the presented concept.

All three performance indicators described in chapter 2 are calculated for the repository in salt for both test cases; namely the

- radiotoxicity inventory in different compartments [Sv],
- radiotoxicity fluxes from compartments [Sv/a] and
- integrated radiotoxicity fluxes from compartments [Sv].

4.4.1 Radiotoxicity inventory in different compartments

The radiotoxicity inventories are calculated only for the waste compartments (boreholes, red lines in Figures 4.10 to 4.15) and the compartments representing the central field, the access and the transfer drifts (blue lines). With the existing tools it is presently not possible to export the radiotoxicity inventory in the overlying rock compartment. Additionally to the calculated inventories in the compartments of the repository the

black line represents the decay corrected initial inventory (indicated with 'total' in Figures 4.10 to 4.15).

As already mentioned in chapter 4.2.2 the radiotoxicity inventory in the waste compartment is the mobilised radiotoxicity inventory. The gap between the curves of the total inventory and the mobilised inventory represents the radiotoxicity inventory remaining in the waste forms. After the release of radionuclides into the geosphere the radiotoxicity inventory in the overlying rock and the radiotoxicity released to the biosphere have also take into account.

4.4.1.1 Test case: Failure of shaft and drift seals

Figures 4.10 to 4.12 show the temporal evolution of the radiotoxic inventory of all radionuclides, of Tc-99 and of I-129, respectively.

In all figures it can be seen that the brine intruding via the shaft reaches the waste canisters in the first compartments (SF1 and SF2) after a few years. At this time the canister failure starts and radionuclides are mobilised. The smaller fraction released from SF2 reveals that the brine does not reach all boreholes of SF2. There is no release from the backmost waste compartments HLW and ILW.

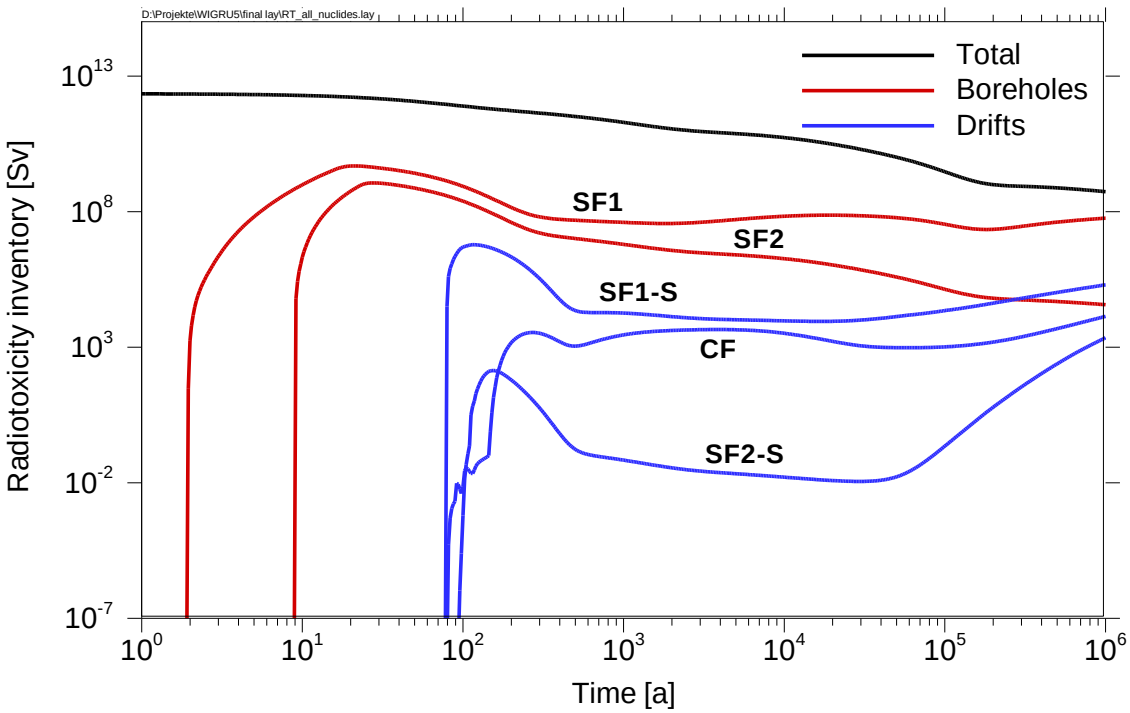

Fig. 4.10 Radiotoxicity inventory of all radionuclides in different compartments

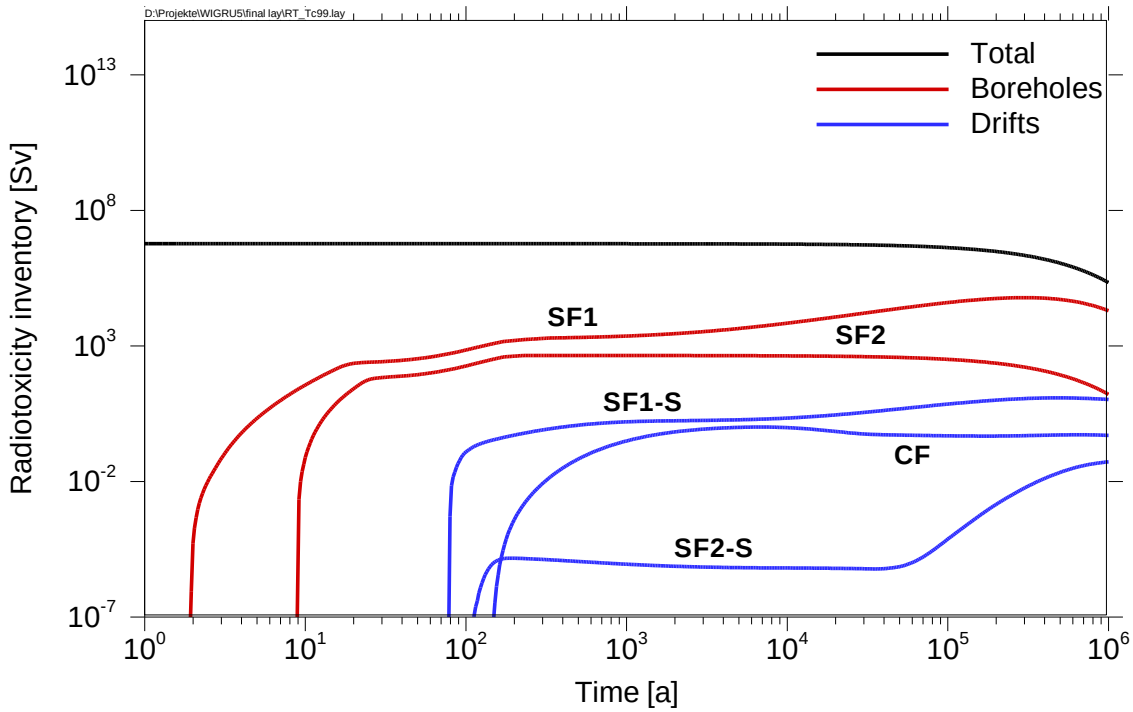

Fig. 4.11 Radiotoxicity inventory of Tc-99 in different compartments

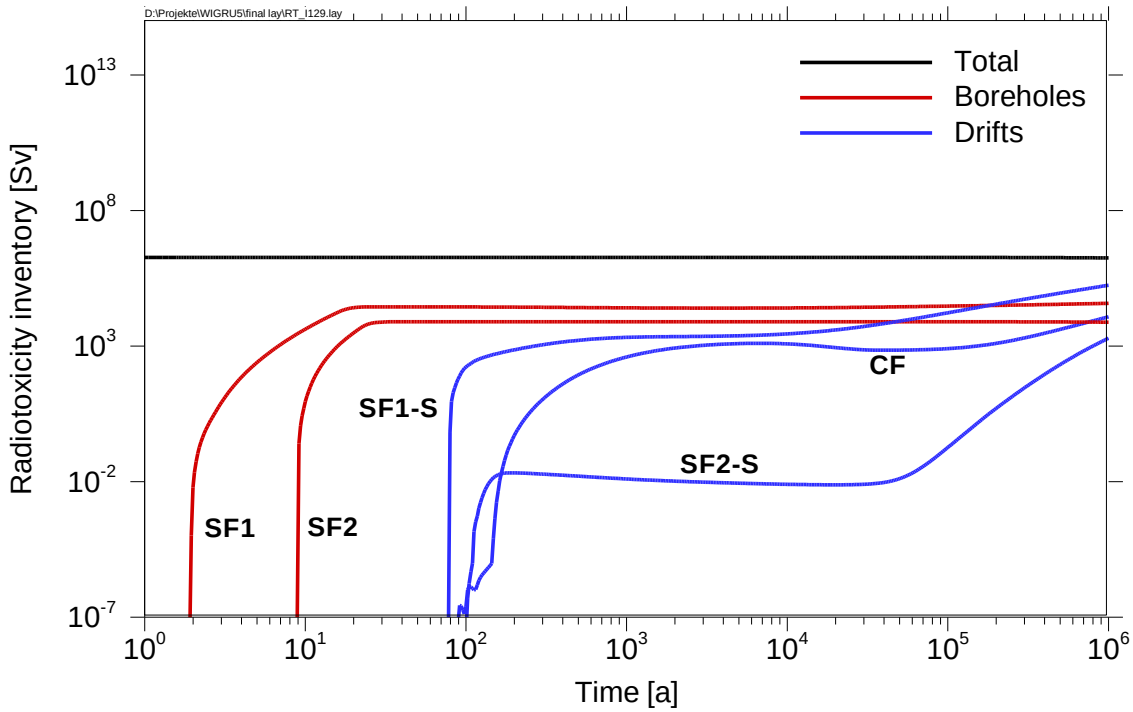

Fig. 4.12 Radiotoxicity inventory of I-129 in different compartments

The instant release of radionuclides from the gap (IRF) leads to a rapid increase of the mobilised radiotoxicity (Figure 4.10). After the IRF mobilisation the mobilisation is dominated by the slower rates from the metal parts and the fuel matrix. The amount of

mobilised radionuclides can not compensate the decay of the short-lived radionuclides. Consequently, the radiotoxicity inventory in the waste compartments decreases with time.

When convergence decreases the volumes of cavities and void spaces to a certain value, the convergence stops and diffusion determines the transport of radionuclides through the repository. This leads to an increase of the radiotoxicity inventory in the drift compartments (SF1-S, SF2-S, CF).

The total IRF of Tc-99 and I-129 are mobilised within a few decades corresponding to the canister failure. After the release of the IRF the amount of the mobilised radiotoxicity is controlled by the mobilisation rates of the other constituents of the spent fuel elements. For Tc-99 the mobilisation from metal parts and the fuel matrix causes an increase of the radiotoxicity inventory and yields a peak around $5.0 \cdot 10^5$ years. Due to its shorter half-life the radiotoxicity decreases by radioactive decay (Figure 4.11). Since I-129 is not contained in the metal parts of the spent fuel elements the radiotoxicity inventory increases only slightly during the period investigated representing the slow mobilisation rate from the fuel matrix. Owing to its long half-life the diffusion-controlled increase in the drift compartments at late times is quite distinctive (Figure 4.12).

4.4.1.2 Test case: Fluid reservoir

Figures 4.13 to 4.15 show the temporal evolution of the radiotoxicity inventory of all radionuclides, of Tc-99 and of I-129, respectively. The main difference to the first test case is the earlier interaction between the brine and the waste canisters, since intrusion from the brine inclusions starts immediately after repository closure. Mobilisation starts in the section SF2, where the reservoirs are located, and shortly later in the sections SF1, HLW and ILW. (In fact, the two curves of the radiotoxicity inventory in SF1 and SF2 are almost identical in the logarithmic illustration in Figures 4.13 to 4.15 and are marked with the notation SF1/SF2.)

Due to the mobilisation in all waste compartments the overall mobilisation is considerably larger in the second test case for the waste compartments. A striking difference to the first case is the time lag between the radiotoxicity inventory in the central field (CF) and the SF-compartments. The comparably low radiotoxicity inventory in the central field indicates the limited advective flow through the repository due to the low brine vol-

ume in the second test case. Moreover the intact drift seals retard the migration of the radionuclides from the drifts into the central field. Both effects are finally responsible for the much lower maximum effective dose rates in the second test case.

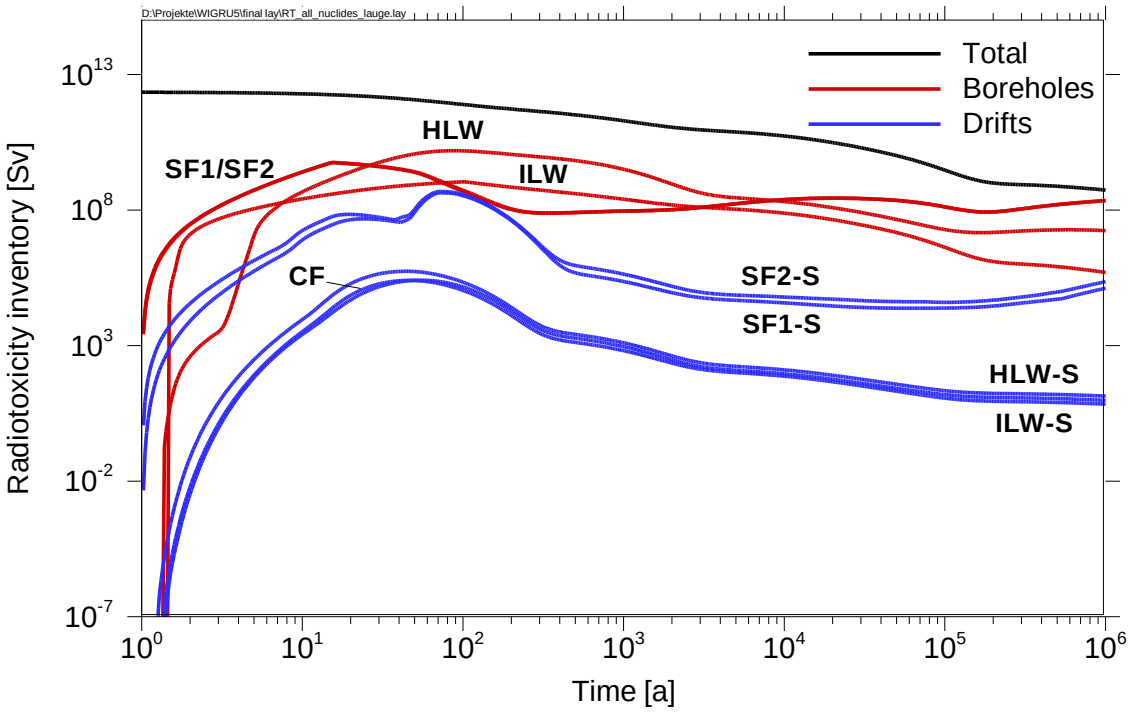

Fig. 4.13 Radiotoxicity inventory of all radionuclides in different compartments

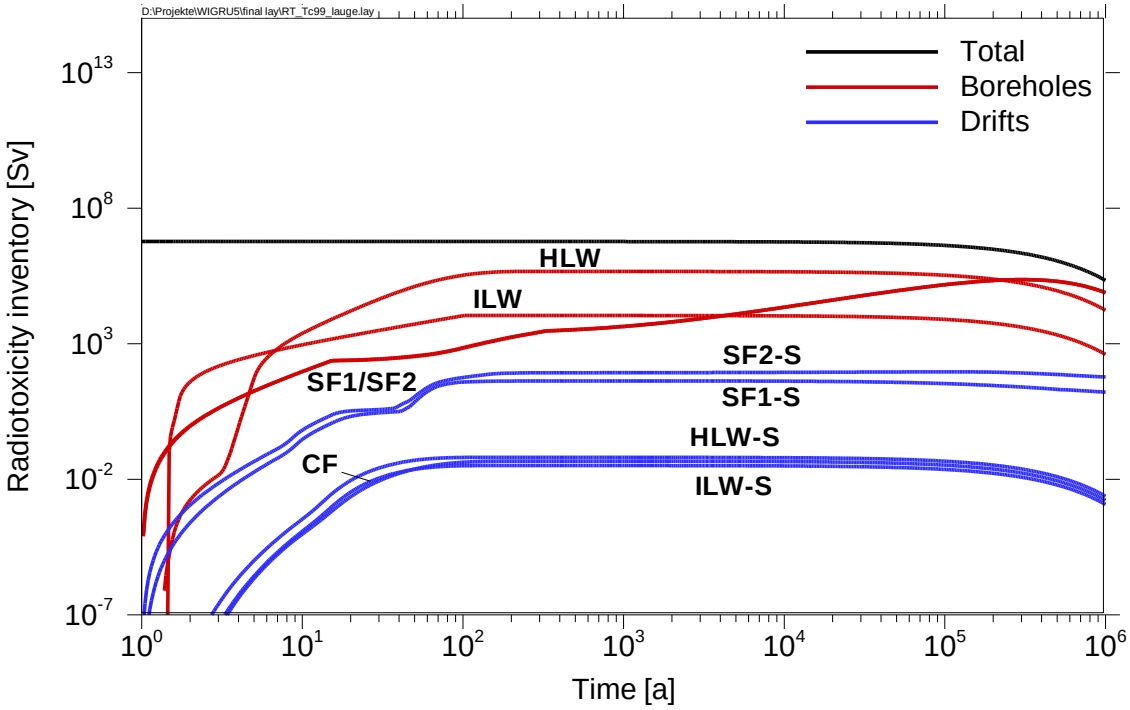

Fig. 4.14 Radiotoxicity inventory of Tc-99 in different compartments

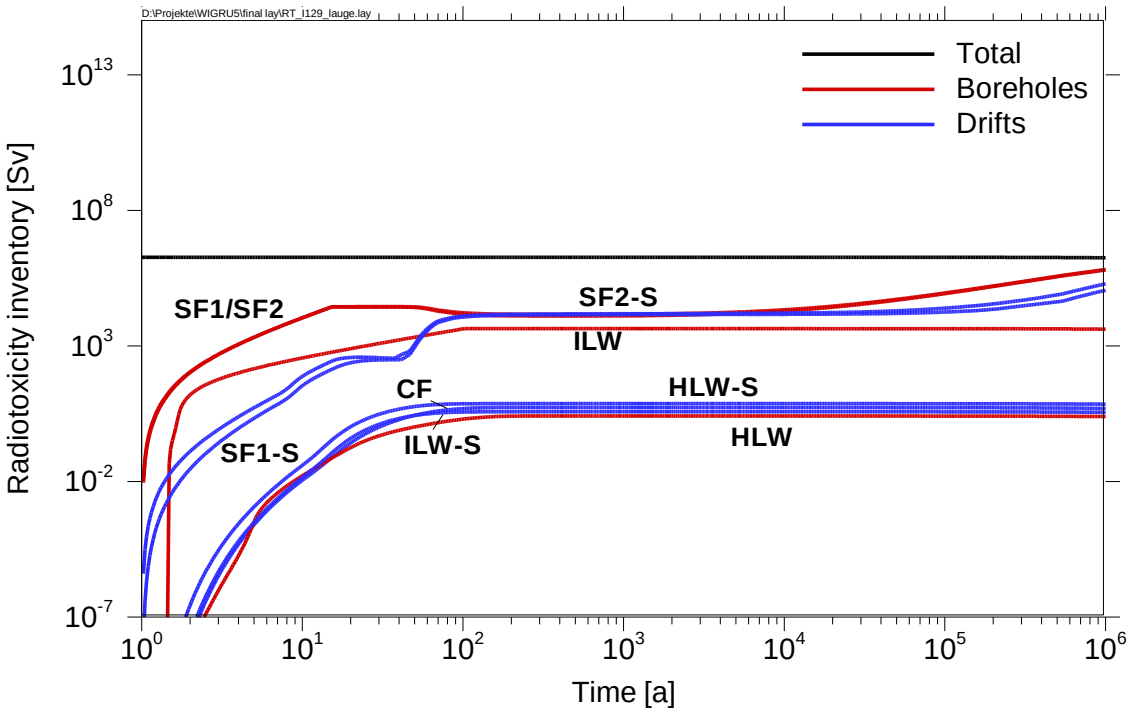

Fig. 4.15 Radiotoxicity inventory of I-129 in different compartments

The low radiotoxicity inventory of I-129 in the HLW section (Figure 4.15) reflects the low percentage of I-129 in the HLW compartment (Table 4.2).

4.4.2 Radiotoxicity fluxes from compartments

Radiotoxicity fluxes were calculated from the waste compartments (SF1, SF2, HLW and ILW), from the repository and from the overlying rock for the sum of all radionuclides as well as for Tc-99 and I-129. The radiotoxicity flux from a waste compartment represents the overall flux from the corresponding boreholes in this compartment. A flux out of a borehole is positive, a flux into a borehole is negative, i.e. a positive flux from one borehole can compensate a negative flux into another borehole and vice versa.

The radiotoxicity flux from the repository is the flux from the shaft to the overlying rock. The radiotoxicity flux from the overlying rock is determined by multiplying the activity fluxes calculated using the far field model by ingestion dose coefficients.

4.4.2.1 Test case: Failure of shaft and drift seals

In the first test case only a release from the waste compartment SF1, which is located near the shaft, takes place (Figure 4.16). There is no flux from any other waste compartment, because the intruding brine reaches these compartments after the borehole plugs are sealed.

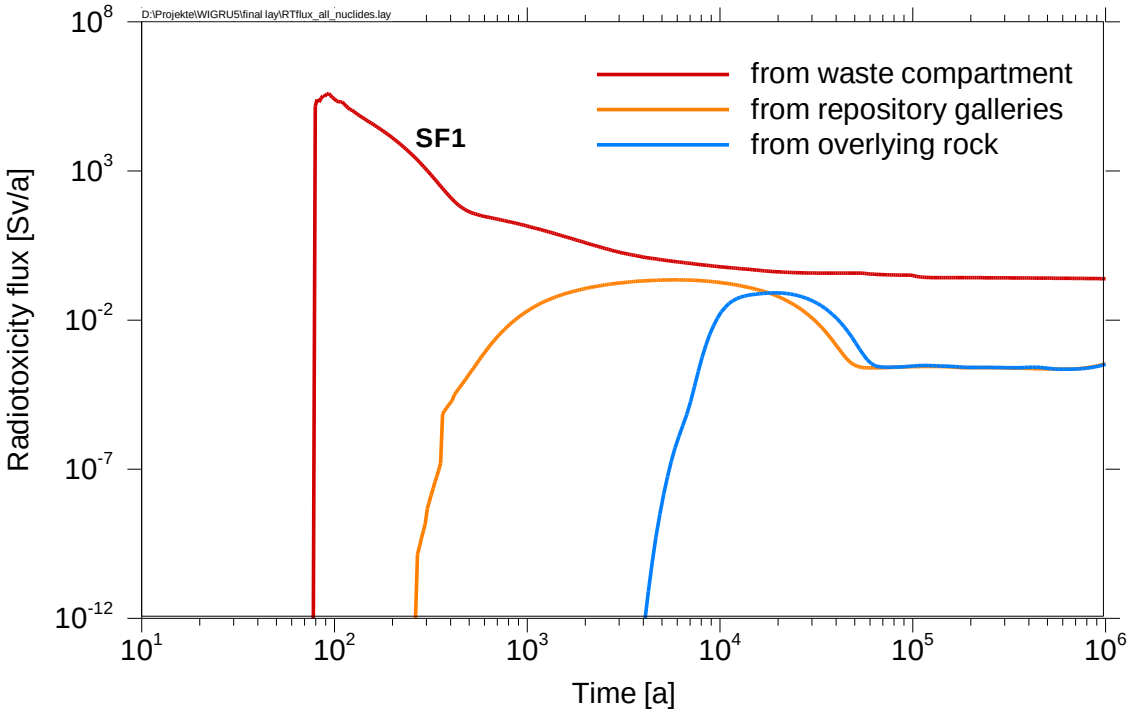

Fig. 4.16 Radiotoxicity flux from different compartments for all radionuclides

The small spikes at the beginning of the curve (on the top of the peak around 100 years) representing the flux from the waste compartment SF1 are caused by the fact that this compartment is the sum of several boreholes, which are not reached by the inflowing fluid at the same time. Therefore some boreholes have a positive flux, whereas others are still in the inflow period. If the intruding brine is already contaminated by radionuclides released from other boreholes, there is a negative radiotoxicity flux. The summation of the positive fluxes and some small negative fluxes is responsible for the small spikes. This effect can be seen in several figures that will follow.

The total flux decreases from one compartment to the next. The compartment repository galleries is, even with its failed geotechnical barriers, the most effective compartment regarding the reduction of the radiotoxicity. The reduction of the maximum peak of the radiotoxicity flux from the waste package to the flux from the central field and the

transfer and access drifts is six orders of magnitude, whereas the overlying rock only contributes about one order of magnitude to the reduction. However, this reduction can be better illustrated by integrated radiotoxicity fluxes (see chapter 4.4.3).

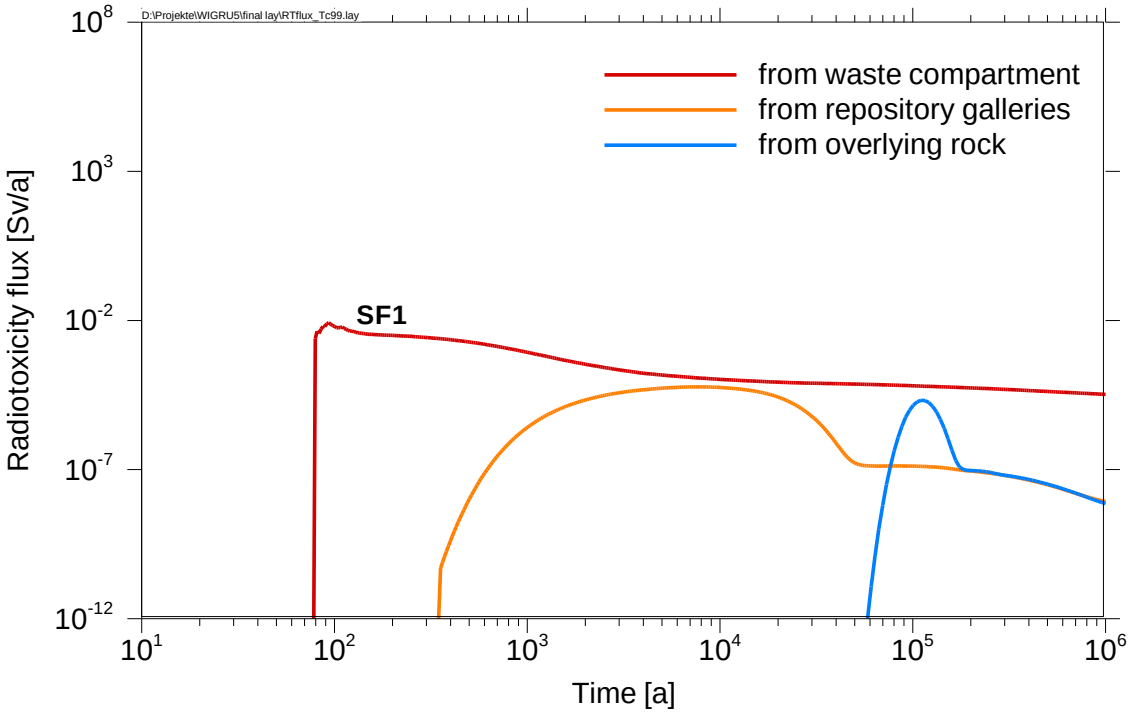

Fig. 4.17 Radiotoxicity flux from different compartments for Tc-99

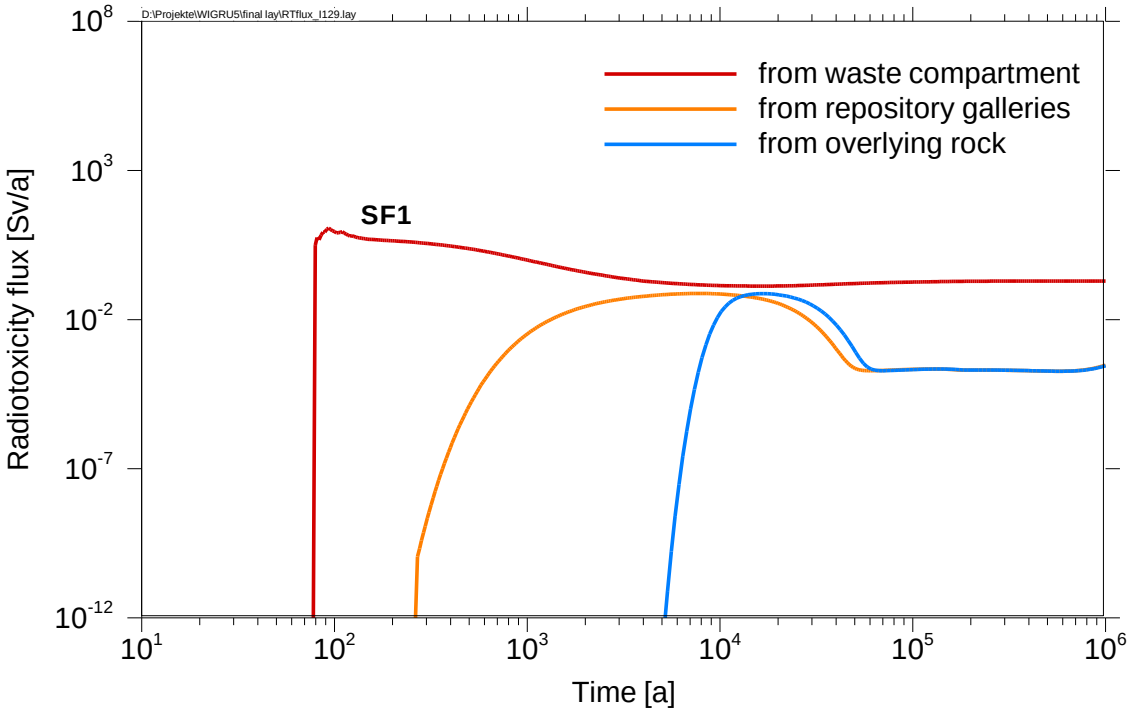

Fig. 4.18 Radiotoxicity flux from different compartments for I-129

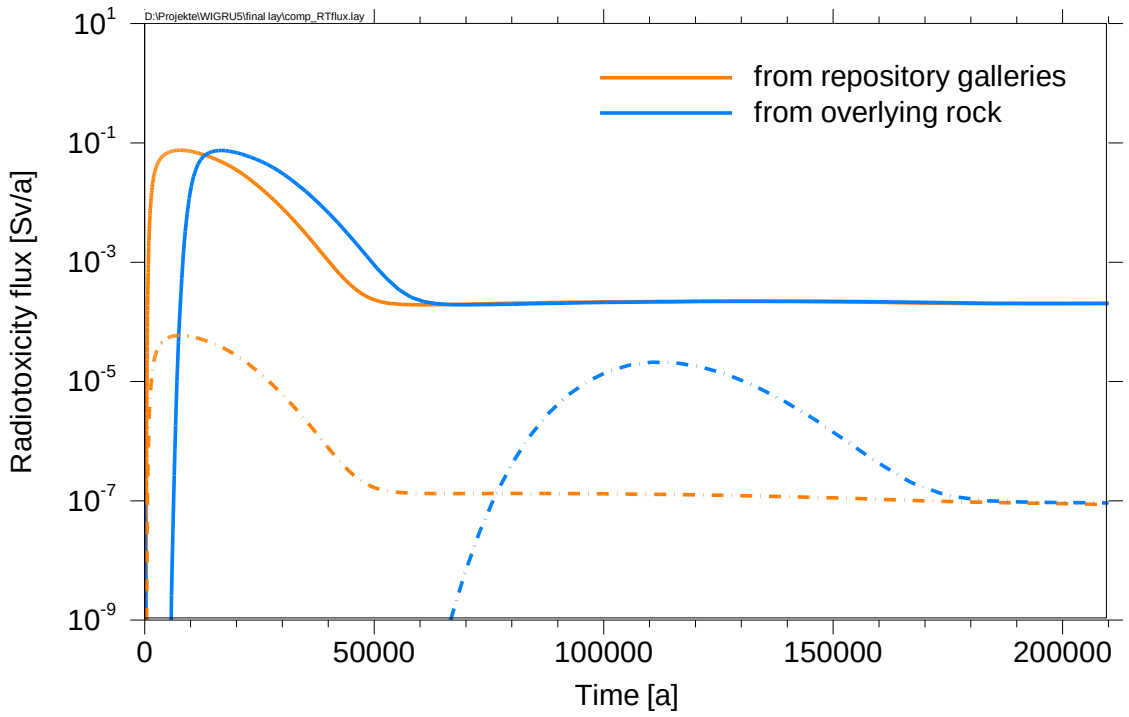

Fig. 4.19 Comparison of the radiotoxicity fluxes from the repository galleries and from the overlying rock for I-129 (solid line) and Tc-99 (dash and dot line)

The radiotoxicity fluxes of Tc-99 and I-129 are shown in Figure 4.17 and Figure 4.18, respectively. For the fluxes from the waste compartment SF1 the shapes of the curves are quite similar for both radionuclides. An important difference is the time-development of the fluxes from the repository galleries and from the overlying rock.

Figure 4.19 compares both fluxes for Tc-99 and I-129 on a linear x-axis. On a linear x-axis differences can be more easily identified. Due to its low sorption coefficient and its long half live I-129 passes the overlying rock without any considerable reduction (solid lines). The retardation caused by the overlying rock is about 5 000 years. In contrast to I-129 the radiotoxicity flux of Tc-99 is retarded for more than 65 000 years.

4.4.2.2 Test case: Fluid reservoir

The main difference of the radionuclide fluxes in the second test case (Figures 4.20 to 4.22) compared to the first test case is the occurrence of a radiotoxicity flux from compartment SF2. In contrast to the first case the brine from the reservoirs is in contact with the waste canisters from the beginning of the calculations and accordingly the mobilisation processes start earlier. Moreover, the brine reservoirs are located in the

backmost SF compartment allowing the brine to interact with more canisters than in the first test case. Consequently, the radiotoxicity fluxes from the waste compartments are about two orders of magnitude higher in the second test case.

Due to the intact shaft and drift seals the brine inflow to and outflow from the repository in is only a small fraction of the ones in the first test case. Thus the fluxes from the repository and the overlying rock are significantly lower (about four orders of magnitude). A discussion on the performance of the different compartments for this test case and a comparison of both test cases is provided in more detail in chapter 4.4.3.

For the discussion on the radiotoxicity fluxes in the second test case the compartment SF2, where the fluid reservoirs are located, is of particular importance.

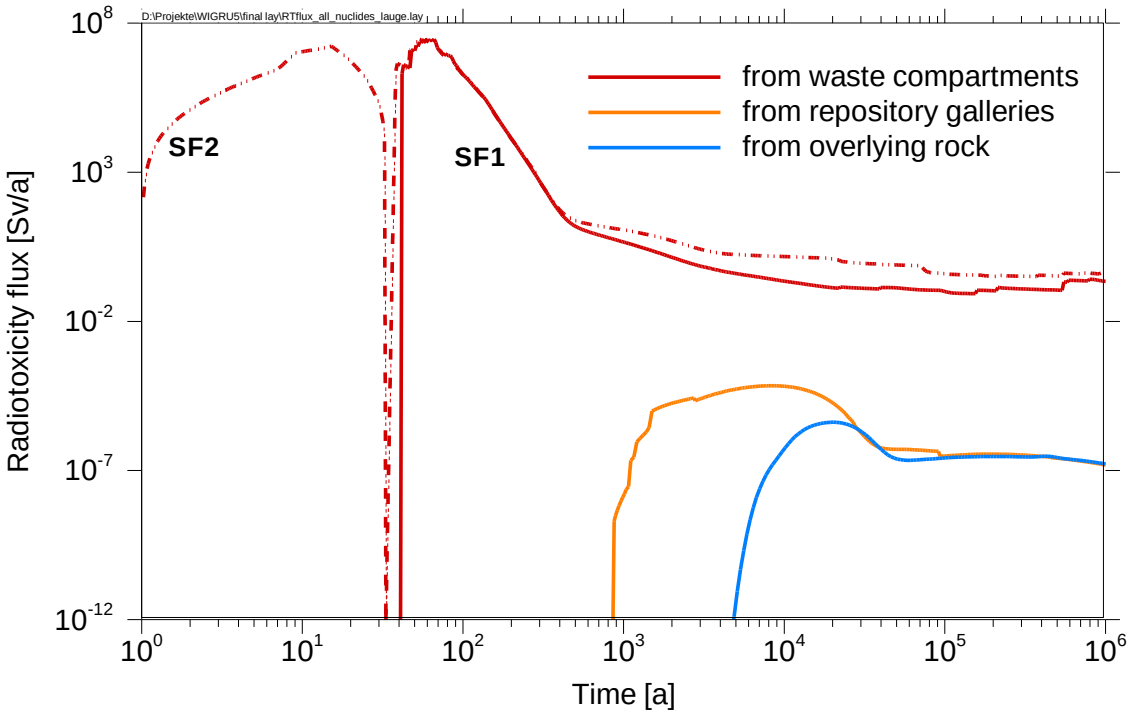

Fig. 4.20 Radiotoxicity flux from different compartments for all radionuclides

Figures 4.20 to 4.22 indicate that a radiotoxicity flux from the compartment SF2 starts shortly after repository closure. After about 20 to 30 years this flux decreases. For the sum of all nuclides and for I-129 this flux actually becomes negative, i.e. the flow into the boreholes is higher than the flow from the boreholes into the drifts (see introductory part of chapter 4.4.2). However, for Tc-99 only a small decrease can be seen in Figure 4.21.

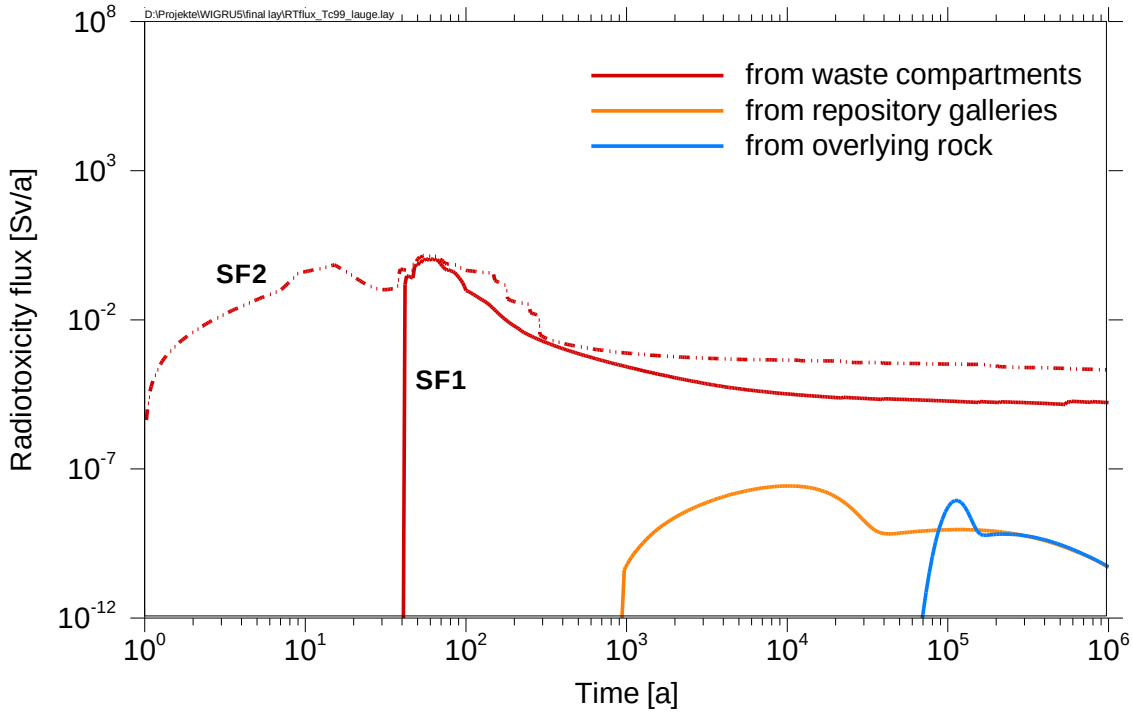

Fig. 4.21 Radiotoxicity flux from different compartments for Tc-99

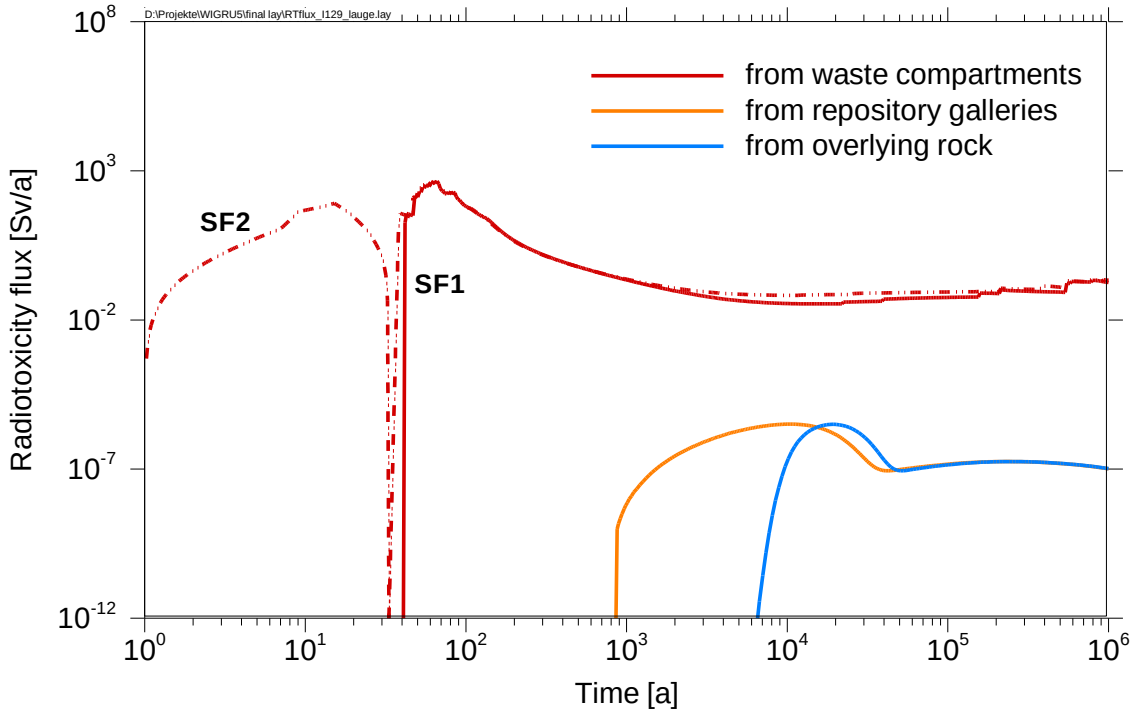

Fig. 4.22 Radiotoxicity flux from different compartments for I-129

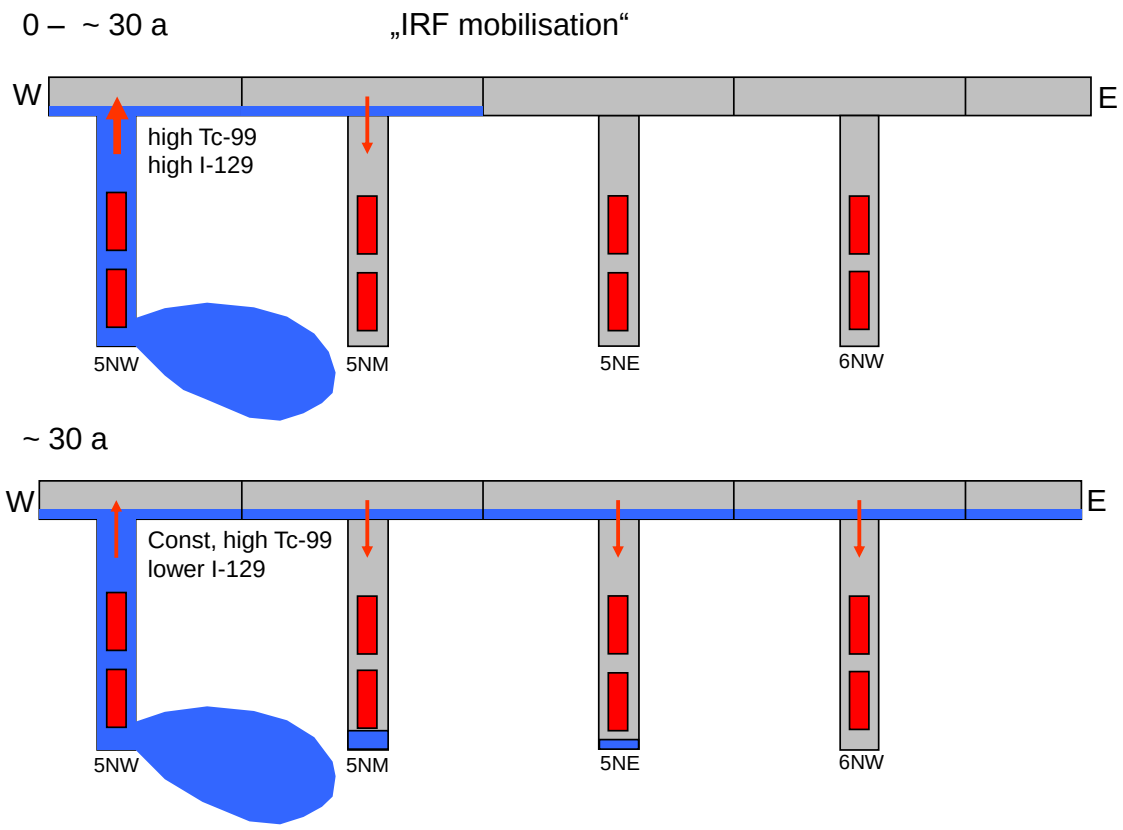

Fig. 4.23 The behaviour of the radiotoxicity fluxes of Tc-99 and I-129 during different stages of the second test case. Red arrows represent radiotoxicity fluxes.

This decrease and the different behaviour of Tc-99 and I-129 can be explained with Figure 4.23. There are two types of waste segments in compartment SF2: two segments with a connected fluid reservoir (e. g. 5NW) and 34 segments without a connected fluid reservoir (e. g. 5NM, 5NE, 6NW). The processes for the starting period of up to about 30 years are schematically shown in Figure 4.23: In boreholes with a connected fluid reservoir the mobilisation process starts immediately after the inflow of brine from the fluid reservoir. The decrease of the volume of cavities and void spaces due to convergence yields a flow of contaminated brine out of the boreholes and a transport of the mobilised radionuclides to the surrounding drifts. In the first stage of mobilisation all radionuclides with a high IRF such as Tc-99 and I-129 contribute to this radiotoxicity flux (upper Figure 4.23). The red arrows represent the radiotoxicity fluxes. The sum of these fluxes is illustrated by the curves for SF2 in Figures 4.20 to 4.22.

After about 30 years the situation is different (lower Figure 4.23). The flux from both filled boreholes is distributed to the surrounding drift segments and more and more boreholes become filled with brine. As long as the (positively counted) radiotoxicity flux

from the boreholes with a connected fluid reservoir is larger than the (negatively counted) radiotoxicity fluxes into the other boreholes the flux remains positive.

But as soon as the concentration of radionuclides mobilised due to the IRF decreases and the lower mobilisation rates from the metal parts and fuel matrix start to dominate the mobilisation process, the radiotoxicity flux from the boreholes mixed with uncontaminated brine from the fluid reservoirs decreases as well. Consequently the overall radiotoxicity flux from compartment SF2 decreases.

Radionuclides, such as I-129, that are not contained in the metal parts of a spent fuel element are mobilised with a very low mobilisation rate. The radiotoxicity flux of these radionuclides can become negative (Figure 4.22).

In contrast to these radionuclides the radiotoxicity flux of Tc-99 decreases only slightly. This effect can be explained by the fact that Tc-99 (and e. g. also C-14, Ni-59, Mo-63) is contained to some extent in the metal parts of spent fuel elements (Table 4.5). For the metal parts a higher mobilisation rate is assumed than for the fuel matrix. This faster mobilisation rate yields a higher concentration of Tc-99 in the borehole and thus a higher radiotoxicity flux of Tc-99 out of the borehole at early times. This effect almost compensates the negative fluxes of Tc-99 due to fluxes to other boreholes in the compartment.

Since the radionuclides contained in the metal parts contribute only a small portion to the overall radiotoxicity flux, the radiotoxicity flux of the sum of all radionuclides, which is dominated by Se-79, Cs-135 and I-129 (Table 4.13), becomes negative between 30 to 40 years (Figure 4.20).

This example shows that the use of a complex repository model with a detailed segment structure and an appropriate performance indicator allows, on the one hand, a detailed description of transport processes inside the repository. This is very useful for the modeller to confirm his understanding of the modelled processes. On the other hand, this complexity makes the illustration of the results for non-experts more difficult. Especially in a repository with a looped structure, the interpretation of the results can become quite awkward. It is very important to chose a well-adapted compartment structure for a given repository concept.

4.4.3 Integrated radiotoxicity fluxes from compartments

In the following two sections first the results of the integrated radiotoxicity fluxes for both test cases are presented (Figures 4.24 to 4.29). The discussion of the results follows by comparing both test cases at the end of chapter 4.4.3.3.

One important advantage of this indicator is the possibility to compare the integrated fluxes of the radiotoxicity with the initially emplaced radiotoxicity in the waste compartments in a comprehensive way. Therefore the initially emplaced inventory is added to Figures 4.24 to 4.29 as a dashed horizontal line.

4.4.3.1 Test case: Failure of shaft and drift seals

The overall radiotoxicity inventory initially emplaced is $2.25 \cdot 10^{12}$ Sv (Figure 4.10).

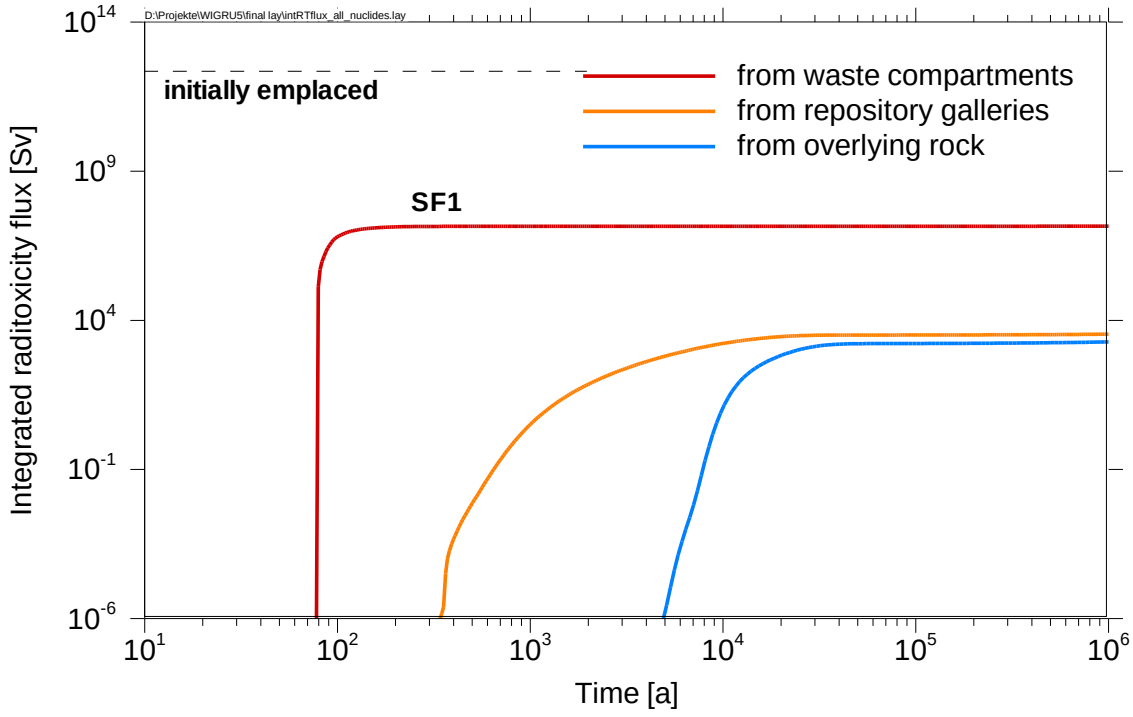

Fig. 4.24 Integrated radiotoxicity flux from different compartments for all radionuclides. The initially emplaced radiotoxicity inventory is shown for comparison

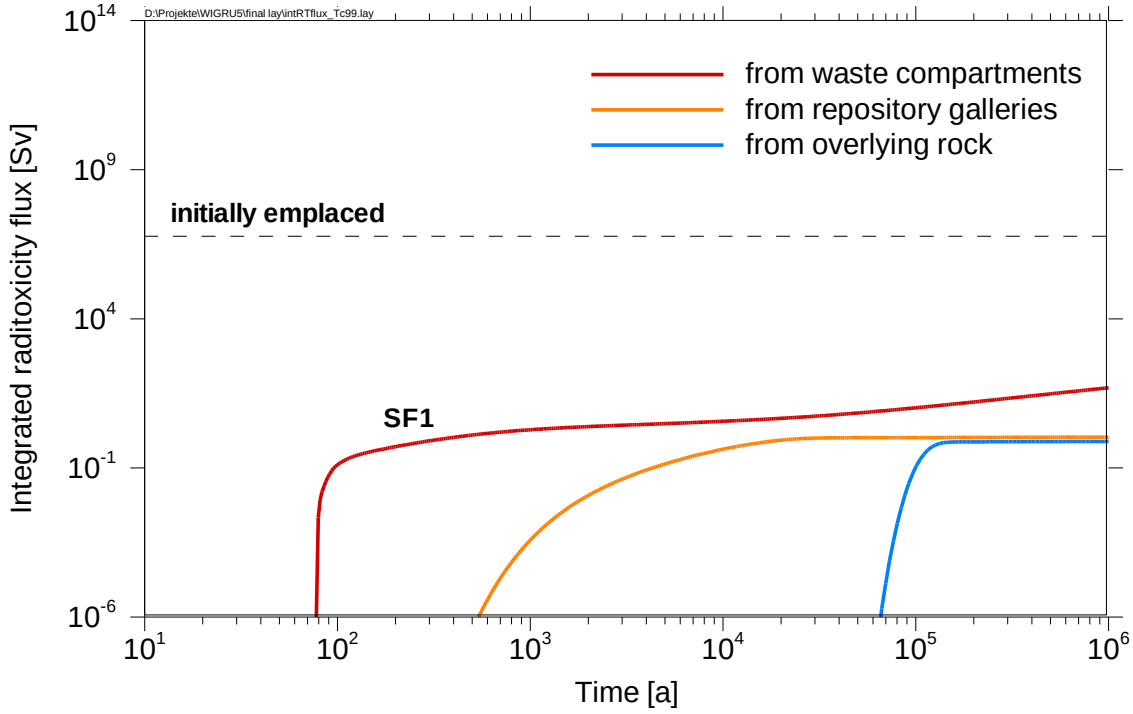

Fig. 4.25 Integrated radiotoxicity flux from different compartments for Tc-99. The initially emplaced radiotoxicity inventory is shown for comparison

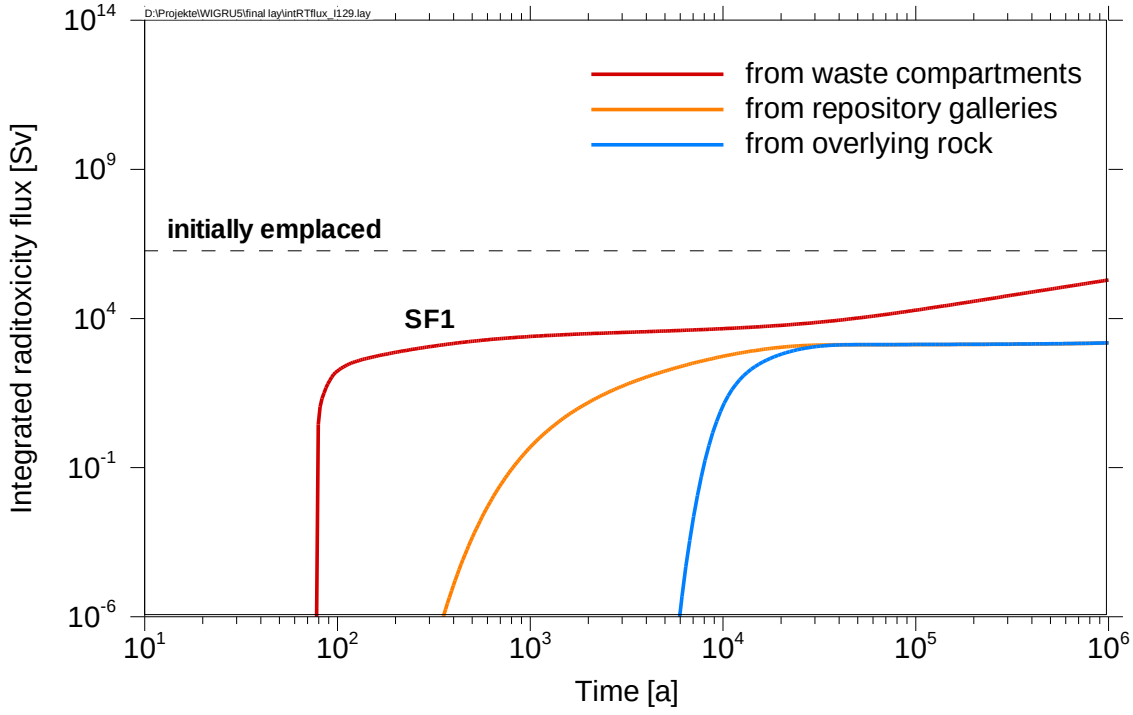

Fig. 4.26 Integrated radiotoxicity flux from different compartments for I-129. The initially emplaced radiotoxicity inventory is shown for comparison

The total release of all radionuclides within one million years is $1.45 \cdot 10^{7}$ Sv from the waste compartments (only from compartment SF1, there is no mobilisation in the other waste compartments), $3.46 \cdot 10^{3}$ Sv from the repository galleries and $1.91 \cdot 10^{3}$ Sv from the overlying rock (Figure 4.24). The release from the waste compartment starts after 80 years, after 270 years from the repository galleries and after 2 680 years from the overlying rock.

For Tc-99 the initially emplaced radiotoxicity inventory is $5.90 \cdot 10^{6}$ Sv (Figure 4.25). The total release of Tc-99 within one million years is $4.89 \cdot 10^{1}$ Sv from the waste compartments (only SF1), 1.08 Sv from the repository galleries and $7.76 \cdot 10^{-1}$ Sv from the overlying rock. The release from the waste compartment starts after 80 years, after 355 years from the repository galleries and after 40 240 years from the overlying rock.

For I-129 the initially emplaced radiotoxicity inventory is $1.87 \cdot 10^{6}$ Sv (Figure 4.26). The total release of I-129 within one million years is $1.95 \cdot 10^{5}$ Sv from the waste compartments (only SF1), $1.53 \cdot 10^{3}$ Sv from the repository galleries and from the overlying rock. The release from the waste compartment starts after 80 years, after 269 years from the repository galleries and after 3 700 years from the overlying rock.

4.4.3.2 Test case: Fluid reservoir

The initially emplaced inventory is $2.25 \cdot 10^{12}$ Sv (Figure 4.10). The total release within one million years is $1.71 \cdot 10^{9}$ Sv from the waste compartments ($7.17 \cdot 10^{8}$ Sv from SF1 and $9.90 \cdot 10^{8}$ Sv from SF2), 1.21 Sv from the repository galleries and $3.11 \cdot 10^{-1}$ Sv from the overlying rock (Figure 4.27). The release from the waste compartments starts shortly after repository closure in SF2 and after 48 years in SF1, after 873 years from the repository galleries and after 3 223 years from the overlying rock.

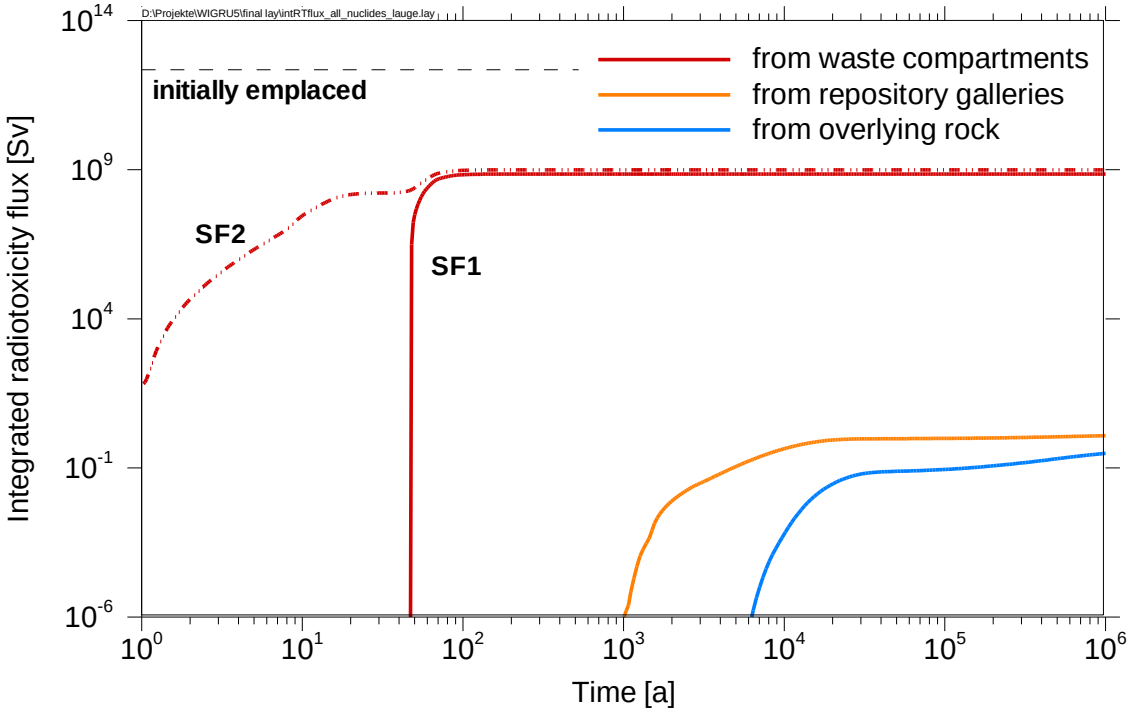

Fig. 4.27 Integrated radiotoxicity flux from different compartments for all radionuclides. The initially emplaced radiotoxicity inventory is shown for comparison

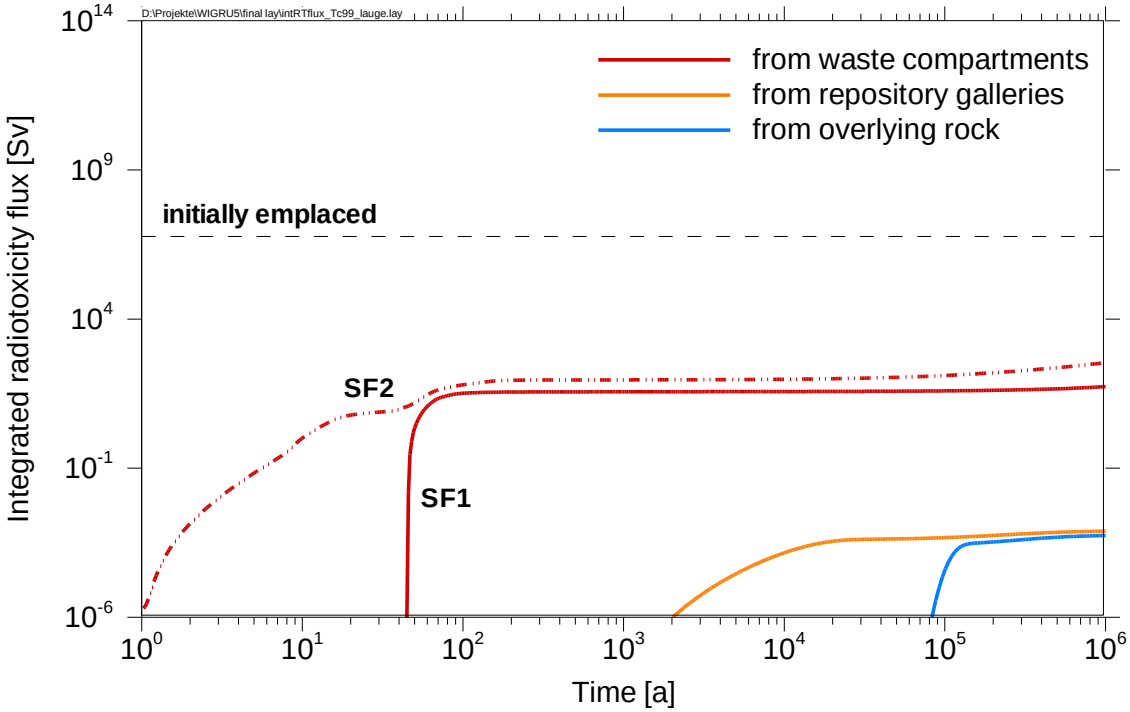

Fig. 4.28 Integrated radiotoxicity flux from different compartments for Tc-99. The initially emplaced radiotoxicity inventory is shown for comparison

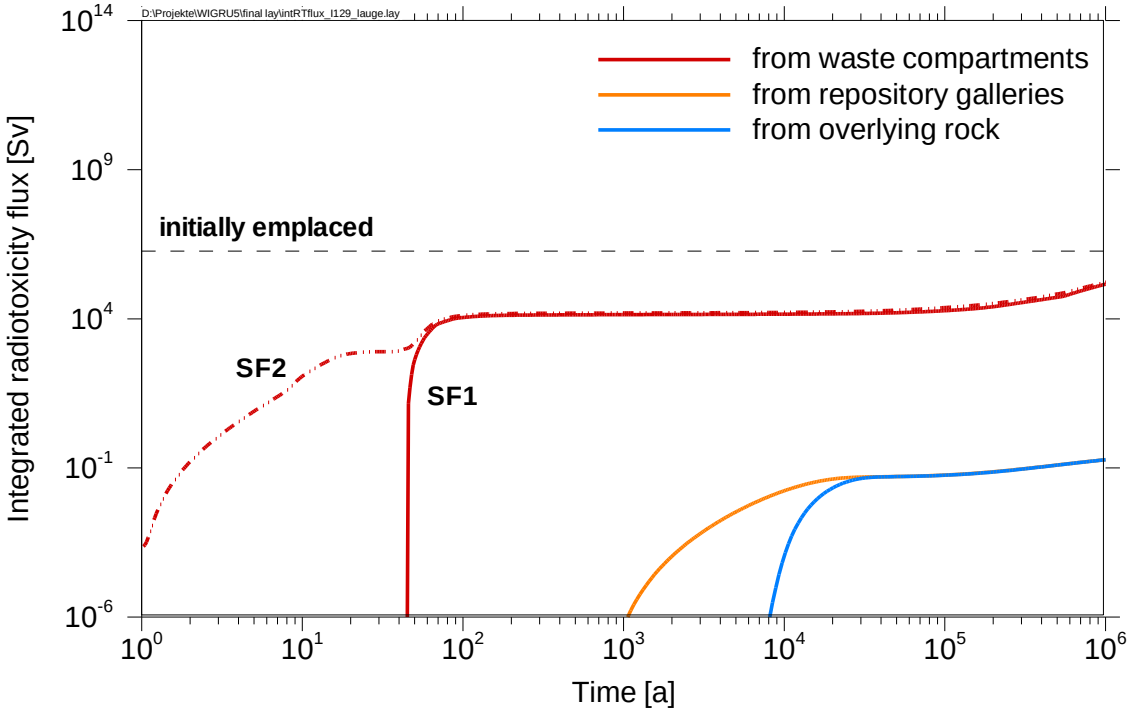

Fig. 4.29 Integrated radiotoxicity flux from different compartments for I-129. The initially emplaced radiotoxicity inventory is shown for comparison

For Tc-99 the initially emplaced radiotoxicity inventory is $5.90 \cdot 10^{6}$ Sv (Figure 4.28). The total release of Tc-99 within one million years is $4.00 \cdot 10^{2}$ Sv from the waste compartments ($5.45 \cdot 10^{1}$ Sv from SF1 and $3.45 \cdot 10^{2}$ Sv from SF2), $7.71 \cdot 10^{-4}$ Sv from the repository galleries and $5.52 \cdot 10^{-4}$ Sv from the overlying rock. The release from the waste compartments starts shortly after repository closure in SF2 and after 48 years in SF1, after 968 years from the repository galleries and after 40 240 years from the overlying rock.

For I-129 the initially emplaced radiotoxicity inventory is $1.87 \cdot 10^{6}$ Sv (Figure 4.29). The total release of I-129 within one million years is $3.14 \cdot 10^{5}$ Sv from the waste compartments ($1.45 \cdot 10^{5}$ Sv from SF1 and $1.69 \cdot 10^{5}$ Sv from SF2), $1.89 \cdot 10^{-1}$ Sv from the repository galleries and from the overlying rock. The release from the waste compartments starts shortly after repository closure in SF2 and after 48 years in SF1, after 873 years from the repository galleries and after 4 450 years from the overlying rock.

4.4.3.3 Discussion of the results by comparing the test cases

Tables 4.14 to 4.16 sum up the relations of the integrated radiotoxicity flux from the different compartment to the total emplaced radiotoxicity inventory after one million years ($2.25 \cdot 10^{12}$ Sv). The total reduction of the radiotoxicity in the whole repository system is about nine orders of magnitude for the first test case and 13 orders of magnitude for the second test case. The corresponding different radiological consequences are already illustrated by the safety indicators for both test cases.

Tab. 4.14 Fraction of the integrated radiotoxicity flux from the different compartments to the total emplaced radiotoxicity ($2.25 \cdot 10^{12}$ Sv) after 10^6 years

Compartment	Test case 1	Test case 2
Waste compartments	$6.4 \cdot 10^{-6}$	$7.6 \cdot 10^{-4}$
Repository galleries	$1.5 \cdot 10^{-9}$	$5.4 \cdot 10^{-13}$
Overlying rock	$8.5 \cdot 10^{-10}$	$1.4 \cdot 10^{-13}$

In addition to these radiological consequences the application of performance indicators reveals the particular importance of the geotechnical barriers (drift and shaft seal) by comparing the reduction of the integrated radiotoxicity fluxes from the waste compartments and from the repository. The reduction is only about three orders of magnitude for the first test case but nine orders of magnitude in the second test case. The seals hinder the inflow of brine from outside the repository thus reducing advective flow through the repository.

In second test case the brine from the reservoirs is immediately in contact with the waste. The mobilisation of radionuclides is much higher and the radiotoxicity flux from the waste compartments is higher by two orders of magnitude Due to the intact geotechnical barriers the transport of radionuclides is retarded significantly, though, and the resulting flux from the repository galleries is small compared to the first test case.

The effect of the overlying rock is quite marginal, for the sum of all radionuclides the reduction factor is in both test cases smaller than 0.5. As already identified by the performance indicator “Radiotoxicity fluxes from compartments” the reduction effect for I-129 is zero, since it has a very low sorption coefficient.

The high mobility of I-129 is illustrated by comparing the results with Tc-99 (Tables 4.15 and 4.16). The emplaced radiotoxicity inventory is nearly the same, but for both test cases the total integrated radiotoxicity flux of I-129 from the repository and the overlying rock is nearly four orders of magnitude higher than the flux of Tc-99. Due to its lower solubility limit a considerable fraction of Tc-99 is immobilised by precipitation. In both test cases this process takes place in the waste compartments such that the radiotoxicity flux of Tc-99 is about five orders of magnitudes lower than for I-129.

Tab. 4.15 Fraction of the integrated radiotoxicity flux from the different compartments to the emplaced radiotoxicity of Tc-99 ($5.90 \cdot 10^{6}$ Sv) after 10^{6} years

Compartment	Test case 1	Test case 2
Waste compartments	$8.3 \cdot 10^{-6}$	$6.8 \cdot 10^{-5}$
Repository galleries	$1.8 \cdot 10^{-7}$	$1.3 \cdot 10^{-10}$
Overlying rock	$1.3 \cdot 10^{-7}$	$9.4 \cdot 10^{-11}$

Tab. 4.16 Fraction of the integrated radiotoxicity flux from the different compartments to the total emplaced radiotoxicity of I-129 ($1.87 \cdot 10^{6}$ Sv) after 10^{6} years

Compartment	Test case 1	Test case 2
Waste compartments	$1.0 \cdot 10^{-1}$	$1.7 \cdot 10^{-1}$
Repository galleries	$8.2 \cdot 10^{-4}$	$1.0 \cdot 10^{-7}$
Overlying rock	$8.2 \cdot 10^{-4}$	$1.0 \cdot 10^{-7}$

Finally one can conclude that for the integrated PA calculations performed in this study the proposed set of performance indicators are useful to improve understanding of the role played by different system components and to foster communication of these issues. The three indicators give useful information to carry out such an analysis of the repository system. All three indicators should be used conjointly since they reflect different aspects of the performance of the repository system. Deriving conclusions on the basis of one performance indicator may be misleading. A telling example is the performance indicator “Integrated radiotoxicity fluxes from compartments” discussed in this chapter. This performance indicator may cover some details that are better illustrated by the two other indicators. For example the complex processes in the repository at the beginning of the second test case (Figure 4.23) could be overlooked by just using the integrated fluxes (Figure 4.27). Figure 4.20 shows a lot more details of these processes.

5 Clay formations

In this chapter the use of safety and performance indicators for nuclear waste repositories in clay formations is examined. For the calculation of the different safety and performance indicators, the results from a recent generic study for a repository in a clay formation /RUE 07/ are used and newly evaluated. In contrast to the simulations for the salt host rock presented before, only spent fuel was taken into account. The aim of the work presented here is neither to develop new calculation tools nor to perform extensive performance assessment calculations, but to perform a first test of the indicators on existing data to identify their suitability and to find out potential needs for future developments. Most of the curves for the indicators for the repository in clay are plotted for a period of time up to 10^8 million years, which is longer as the normal observation period in long-term safety analyses. This was done since the curves show interesting aspects even beyond one million years. The time span later than one million years is indicated by a grey shaded area.

5.1 Concept, model and data

This section summarises the concept of the repository in clay and the input data used for the integrated performance assessment calculations. The description of the latter is summarised from /RUE 07/.

5.1.1 Repository concept

The repository concept considered here was developed by DBE Technology /JOB 07/. In the following, the data of the geometric layout needed as input for integrated performance assessment calculation is described.

The repository layout is shown in Figure 5.1. The concept is based on the disposal of spent fuel canisters (BSK-3) in vertical boreholes of 50 m in length including the borehole seal. Three canisters are disposed of in each of the boreholes. The BSK-3 canisters are steel canisters designed to hold the rods of three spent fuel elements with about 1 600 kg heavy metal in total and have a diameter of 0.43 m and a length of 4.98 m. The boreholes are arranged in a hexagonal layout. This arrangement was cho-

sen since it is the most favourable with regard to the temperature evolution and required space. The drift distance is therefore √3/2 times the borehole distance. The actual value for the borehole distance was calculated by the DBE to be 50 m to fulfil the thermal constraint that the maximum temperature in the bentonite should not exceed 100°C.

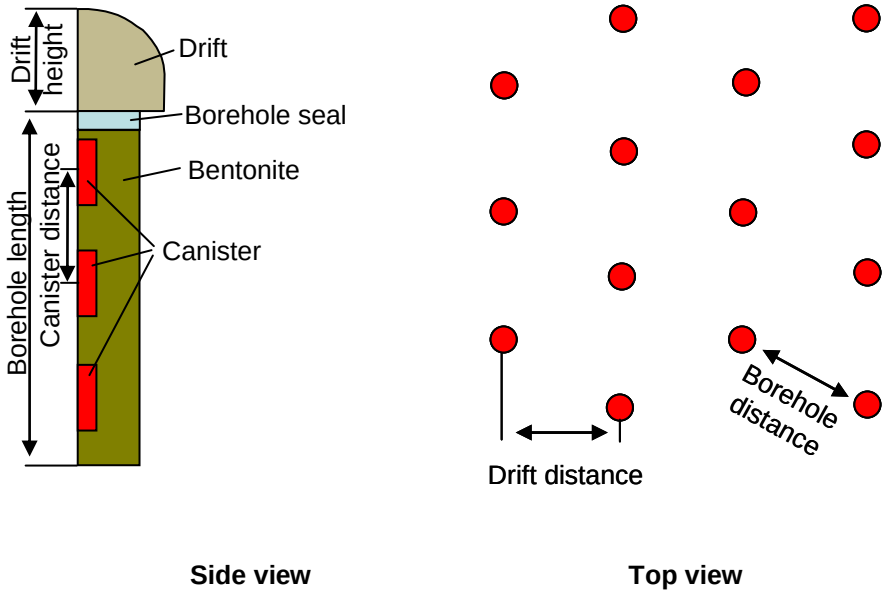

Fig. 5.1 Repository layout

5.1.2 Model and compartments

Figure 5.2 shows a simplified sketch of the repository system. The repository system and the reference scenario for the repository can be described as follows: the containers are stored in vertical boreholes holding five containers each. The cavity around the containers is backfilled with bentonite. It is assumed that before any containers corrode, the bentonite and those parts of the host rock formation that were desaturated during the construction of the repository are re-saturated and all pathways in the bentonite and the excavation-disturbed zone (EDZ) are closed by the swelling process. As soon as the first containers fail, the radionuclides are mobilized and transported. Part of the radionuclides precipitate again in the near-field due to solubility limits. For the reference scenario it is assumed that the mobilized radionuclides are exclusively transported by diffusion through the technical barriers, the host rock itself, and any overlying, similarly impermeable rock strata up to the water-bearing overburden. In all these

areas, the radionuclides are retained by sorption. If a contamination of groundwater occurs, the population is exposed to radiation if it uses the groundwater as drinking water or for foodstuff production.

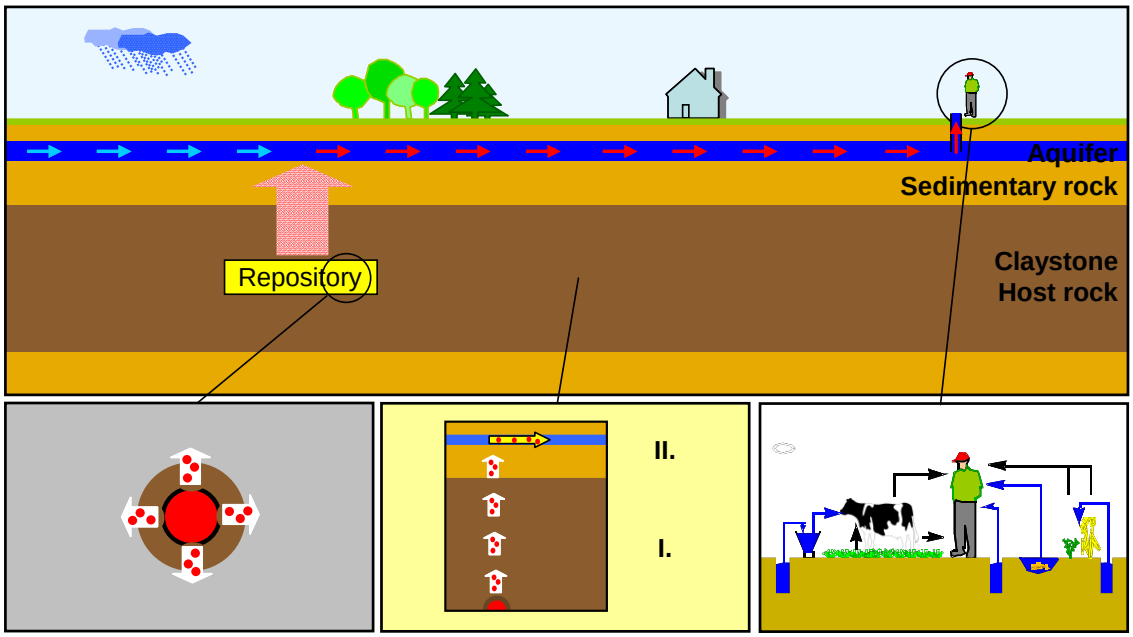

Fig. 5.2 Schematic representation of the reference case

For the modelling of the radionuclide transport the EMOS module CLAYPOS was used. CLAYPOS simulates a single waste canister for high level waste in low-permeable media. It is based on a one-dimensional geometry. For the waste canister two processes are modelled. After the failure of the waste canister, the mobilisation from the waste is modelled for three different fractions; instant release fraction (IRF), claddings (metal parts) and waste matrix. For each fraction a different mobilisation rate is used.

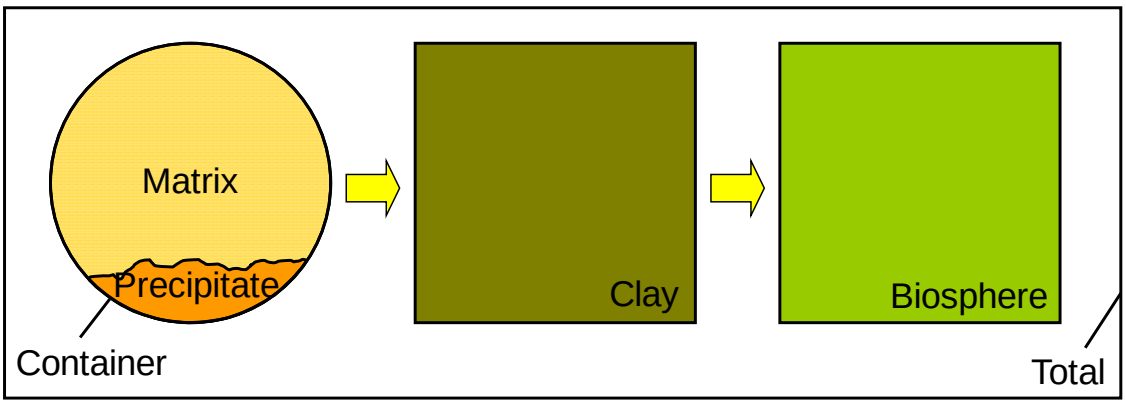

Fig. 5.3 Compartments distinguished for the repository in a clay formation

For the domain of the bentonite and the clay barrier, the diffusive transport and the retention by linear sorption according to the Henry isotherm are modelled. The radioactive decay is taken into account in the whole domain. The outer boundary condition is defined by the water flow in the aquifer.

Figure 5.3 shows the different compartments that are distinguished for the calculation of the performance indicators for the repository in a clay formation. Different colours represent the different compartments that are used for the calculation of the inventories. The yellow arrows represent those compartment boundaries where radionuclide fluxes are calculated. The different compartments are:

- **Matrix:** This compartment represents the non-mobilised radionuclides in the spent fuel matrix
- **Precipitate:** This compartment represents those nuclides that were mobilised from the matrix, but are precipitated since solubility limits are reached.
- **Container[5]:** This compartment is only used for the calculation of the radionuclide flux from both of the preceding compartments (matrix and precipitate) to the clay formation.
- **Clay:** This compartment represents both, the geotechnical (bentonite) and the geological barrier (clay rock). In the current implementation of CLAYPOS it is not possible to distinguish between those two parts of the compartment with respect to the calculation of the performance indicators.
- **Biosphere:** This compartment includes all radionuclides which left the host rock formation. This includes not only the biosphere, but also the aquifer.
- **Total:** This compartment includes all compartments given above. It therefore represents the decay-corrected initial inventory.

[5] The term container is used in the following to denote the compartment while the term canister is used for the physical containment of the waste package.

5.1.3 Input data

This section describes the input data used in /RUE 07/ for the integrated performance assessment calculation for the clay formation. The input data are arranged in five different categories:

- geometry,
- source-term,
- near-field,
- host-rock and
- biosphere.

The far-field transport in the aquifer is not considered here; therefore no data are given for this compartment.

5.1.3.1 Geometry

The geometry input data are given in Table 5.1. A borehole distance of 50 m with three canisters in each borehole was used. This borehole distance results in an area of the hexagonal reference cell of 2 165.1 m^2.

Tab. 5.1 Geometry input data for the Opalinus Clay

Parameter		Value
Borehole length	[m]	50
Numbers of canisters per borehole	[-]	3
Area of the hexagonal reference cell	[m^2]	2 165.06
Width of the CLAYPOS model	[m]	46.53
Transport length in the bentonite	[m]	10
Transport length in the host rock	[m]	30

The transport distances in the bentonite are calculated from the drift height and the one in the host rock from the thickness of the host rock and the repository layout under the assumption that the repository is located exactly in the middle of the clay layer.

5.1.3.2 Source term

The radionuclide inventory is given in Table 5.3 for an interim storage time of 10 years. An additional interim storage time of 63 years was taken into account in the model calculations to fulfil the temperature requirements calculated by DBE. The data for the whole inventory are based on the assumption that 8 550 tonnes heavy metal (t_{HM}) are expected in Germany. Each canister holds 1.6 t_{HM} resulting in a total number of 5 350 canisters.

Tab. 5.2 BSK-3 canister data

Parameter		Value
Length	[m]	4.98
Diameter	[m]	0.43
Wall thickness	[m]	0.05
Void volume	[m^3]	0.30
Inventory	[t_{HM}]	1.6
Life-time	[a]	2 500

In the program CLAYPOS, the three canisters of each borehole are modelled as one. Therefore, the hypothetical canister in the CLAYPOS simulation has three times the inventory of a canister as given in Table 5.3.

Tab. 5.3 Radionuclide inventory

Nuclide	Half-life [a]	Canister [Bq]	Total [Bq]	Total [Sv]
C-14	$5.730 \cdot 10^{3}$	$3.020 \cdot 10^{10}$	$1.616 \cdot 10^{14}$	$9.371 \cdot 10^{04}$
Cl-36	$3.000 \cdot 10^{5}$	$5.493 \cdot 10^{08}$	$2.939 \cdot 10^{12}$	$2.733 \cdot 10^{03}$
Co-60	$5.272 \cdot 10^{0}$	$1.634 \cdot 10^{14}$	$8.743 \cdot 10^{17}$	$2.972 \cdot 10^{09}$
Ni-59	$7.500 \cdot 10^{4}$	$9.626 \cdot 10^{10}$	$5.150 \cdot 10^{14}$	$3.244 \cdot 10^{04}$
Ni-63	$1.000 \cdot 10^{2}$	$1.371 \cdot 10^{13}$	$7.333 \cdot 10^{16}$	$1.100 \cdot 10^{07}$
Se-79	$1.100 \cdot 10^{6}$	$2.796 \cdot 10^{10}$	$1.496 \cdot 10^{14}$	$4.348 \cdot 10^{05}$
Sr-90	$2.864 \cdot 10^{3}$	$3.756 \cdot 10^{15}$	$2.009 \cdot 10^{19}$	$6.179 \cdot 10^{11}$
Zr-93	$1.500 \cdot 10^{6}$	$1.341 \cdot 10^{11}$	$7.172 \cdot 10^{14}$	$8.753 \cdot 10^{05}$
Nb-94	$2.000 \cdot 10^{4}$	$1.013 \cdot 10^{05}$	$5.421 \cdot 10^{08}$	$9.213 \cdot 10^{-01}$
Mo-93	$3.500 \cdot 10^{3}$	$7.148 \cdot 10^{07}$	$3.824 \cdot 10^{11}$	$1.231 \cdot 10^{03}$

Nuclide	Half-life [a]	Canister [Bq]	Total [Bq]	Total [Sv]
Tc-99	$2.100 \cdot 10^{5}$	$4.066 \cdot 10^{11}$	$2.175 \cdot 10^{15}$	$1.392 \cdot 10^{06}$
Sn-126	$2.345 \cdot 10^{5}$	$4.964 \cdot 10^{10}$	$2.656 \cdot 10^{14}$	$1.356 \cdot 10^{06}$
I-129	$1.570 \cdot 10^{7}$	$3.222 \cdot 10^{09}$	$1.724 \cdot 10^{13}$	$1.906 \cdot 10^{06}$
Cs-135	$2.000 \cdot 10^{6}$	$3.481 \cdot 10^{10}$	$1.863 \cdot 10^{14}$	$3.725 \cdot 10^{05}$
Cs-137	$3.017 \cdot 10^{1}$	$6.324 \cdot 10^{15}$	$3.383 \cdot 10^{19}$	$4.408 \cdot 10^{11}$
Sm-151	$9.300 \cdot 10^{1}$	$1.092 \cdot 10^{14}$	$5.844 \cdot 10^{17}$	$5.735 \cdot 10^{07}$
Ra-226	$1.600 \cdot 10^{3}$	$1.691 \cdot 10^{04}$	$9.048 \cdot 10^{07}$	$2.548 \cdot 10^{01}$
Th-229	$7.880 \cdot 10^{3}$	$1.032 \cdot 10^{04}$	$5.519 \cdot 10^{07}$	$3.396 \cdot 10^{01}$
Th-230	$7.540 \cdot 10^{4}$	$6.280 \cdot 10^{06}$	$3.360 \cdot 10^{10}$	$7.066 \cdot 10^{03}$
Th-232	$1.405 \cdot 10^{10}$	$8.118 \cdot 10^{00}$	$4.343 \cdot 10^{04}$	$9.999 \cdot 10^{-03}$
Pa-231	$3.276 \cdot 10^{4}$	$2.029 \cdot 10^{06}$	$1.085 \cdot 10^{10}$	$7.717 \cdot 10^{03}$
U-233	$1.592 \cdot 10^{5}$	$5.795 \cdot 10^{06}$	$3.100 \cdot 10^{10}$	$1.581 \cdot 10^{03}$
U-234	$2.455 \cdot 10^{5}$	$6.609 \cdot 10^{10}$	$3.536 \cdot 10^{14}$	$1.733 \cdot 10^{07}$
U-235	$7.038 \cdot 10^{8}$	$7.969 \cdot 10^{08}$	$4.263 \cdot 10^{12}$	$2.028 \cdot 10^{05}$
U-236	$2.342 \cdot 10^{7}$	$1.348 \cdot 10^{10}$	$7.210 \cdot 10^{13}$	$2.729 \cdot 10^{07}$
U-238	$4.468 \cdot 10^{9}$	$1.953 \cdot 10^{10}$	$1.045 \cdot 10^{14}$	$5.110 \cdot 10^{06}$
Np-237	$2.144 \cdot 10^{6}$	$2.153 \cdot 10^{10}$	$1.152 \cdot 10^{14}$	$1.287 \cdot 10^{07}$
Pu-238	$8.774 \cdot 10^{1}$	$4.747 \cdot 10^{14}$	$2.540 \cdot 10^{18}$	$5.841 \cdot 10^{11}$
Pu-239	$2.411 \cdot 10^{4}$	$3.465 \cdot 10^{13}$	$1.854 \cdot 10^{17}$	$4.634 \cdot 10^{10}$
Pu-240	$6.563 \cdot 10^{3}$	$8.160 \cdot 10^{13}$	$4.366 \cdot 10^{17}$	$1.091 \cdot 10^{11}$
Pu-241	$1.435 \cdot 10^{1}$	$1.387 \cdot 10^{16}$	$7.419 \cdot 10^{19}$	$3.562 \cdot 10^{11}$
Pu-242	$3.750 \cdot 10^{5}$	$6.035 \cdot 10^{11}$	$3.229 \cdot 10^{15}$	$1.398 \cdot 10^{09}$
Am-241	$4.322 \cdot 10^{2}$	$3.277 \cdot 10^{14}$	$1.753 \cdot 10^{18}$	$3.516 \cdot 10^{11}$
Am-242m	$1.410 \cdot 10^{3}$	$3.228 \cdot 10^{12}$	$1.727 \cdot 10^{16}$	$3.281 \cdot 10^{09}$
Am-243	$7.37 \cdot 10^{3}$	$5.740 \cdot 10^{12}$	$3.071 \cdot 10^{16}$	$6.176 \cdot 10^{09}$
Cm-244	$1.810 \cdot 10^{1}$	$8.996 \cdot 10^{14}$	$4.813 \cdot 10^{18}$	$5.785 \cdot 10^{11}$
Cm-245	$8.500 \cdot 10^{3}$	$3.484 \cdot 10^{11}$	$1.864 \cdot 10^{15}$	$3.914 \cdot 10^{08}$

A canister life-time of 2 500 years was assumed and further on it was conservatively assumed that all canisters in the repository fail at the same time. After the canister has failed, the radionuclides are released from the three different fractions of the spent fuel elements with the release rates given in Table 5.4. The distribution of the elements on

the three fractions in the fuel elements is given in Table 5.5 in per cent of the total inventory.

Tab. 5.4 Mobilisation rates for different fuel fractions

	Metal parts	Fuel Matrix	IRF
Mobilisation rate [a^{-1}]	$3.6 \cdot 10^{-3}$	$1.0 \cdot 10^{-6}$	instantaneous

Tab. 5.5 Relative inventory in the different fuel fractions in per cent

Element	Metal parts	Fuel Matrix	IRF
C	72.20	26.41	1.39
Cl	0.00	94.00	6.00
Ni, Mo, Nb	99.50	0.47	0.03
Sn	0.00	98.00	2.00
I, Se	0.00	97.00	3.00
Cs	0.00	96.00	4.00
Rb, H	0.00	95.00	5.00
Sr, Sm, Pb	0.00	99.90	0.10
Zr	9.40	86.07	4.53
Tc	0.10	99.89	0.01
Pd, Cm, Am, Pu, Pa, U, Th, Ac, Np, Ra	0.00	99.99	0.01

After the radionuclides are mobilised from the waste into the water filled void volume inside the canister, some radionuclides may be precipitated if they reach their solubility limits within this volume. The data for the solubility limit for each element are given in Table 5.6 according to data from /NAG 02/.

Tab. 5.6 Solubility limits in [$mol \cdot l^{-1}$], “high” denotes no solubility limit

Element	Value	Element	Value	Element	Value
C	high	Tc	$4 \cdot 10^{-9}$	Ra	$2 \cdot 10^{-11}$
Cl	high	Pd	$5 \cdot 10^{-8}$	Ac	$1 \cdot 10^{-6}$
Ca	$1 \cdot 10^{-2}$	Ag	$3 \cdot 10^{-6}$	Th	$7 \cdot 10^{-7}$
Ni	$3 \cdot 10^{-5}$	Sn	$1 \cdot 10^{-8}$	Pa	$1 \cdot 10^{-8}$
Se	$5 \cdot 10^{-9}$	I	high	U	$3 \cdot 10^{-9}$

Element	Value	Element	Value	Element	Value
Sr	$2 \cdot 10^{-5}$	Cs	high	Np	$5 \cdot 10^{-9}$
Zr	$2 \cdot 10^{-9}$	Sm	$5 \cdot 10^{-7}$	Pu	$5 \cdot 10^{-8}$
Nb	$3 \cdot 10^{-5}$	Pb	$2 \cdot 10^{-6}$	Am	$1 \cdot 10^{-6}$
Mo	$1 \cdot 10^{-6}$	Po	high	Cm	$1 \cdot 10^{-6}$

5.1.3.3 Near field

The transport length in the bentonite is 10 m. It is assumed that the drifts are filled with bentonite with a dry density of $\rho = 2\,760$ kg·m^{-3}. This value is also assumed for the borehole seals. The data for the element-specific transport parameter values such as the distribution coefficients K_d, the diffusion accessible porosity n and the diffusion coefficient D_p are listed in Table 5.7 according to data from /NAG 02/.

5.1.3.4 Host rock

The transport length in the host rock is 30 m. The density of the Opalinus Clay is 2 400 kg·m^{-3}. All other values for the element-specific transport parameters for the host rock are listed in Table 5.7 according to data from /NAG 02/.

Tab. 5.7 Near-field and host rock transport parameter values

Element	Bentonite			Host rock		
	K_d [m^3·kg^{-1}]	n [-]	D_p [m^2·s^{-1}]	K_d [m^3·kg^{-1}]	n [-]	D_p [m^2·s^{-1}]
C	0	0.36	$5.55 \cdot 10^{-10}$	0	0.12	$8.33 \cdot 10^{-11}$
Cl	0	0.05	$6.00 \cdot 10^{-10}$	0	0.06	$1.67 \cdot 10^{-11}$
Ca	0.003	0.36	$5.55 \cdot 10^{-10}$	0.001	0.12	$8.33 \cdot 10^{-11}$
Ni	0.2	0.36	$5.55 \cdot 10^{-10}$	0.9	0.12	$8.33 \cdot 10^{-11}$
Se	0	0.05	$6.00 \cdot 10^{-10}$	0	0.06	$1.67 \cdot 10^{-11}$
Sr	0.003	0.36	$5.55 \cdot 10^{-10}$	0.001	0.12	$8.33 \cdot 10^{-11}$
Zr	80	0.36	$5.55 \cdot 10^{-10}$	10	0.12	$8.33 \cdot 10^{-11}$
Nb	30	0.36	$5.55 \cdot 10^{-10}$	4	0.12	$8.33 \cdot 10^{-11}$
Mo	0	0.05	$6.00 \cdot 10^{-10}$	0.01	0.06	$1.67 \cdot 10^{-11}$
Tc	60	0.36	$5.55 \cdot 10^{-10}$	50	0.12	$8.33 \cdot 10^{-11}$

Element	Bentonite			Host rock		
	K_d [$m^3 \cdot kg^{-1}$]	n [-]	D_p [$m^2 \cdot s^{-1}$]	K_d [$m^3 \cdot kg^{-1}$]	n [-]	D_p [$m^2 \cdot s^{-1}$]
Pd	5	0.36	$5.55 \cdot 10^{-10}$	5	0.12	$8.33 \cdot 10^{-11}$
Sn	800	0.36	$5.55 \cdot 10^{-10}$	100	0.12	$8.33 \cdot 10^{-11}$
I	$5 \cdot 10^{-4}$	0.05	$6.00 \cdot 10^{-10}$	$3 \cdot 10^{-5}$	0.06	$1.67 \cdot 10^{-11}$
Cs	0.1	0.36	$5.55 \cdot 10^{-10}$	0.5	0.12	$8.33 \cdot 10^{-11}$
Sm	4	0.36	$5.55 \cdot 10^{-10}$	50	0.12	$8.33 \cdot 10^{-11}$
Eu	4	0.36	$5.55 \cdot 10^{-10}$	50	0.12	$8.33 \cdot 10^{-11}$
Pb	7	0.36	$5.55 \cdot 10^{-10}$	2	0.12	$8.33 \cdot 10^{-11}$
Po	0.06	0.05	$6.00 \cdot 10^{-10}$	0.1	0.06	$1.67 \cdot 10^{-11}$
Ra	0.002	0.36	$5.55 \cdot 10^{-10}$	$7 \cdot 10^{-4}$	0.12	$8.33 \cdot 10^{-11}$
Ac	20	0.36	$5.55 \cdot 10^{-10}$	10	0.12	$8.33 \cdot 10^{-11}$
Th	60	0.36	$5.55 \cdot 10^{-10}$	50	0.12	$8.33 \cdot 10^{-11}$
Pa	5	0.36	$5.55 \cdot 10^{-10}$	5	0.12	$8.33 \cdot 10^{-11}$
U	40	0.36	$5.55 \cdot 10^{-10}$	20	0.12	$8.33 \cdot 10^{-11}$
Np	60	0.36	$5.55 \cdot 10^{-10}$	50	0.12	$8.33 \cdot 10^{-11}$
Pu	20	0.36	$5.55 \cdot 10^{-10}$	20	0.12	$8.33 \cdot 10^{-11}$
Am	20	0.36	$5.55 \cdot 10^{-10}$	10	0.12	$8.33 \cdot 10^{-11}$
Cm	20	0.36	$5.55 \cdot 10^{-10}$	10	0.12	$8.33 \cdot 10^{-11}$

5.1.3.5 Biosphere

The potential radiation exposure of the age class > 17 a was calculated with the module EXCON using the dose conversion factors in accordance to the German regulations given in Table 5.8. A groundwater flow of 10^5 $m^3 \cdot a^{-1}$ was assumed in the module CLAYPOS to convert the radionuclide flux from the clay formation to concentration values. Table 5.9 additionally gives the dose coefficients for ingestion used to calculate the radiotoxicity values for the safety and performance indicators. Dose coefficients of short-lived daughter nuclides that are not explicitly included in the calculation are added to their mother nuclides under the assumption of radioactive equilibrium.

Tab. 5.8 Dose conversion factors (DCF) in $Sv \cdot a^{-1}$ / $Bq \cdot m^{-3}$

Activation and fission products		Th- and Np- series		U- and Ac-series	
Nuclide	DCF	Nuclide	DCF	Nuclide	DCF
C-14	$4.6 \cdot 10^{-8}$	Cm-248	$5.0 \cdot 10^{-6}$	Cm-246	$8.0 \cdot 10^{-7}$
Cl-36	$3.5 \cdot 10^{-8}$	Pu-244	$3.0 \cdot 10^{-6}$	Pu-242	$9.4 \cdot 10^{-7}$
Ca-41	$2.0 \cdot 10^{-9}$	Cm-244	$3.8 \cdot 10^{-7}$	Am-242m	$7.6 \cdot 10^{-7}$
Co-60	$3.9 \cdot 10^{-6}$	Pu-240	$9.6 \cdot 10^{-7}$	U-238	$7.1 \cdot 10^{-7}$
Ni-59	$4.9 \cdot 10^{-9}$	U-236	$5.6 \cdot 10^{-7}$	Pu-238	$7.5 \cdot 10^{-7}$
Ni-63	$1.1 \cdot 10^{-9}$	Th-232	$1.1 \cdot 10^{-4}$	Th-234	$4.8 \cdot 10^{-9}$
Se-79	$3.4 \cdot 10^{-7}$	Ra-228	$2.4 \cdot 10^{-6}$	U-234	$1.4 \cdot 10^{-6}$
Rb-87	$1.3 \cdot 10^{-7}$	U-232	$5.4 \cdot 10^{-6}$	Th-230	$3.7 \cdot 10^{-5}$
Sr-90	$1.8 \cdot 10^{-7}$	Th-228	$1.3 \cdot 10^{-6}$	Ra-226	$3.0 \cdot 10^{-5}$
Zr-93	$3.7 \cdot 10^{-8}$	Cm-245	$1.4 \cdot 10^{-6}$	Pb-210	$2.3 \cdot 10^{-6}$
Mo-93	$3.2 \cdot 10^{-7}$	Pu-241	$1.8 \cdot 10^{-8}$	Po-210	$4.9 \cdot 10^{-6}$
Nb-94	$3.1 \cdot 10^{-6}$	Am-241	$8.0 \cdot 10^{-7}$	Cm-247	$2.9 \cdot 10^{-6}$
Tc-99	$8.8 \cdot 10^{-9}$	Np-237	$4.7 \cdot 10^{-6}$	Am-243	$2.0 \cdot 10^{-6}$
Pd-107	$1.9 \cdot 10^{-9}$	U-233	$3.9 \cdot 10^{-6}$	Pu-239	$9.8 \cdot 10^{-7}$
Sn-126	$1.6 \cdot 10^{-5}$	Pa-233	$8.8 \cdot 10^{-9}$	U-235	$3.3 \cdot 10^{-6}$
I-129	$5.6 \cdot 10^{-7}$	Th-229	$1.7 \cdot 10^{-5}$	Pa-231	$4.0 \cdot 10^{-5}$
Cs-135	$5.7 \cdot 10^{-8}$	Ra-225	$1.1 \cdot 10^{-7}$	Ac-227	$1.0 \cdot 10^{-5}$
Cs-137	$9.5 \cdot 10^{-7}$	Ac-225	$3.7 \cdot 10^{-8}$	Th-227	$1.9 \cdot 10^{-8}$
Sm-151	$3.2 \cdot 10^{-10}$			Ra-223	$1.1 \cdot 10^{-7}$

Tab. 5.9 Dose coefficients for ingestion in Sv/Bq to calculate the radiotoxicity[6]

Activation and fission products		Th- and Np- series		U- and Ac-series	
Nuclide	Dose coefficient	Nuclide	Dose coefficient	Nuclide	Dose coefficient
C-14	$5.80 \cdot 10^{-10}$	Cm-244	$1.20 \cdot 10^{-07}$	Pu-242 +	$4.30 \cdot 10^{-07}$
Cl-36	$9.30 \cdot 10^{-10}$	Pu-240	$2.50 \cdot 10^{-07}$	Am-242m +	$1.90 \cdot 10^{-07}$
Co-60	$3.40 \cdot 10^{-09}$	U-236 +	$3.77 \cdot 10^{-07}$	Pu-238	$2.30 \cdot 10^{-07}$
Ni-59	$6.30 \cdot 10^{-11}$	Th-232	$2.30 \cdot 10^{-07}$	U-238 +	$4.89 \cdot 10^{-08}$
Ni-63	$1.50 \cdot 10^{-10}$	Ra-228 +	$8.34 \cdot 10^{-07}$	U-234	$4.90 \cdot 10^{-08}$
Se-79	$2.90 \cdot 10^{-09}$	Cm-245	$2.10 \cdot 10^{-07}$	Th-230	$2.10 \cdot 10^{-07}$
Sr-90	$3.07 \cdot 10^{-08}$	Pu-241	$4.80 \cdot 10^{-09}$	Ra-226 +	$2.80 \cdot 10^{-07}$
Zr-93	$1.22 \cdot 10^{-09}$	Am-241	$2.00 \cdot 10^{-07}$	Pb-210	$6.91 \cdot 10^{-07}$
Nb-94	$1.70 \cdot 10^{-09}$	Np-237 +	$1.11 \cdot 10^{-07}$	Am-243 +	$2.01 \cdot 10^{-07}$
Mo-93	$3.22 \cdot 10^{-09}$	U-233	$5.10 \cdot 10^{-08}$	Pu-239	$2.50 \cdot 10^{-07}$
Tc-99	$6.40 \cdot 10^{-10}$	Th-229 +	$6.13 \cdot 10^{-07}$	U-235 +	$4.73 \cdot 10^{-08}$
Sn-126	$5.07 \cdot 10^{-09}$			Pa-231	$7.10 \cdot 10^{-07}$
I-129	$1.10 \cdot 10^{-07}$			Ac-227 +	$1.21 \cdot 10^{-06}$
Cs-135	$2.00 \cdot 10^{-09}$				
Cs-137	$1.30 \cdot 10^{-08}$				
Sm-151	$9.80 \cdot 10^{-11}$				

[6] A plus sign after the nuclide name indicates that the dose coefficient for this nuclide includes the dose coefficient for all daughter nuclides up to the next one given in the table.

5.2 Safety indicators

Performance assessment calculations have been performed with the module CLAYPOS using the input data given above. The output of the module CLAYPOS has been used to calculate those three safety indicators described in chapter 2 for a repository in clay; namely the

- effective dose rate,
- radiotoxicity concentration in the biosphere water, and
- radiotoxicity flux from the geosphere.

The curves for the safety indicators are dominated by the radionuclides C-14, Se-79 and I-129 and to a lower degree also by Cl-36. No other radionuclides are released in a relevant amount from the host rock at any time. C-14 dominates the values of the indicators for early times resulting in the first maximum at about 20 000 years while I-129 dominates the values for late times resulting in the second maximum at about 2 Mio. years.

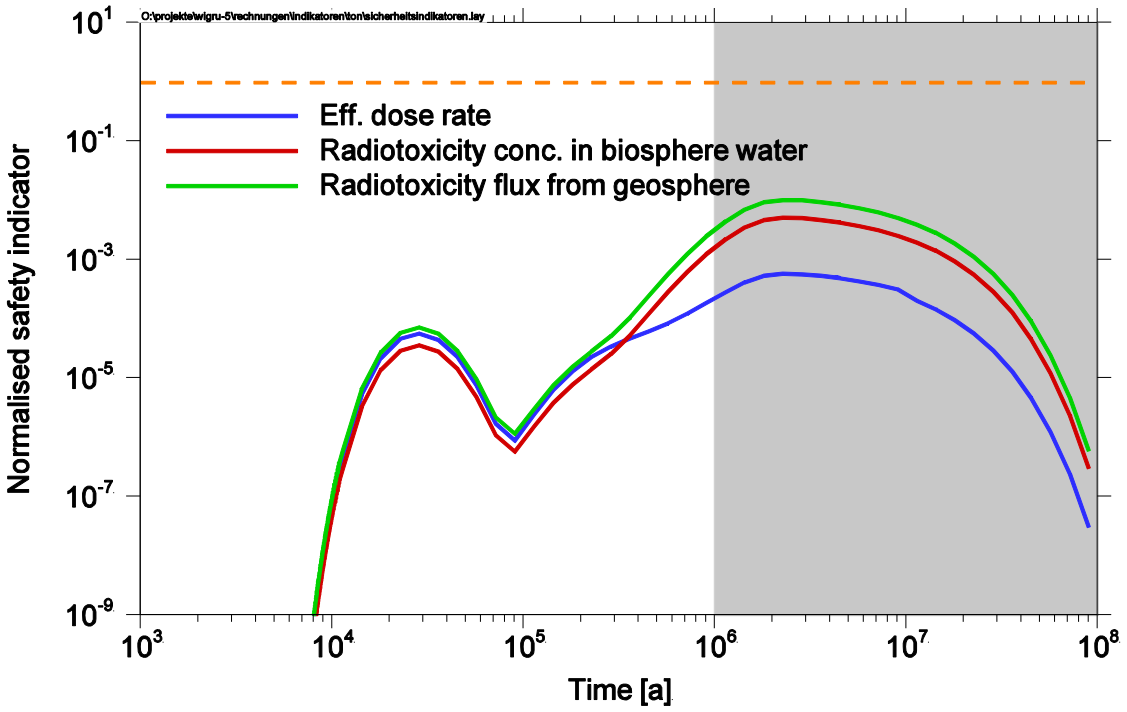

Fig. 5.4 Normalised safety indicators for the reference case

All three safety indicators were normalised by division by their respective reference values described in chapter 3 which are $1 \cdot 10^{-4}$ Sv·a^{-1} for the dose rate, $2 \cdot 10^{-6}$ Sv/m^3 for

the radiotoxicity concentration in the geosphere and 0.1 $Sv \cdot a^{-1}$ for the radiotoxicity flux from the geosphere.

The temporal evolution of all safety indicators is shown for the reference case in Figure 5.4. The three safety indicators show a nearly identical behaviour since only two radionuclides are more or less the only ones that dominate the values of the safety indicators, C-14 at the first and I-129 at the second maximum. The fact that the normalised indicators nearly show the same values is rather by chance.

At times later than 300 000 years, the effective dose rate falls below the two radiotoxicity safety indicators by about one order of magnitude. The reason for the difference in the curves for late times is the different weighing of the radionuclides C-14 and I-129 by the ingestion dose coefficients and the dose conversion factors, respectively. The ratio between the dose conversion factors of I-129 and of C-14 is about 12, while the ratio of the ingestion dose coefficients is about 190. Therefore, the two safety indicators using radiotoxicity values rate the impact of I-129 higher by more than one order of magnitude compared to the one by C-14. This difference between the dose factors and the dose coefficients results in an increase in the curves of the two radiotoxicity indicators for late times, when I-129 is the dominating radionuclide.

Besides the reference case, the calculation of the safety indicators has also been performed for a parameter variation of the diffusion coefficients in the clay. For this parameter variation the diffusion coefficient has been varied by a factor of 10 higher and lower relative to the reference value. The result of this parameter variation is shown in Figure 5.5. The position of the curves in the plot relative to each other is about the same as in the reference case.

Altogether one can summarise that for the integrated performance assessment calculations performed in this generic study, all safety indicators stay far below their respective reference value. The two radiotoxicity safety indicators therefore emphasise the statement of safety of the repository already obtained from the dose rate. Due to the simplicity of the model regarded here, all three safety indicators are determined more or less from the same result of the calculation, namely the flux from the repository. This resulted in the curves showing very similar shapes. For a further testing of the safety indicators for a repository in clay, a more detailed system consisting of additional compartments in the far field will have to be examined.

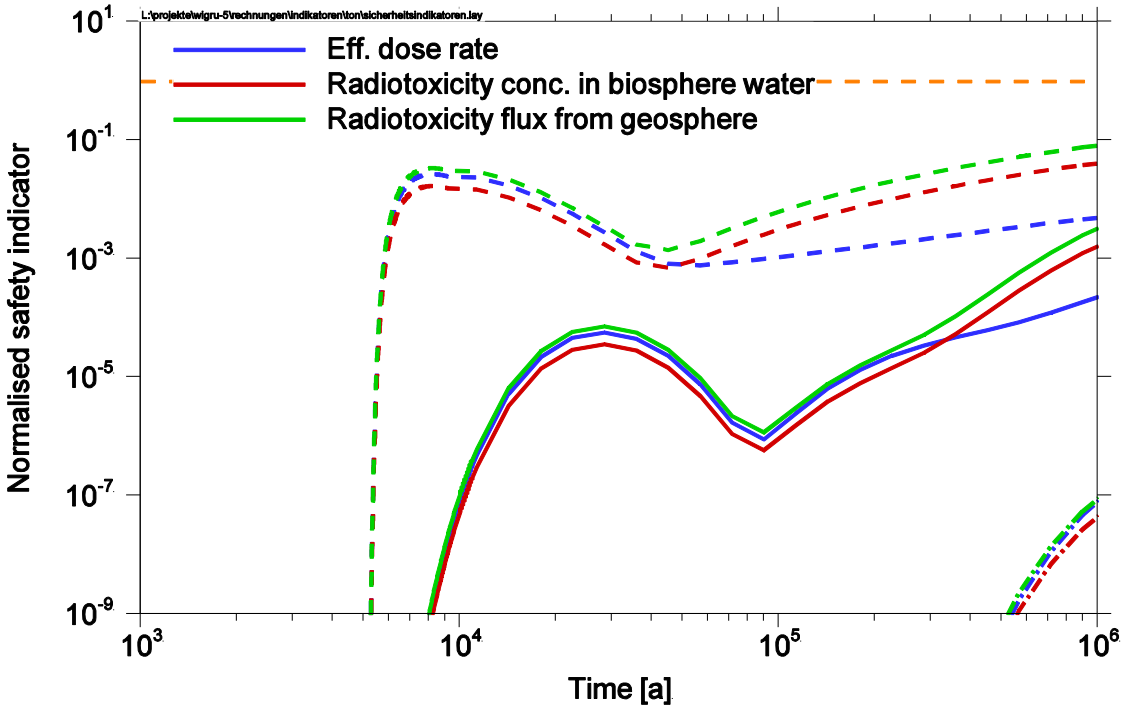

Fig. 5.5 Normalised safety indicators for variations of the diffusion coefficient; solid lines represent the reference case, dashed lines the variation with the diffusion coefficient / 10 and dash-dotted lines the variation with diffusion coefficient · 10.

5.3 Performance indicators

All three performance indicators described in chapter 2 are calculated for the repository in clay; namely the

- radiotoxicity inventory in different compartments,
- radiotoxicity fluxes from compartments and
- integrated radiotoxicity fluxes from compartments.

The radiotoxicity performance indicators are calculated for the sum of the whole nuclide spectrum as well as for Tc-99 and I-129 as two example nuclides. Tc-99 represents a strongly sorbing and solubility limited radionuclide, while I-129 represents a weakly sorbing and non-solubility limited radionuclide. Both radionuclides have long half-lives, so radioactive decay plays only a minor role until 10^6 years.

5.3.1 Inventory in different compartments

Figures 5.6 to 5.8 show the temporal evolution of the radiotoxicity inventory for the sum of all radionuclides and for Tc-99 and I-129. As long as the canisters are intact, all radiotoxicity is located in the waste matrix until after 2 500 years the canisters fail. One fraction of the radionuclides is precipitated while another fraction is released into the clay.

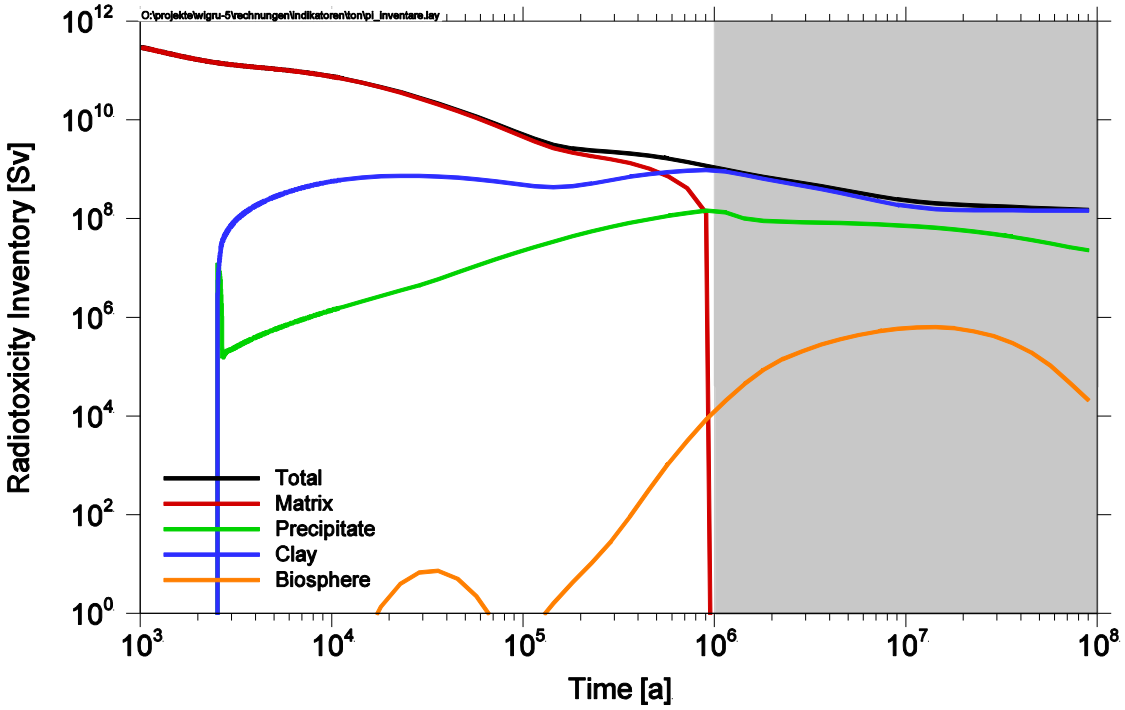

Fig. 5.6 Radiotoxicity inventory of all radionuclides in different compartments

At the time of the canister failure, the radiotoxicity in the precipitate shows a sharp peak (fast increase followed by a fast decrease) and later on rises slowly again (Figure 5.6). This is an effect of the fast release of radionuclides from the instant release fraction and the metal parts. For some radionuclides such as Tc-99 (Figure 5.7), the inventory coming from the instant release fraction and metal parts is large enough to reach the solubility limit shortly after canister failure. Due to the high initial concentration gradient between the canister water and the clay pore water, the diffusive loss of radionuclides from the canister water is high, too. The precipitate is consequently redissolved until the concentration gradient is levelled out – and consequently the diffusive flux is decreasing. At this stage, the long-term release rate exceeds the diffusive flux and the radiotoxicity in the precipitate increases again until about 200 000 years.

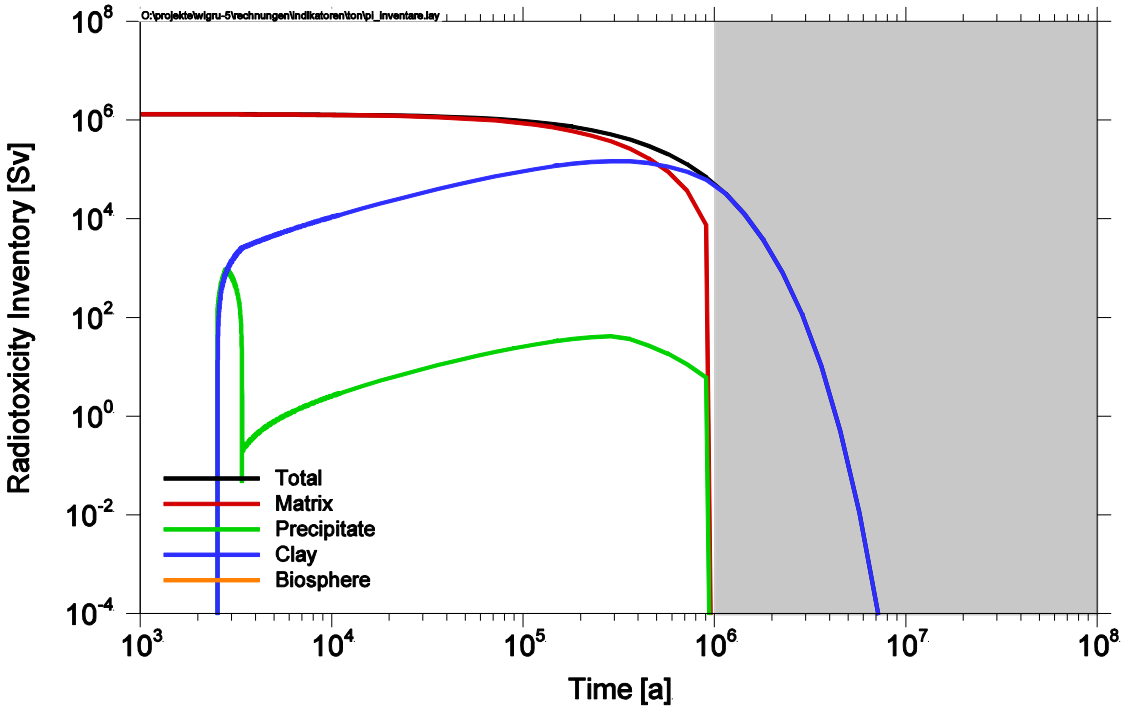

Fig. 5.7 Radiotoxicity inventory of Tc-99 in different compartments

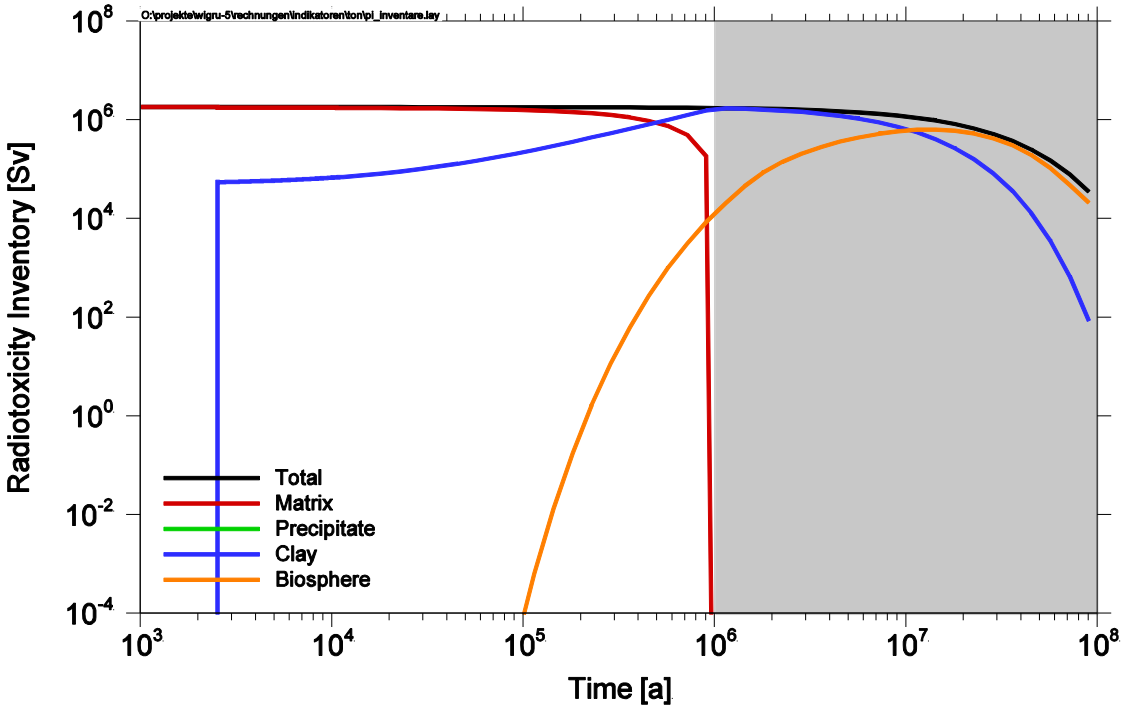

Fig. 5.8 Radiotoxicity inventory of I-129 in different compartments

I-129, as non solubility limited tracer, is more or less directly released from the matrix into the clay (Figure 5.8). The initial release of I-129 leads to a rather high radiotoxicity

in the clay directly after failure of the canister. The following increase of the inventory results from the long term dissolution rate of the waste matrix.

For the sum of all radionuclides, the radiotoxicity in the biosphere is always more than two orders of magnitude below the total radiotoxicity in the system. This is an effect of radionuclide sorption in the clay barriers as can be seen from the differences between the curves shown for Tc-99 and I-129. The strongly sorbing Tc-99 is completely transferred from the waste to the clay within one million years, but then is retained therein. None of the Tc-99 is released from the clay into the biosphere, while the weakly sorbing I-129 passes through the host-rock and is released to the biosphere, so the main part of the inventory of I-129 is in the biosphere after $2 \cdot 10^7$ years.

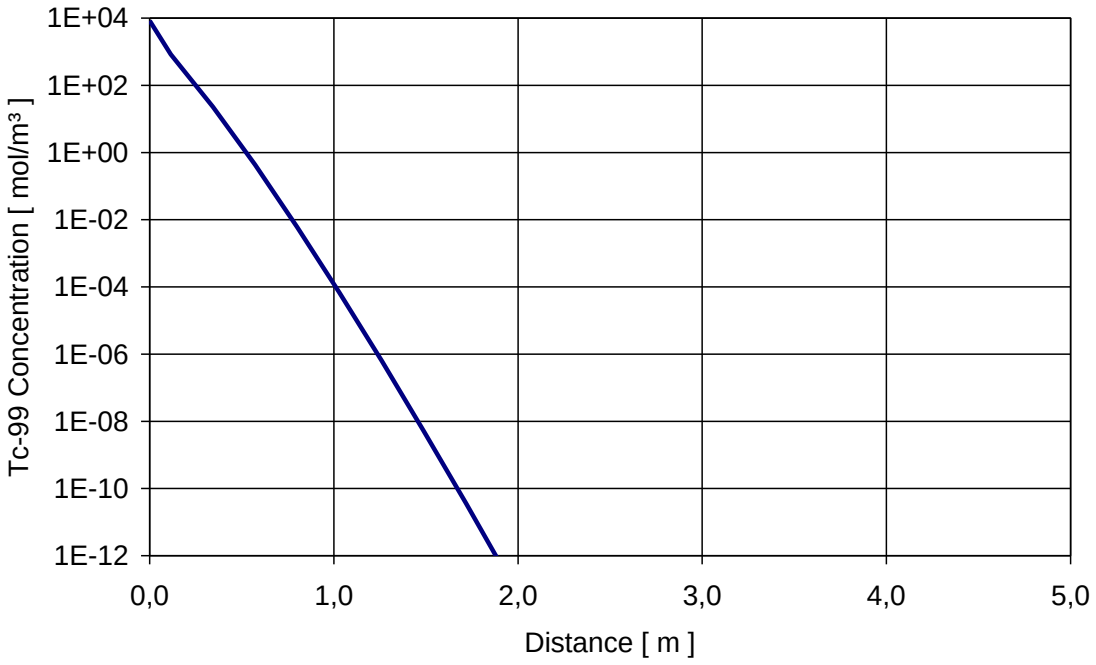

Fig. 5.9 Profile of the Tc-99 concentration after 10^6 years

Figure 5.9 shows the profile of the Tc-99 concentration in the clay pore water after 10^6 years. Tc-99 as strongly sorbing tracer is more or less completely retained within the first few meters i.e. in the geotechnical bentonite barrier. This matter of fact unfortunately can not be quantified by the inventory performance indicators, since the program CLAYPOS currently does not calculate the inventories of the host-rock and the bentonite buffer independently. For the future, however, it is desirable to extend the capabilities of CLAYPOS in such a way that the inventories are calculated independently for each part of the barrier system. Especially if additional overlying low permeable formations exist, like it is the case for the Lower-Cretaceous Clays in Northern

Germany, it will be useful to distinguish between the barrier efficiency of the host rock itself and the additional formations.

5.3.2 Radiotoxicity fluxes from compartments

Radiotoxicity fluxes were calculated from the container and from the clay, on the one hand, for the sum of all radionuclides (Figure 5.10) and, on the other hand, for the single radionuclides Tc-99 and I-129 (Figures 5.11 and 5.12). For the sum of all radionuclides and for I-129 one can see a very high flux from the container at the beginning resulting from the instant release fraction. For Tc-99 one can see a slightly increased flux for the first few hundred years after canister failure resulting from the release from the metal parts.

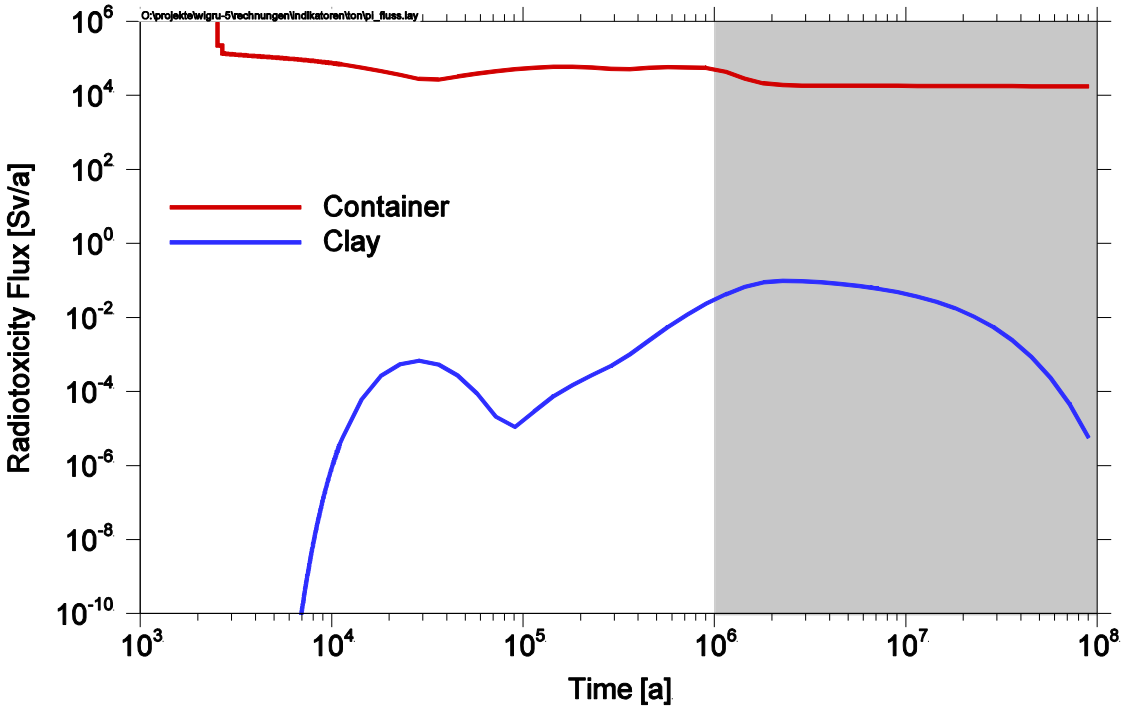

Fig. 5.10 Radiotoxicity flux from different compartments for all radionuclides

The radiotoxicity flux for all radionuclides from the container remains at a high level throughout the whole examined time period of 10^8 years. This is mainly due to a flux of Pb-210, which is constantly produced by its mother nuclides in the Uranium decay series being still present in the precipitate. While all the mother radionuclides have reached their solubility limit, Pb-210 remains below its solubility limit and is released from the container as it is produced, at a constant rate in decay equilibrium.

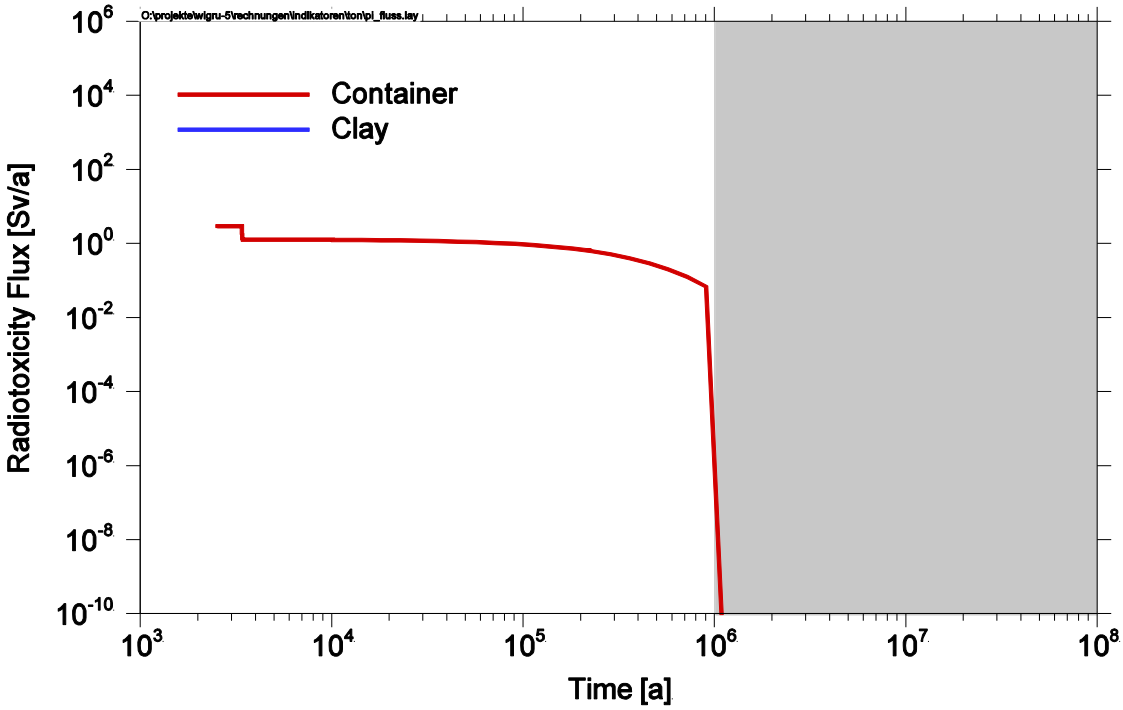

Fig. 5.11 Radiotoxicity flux from different compartments for Tc-99

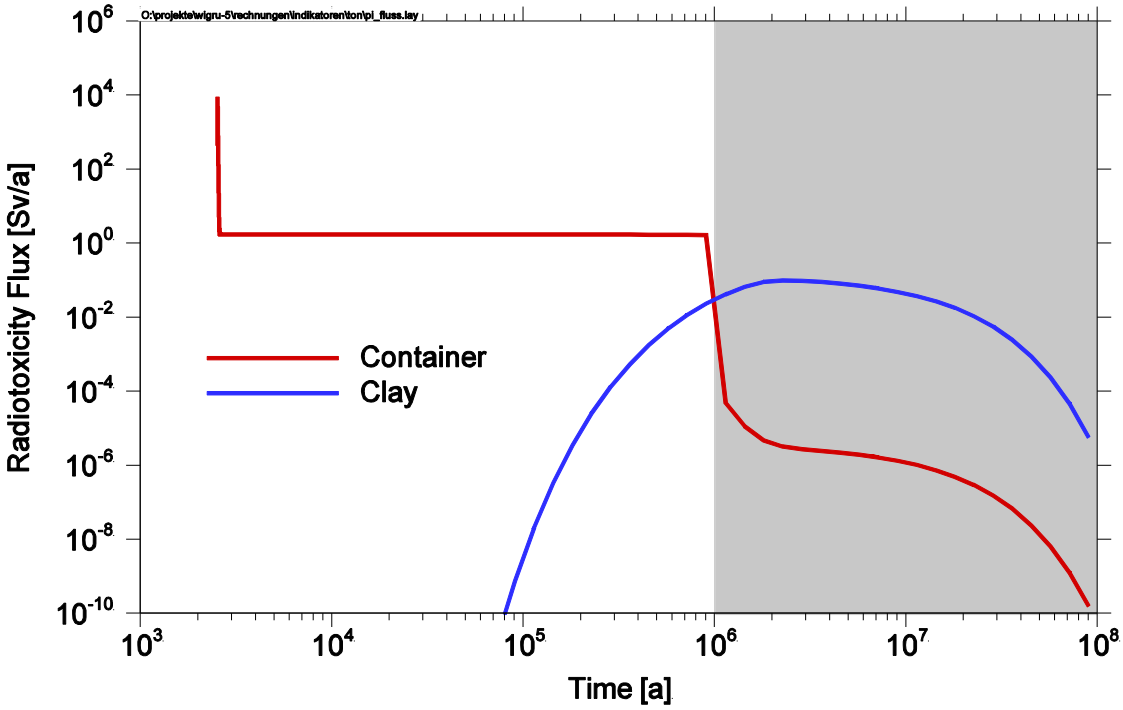

Fig. 5.12 Radiotoxicity flux from different compartments for I-129

The shape of the curve of the radionuclide flux from the clay for the sum of all radionuclides is directly related to the curves of the three safety indicators shown in sec-

tion 5.2, since only dilution, but no transport is regarded in the far-field in this calculation.

After one million years, all radionuclides are released from the matrix. However, the behaviour of the flux from the container is different for different radionuclides depending on its solubility and sorption properties. Due to the high sorption of Tc-99, its concentration in the clay pore water is low and the concentration gradient between the container water and the pore water in the clay remains high. The concentration gradient results in a high radionuclide flux until the precipitate of Tc-99 is completely used up within a short time.

I-129 is not solubility limited and therefore is released from the container at the same constant rate as the matrix dissolves. When the matrix dissolution terminates after 10^6 years, some I-129 still resides in the container water. After 10^6 years, the flux of the radiotoxicity of I-129 from the container is only determined by the diffusion process and controlled by the low concentration difference between the container water and the clay pore water. In contrast to Tc-99, I-129 is a non-sorbing radionuclide and the concentration in the clay pore water of I-129 is comparably high. The further decrease of the radiotoxicity flux of I-129 between $3 \cdot 10^6$ and 10^8 years shown by the curves in Figure 5.12 is only due to the radioactive decay.

5.3.3 Integrated radiotoxicity fluxes from compartments

Figures 5.13 to 5.15 show the integrated radiotoxicity fluxes from the compartments for the sum of all radionuclides and for Tc-99 and I-129. For the sum of all radionuclides the integrated radiotoxicity flux from the clay after 10^8 years is about six orders of magnitude lower than that from the container. This implies that the clay barriers are able to retain 99.9999 % of the radiotoxicity released from the container.

It has to be noted that the sum of the radiotoxicity released from the container might exceed the initially emplaced radiotoxicity. The reason for this effect is that daughter nuclides which are released in some cases have a higher radiotoxicity than their mother nuclides originally emplaced. This effect can lead to a misinterpretation of the radiotoxicity indicators and has to be kept in mind if sum radiotoxicities are used for the interpretation. While for I-129 all radiotoxicity is released from the container after the matrix dissolution, some T-99 has already decayed during transport.

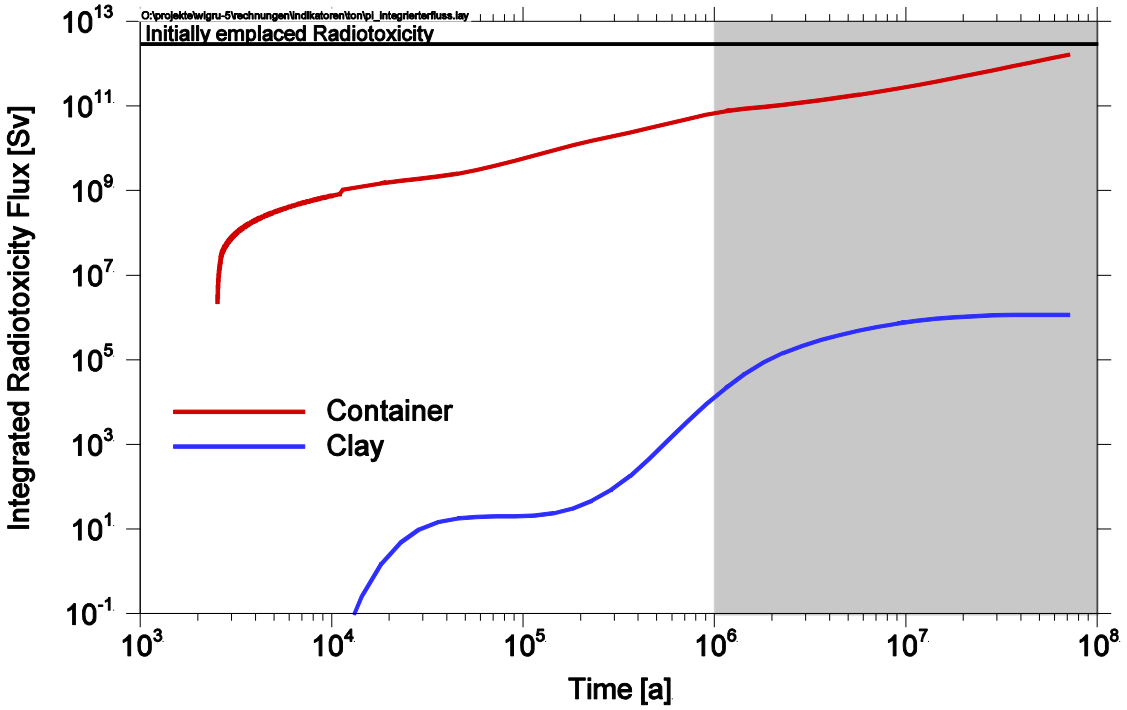

Fig. 5.13 Integrated radiotoxicity flux from different compartments for all radionuclides. The initially emplaced radiotoxicity inventory ($3.10 \cdot 10^{12}$ Sv) is shown for comparison.

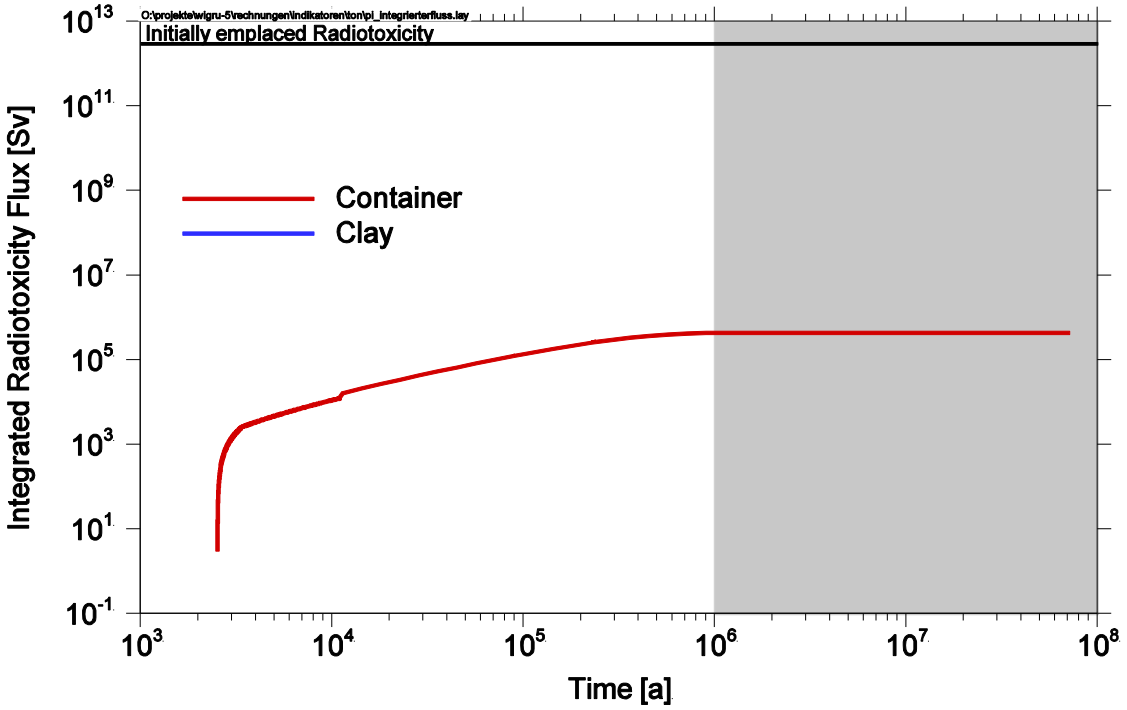

Fig. 5.14 Integrated radiotoxicity flux from different compartments for Tc-99. The initially emplaced radiotoxicity inventory ($1.39 \cdot 10^{6}$ Sv) is shown for comparison.

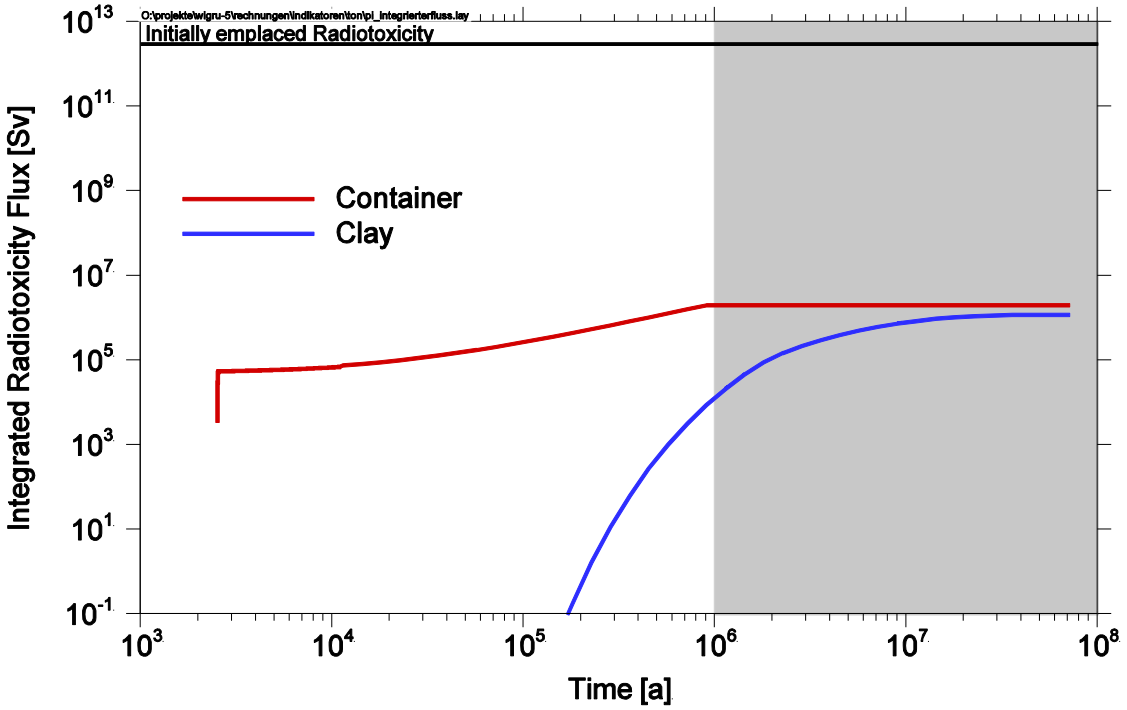

Fig. 5.15 Integrated radiotoxicity flux from different compartments for I-129. The initially emplaced radiotoxicity inventory ($1.90 \cdot 10^6$ Sv) is shown for comparison.

The barrier efficiency is different if single nuclides are examined. On the one hand, for strongly sorbing tracers like Tc-99 all radiotoxicity is retained in the clay, while on the other hand for a weakly sorbing radionuclide like I-129 about 60 % of the radiotoxicity passes through the clay barriers in 10^8 years and only 40 % are retained. Due to technical reasons, it is not possible to distinguish between the contributions of the bentonite buffer and the clay on the overall efficiency to retain radiotoxicity in the repository system.

6 Summary

Three safety and three performance indicators were successfully applied to long-term safety studies for high level waste repositories in salt and clay.

The three safety indicators considered in this report are

- the effective dose rate [Sv/a],
- the radiotoxicity concentration in the biosphere water [Sv/m^3] and
- the radiotoxicity flux from the geosphere (overlying rock) [Sv/a].

Appropriate reference values were identified by determining natural background values and considering a safety margin by constraining the reference value to about one third of the natural background value. For the effective dose rate and the radiotoxicity concentration in the biosphere water two global (regional) reference values were determined. The radiotoxicity flux from the geosphere requires a local site-specific reference value. The general philosophy of this procedure was to keep the reference values comparatively low in order to enhance the confidence in the safety statement given by the corresponding safety indicator. For both case studies the following reference values were identified

- for the effective dose rate: $1 \cdot 10^{-4}$ Sv/a,
- for the radiotoxicity concentration in the biosphere water: $2 \cdot 10^{-6}$ Sv/m^3 and
- for the radiotoxicity flux from the geosphere: 0.1 Sv/a.

Additionally to the three safety indicators three performance indicators were calculated for the repositories in salt and in clay. For the calculation of the performance indicators the repository concept was divided into several compartments. The selection of the compartments depends on the host rock type and in particular on the repository concept. Therefore the results are strongly related to the given concept and can hardly be compared between two different host rock types.

The following performance indicators were considered

- radiotoxicity inventory in different compartments [Sv],

- radiotoxicity fluxes from compartments [Sv/a] and
- integrated radiotoxicity fluxes from compartments [Sv].

In the following sections the results for the safety indicators and performance indicators are summarised. In both sections general results are discussed first, followed by the description of host rock specific results.

6.1.1 Safety indicators

The main advantage of a safety indicator is that such an indicator is a quantitative measure for the safety of the whole repository system. A safety indicator allows a comparison with other repository systems.

Due to the independently derived corresponding reference values the three safety indicators applied in this report provide three different safety statements. These safety statements are:

1. *Individual dose rate*: Human health is not jeopardised by radionuclides released from the repository. All biological effects to a human individual, i.e. the incorporation of radionuclides by humans via different exposition paths /AVV 90/, remain so small that they have no significant impact on human health.
2. *Radiotoxicity concentration in the biosphere water*: The ingestion of the biosphere water that is contaminated with the radionuclide flux from the repository is as harmful as the ingestion of average drinking water provided in Germany (regarding the impact of radionuclides).
3. *Radiotoxicity flux from the geosphere (overlying rock)*: The radiotoxicity flux from the geosphere to a water body, which represents the interface to the biosphere, is lower than the natural radiotoxicity fluxes to this water body.

These three safety indicators were normalised by division by the corresponding reference value in order to facilitate the comparison of them. The combination of the three indicators gives a strong argument for or against the safety of a repository system. The distinctive uncertainties of every single indicator are thus less important for the overall safety assessment.

6.1.1.1 Safety indicators in salt formations

The safety indicators were calculated for a repository system in a salt formation for two test cases:

1. the combined failure of shaft and drift seals and
2. fluid reservoirs inside the repository.

The safety indicators were very close to the reference values in the first test case, only the effective dose rate shows a small margin of about one order of magnitude. In total, the investigation of the three safety indicators increases the confidence in the safety assessment.

For the second test case the margin between the reference value and the calculated value is almost five orders of magnitude. For this test case all three safety indicators give quite similar results. Thus the calculation of the three safety indicators provides a well-founded safety statement for the second test case.

This study is the first detailed calculation of a set of different safety indicators for a repository for HLW in a salt formation in Germany. The applied repository concept has a complex structure and reflects the current state of the art /BUH 08b/. It could be shown that the necessary tools for the calculation and evaluation of the proposed safety indicators are already available. In a next step a systematic sensitivity analysis should be performed for the different safety indicators. Since safety indicators in salt are always based on release scenarios, the determination of the scenario probabilities is a decisive step in assessing the results. If scenario probabilities are available a further type of indicators, risk indicators, could be added to the safety assessment of repository systems.

6.1.1.2 Safety indicators in clay formations

The three safety indicators have been successfully applied to a generic repository in clay. The temporal evolution of the curves for the indicators shows a very similar shape. The differences between the three curves are due to differences in weighing of the radionuclides C-14 and I-129 by the dose factors compared to the one by the dose conversion factors. A very simple model was applied in this study in which only the

near field and the host- rock formation are regarded, but no transport in other formations like other adjacent low permeable formations or the aquifers in the overburden. This fact is the reason for the similar shape of the curves. A different shape of the three indicators curves would only be expected if an additional retention in the far field was considered in the model.

The values of the three indicators relative to their respective reference value are also in the same range. Since the reference values were determined independently, all three indicators confirm about the same degree of safety for the different safety statements. Further testing of the safety indicators for a repository in clay formations with additional low permeable adjacent formations such as the lower Cretaceous Clay in Northern Germany will be performed in the future to better identify the use of and the differences between the three indicators.

6.1.2 Performance indicators

One important shortcoming of safety indicators is that they do not indicate which parts of the repository system (barriers or compartments) contribute to what percentage to the overall safety. For that purpose performance indicators are applied in order to give further arguments regarding the safety of a repository system. Performance indicators aim at providing a measure of the level of quality, reliability or effectiveness of a given compartment of the whole system. In general performance indicators provide valuable additional information to the safety indicators. They are an important element in the decision-making process and they facilitate communication to the regulator and to the public. They give additional valuable information on the repository system and thus increase the system understanding. They play an important role for the optimisation of the repository concept.

In contrast to the safety indicators the performance indicators are dependent on the repository concept. Especially the selection of compartments has a strong influence on the results.

6.1.2.1 Performance indicators in salt formations

The performance indicators were calculated for a repository in a salt formation for two test cases:

1. the combined failure of shaft and drift seals and

2. fluid reservoirs inside the repository.

The results show that a set of performance indicators is needed to get a better understanding for the important processes in a complex repository system in a rock salt formation. In general the radiotoxicity inventories in the selected compartments and the corresponding fluxes between these compartments are good indicators for the evolution of the contaminant transport through the repository system. A partitioning of the repository into compartments was carried out in order to take into account the different sections. This partitioning fosters the understanding of the investigated system. But the inventories and fluxes inside the repository need a lot of interpretation and explanation and require a good knowledge about the repository system. For some compartments it is difficult to interpret the radiotoxicity inventories for the compartments representing the structure of the repository (e. g. SF1-S, SF2-S and CF), since flows inside and between the different compartments can compensate each other.

The most illustrative performance indicator is the integrated radiotoxicity flux from different compartments. If this indicator is compared with the initially emplaced radiotoxicity inventory, the performance of each compartment can be demonstrated in an illustrative way in figures as well as in tables.

Very useful is the additional analysis of single radionuclides. By comparing radionuclides with different characteristics (e. g. different solubility limits or sorption coefficients) a certain process or effect in the repository system can be studied and explained.

The proposed indicators fulfil the goal of providing a measure of the level of quality, reliability and effectiveness of a certain compartment in the presented repository system. They could be used to optimise the system, e. g. to change the arrangement of the different waste sections in the repository. If the repository system is changed, it could be necessary to test further indicators and add them to the proposed set.

6.1.2.2 Performance indicators in clay formations

Three performance indicators have been successfully tested for a repository in clay. Due to the simplicity of the model used in these calculations that accounts for one

compartment only in which the radionuclide transport is taking place, all three performance indicators more or less give the same information in contrast to the more complex repository system in rock salt. Therefore the results are summarised in the following for the first indicator only.

The performance indicator examining the inventory in the different compartments has revealed that the retention of that part of the radionuclides which is actually released from the matrix is achieved by sorption in the clay barriers, while precipitation of radionuclides only plays a minor role for the overall retention. To be able to better distinguish between the role of the matrix and the precipitate for the retention of the radionuclides it would be helpful to study the radiotoxicity fluxes from the matrix to the precipitate / container water and from the precipitate / container water to the near-field bentonite pore water.

A further differentiation in which part of the clay barrier system the radionuclides are retained – engineered bentonite barrier, or host rock – could not be achieved by the performance indicators since only one compartment was taken into account. The reason for both deficiencies is that the current version of the CLAYPOS software is not able to give the inventories and fluxes for different compartments of the clay barrier system independently. This however will be very helpful, in particular to examine multi formation clay barrier systems as they are found in Northern Germany. Further development of the CLAYPOS module in a future project will therefore include the calculation and output of the

- inventories in all compartments of the clay barrier system (bentonite, host rock, adjacent formations),
- radiotoxicity fluxes from all compartments of the clay barrier system and
- radiotoxicity fluxes from the matrix.

Further testing and developments of the use of safety and performance indicators for repositories in clay and the further development of the CLAYPOS module will be performed in the European project PAMINA.

7 Outlook

The tools for calculating and analysing the three proposed safety indicators are available for a repository in rock salt as well as in clay. Only in case that risk based indicators are intended to be used (s. above), the existing codes need to be further adapted. A key problem associated with safety indicators is the determination of appropriate reference values, based on reliable data, in order to give solid safety statements. In particular, the derivation of the reference value for the radiotoxicity flux from the geosphere is subject to high uncertainties. This indicator is to a large extent site-specific. More work is necessary to derive a conclusive reference value for the site considered.

The investigation of the performance indicators clearly showed that it is necessary in a specific study to consider as far as possible the same compartments for each indicator to better compare the indicators and to receive most comprehensive information. This is needed for a detailed interpretation and characterisation of the impact of all processes.

Based on these findings it was revealed that the integrated codes for repositories in rock salt and in clay formations need to be further developed. For rock salt the near-field module LOPOS has to be enabled to calculate the inventories in and fluxes from the precipitate. The consideration of this additional compartment is essential to estimate the contribution of precipitation to the barrier effect of the near field compartments, which could be quite high for several radionuclides. Furthermore the geosphere model CHETLIN needs to be modified to calculate activity and/or radiotoxicity inventories in the total geosphere compartment for every time step. This is necessary to make a complete mass balance, i.e. to compare the distribution of the inventory in all parts of the repository system with the initially emplaced inventory.

For performance indicators in clay formations it is currently not possible to distinguish between the compartments buffer and host-rock formation; both have been summarised to one compartment “clay” in this study. However, in order to judge the barrier function of the engineered and geological barriers it is important to know the contributions of the buffer and the host-rock. In case a more complex geological system (including adjacent formations to the host rock) is considered, the development of CHETLIN described above is also needed for clay formations.

8 References

/AVV 90/ Allgemeine Verwaltungsvorschrift zu § 45 Strahlenschutzverordnung: Ermittlung der Strahlenexposition durch die Ableitung radioaktiver Stoffe aus kerntechnischen Anlagen oder Einrichtungen (21. Februar 1990). Erschienen im Bundesanzeiger, 42. Jg. Nummer 64a, 1990.

/BAL 07/ Baltes, B.; Röhlig, K.-J., Kindt, A.: Sicherheitsanforderungen an die Endlagerung hochradioaktiver Abfälle in tiefen geologischen Formationen. Gesellschaft für Anlagen- und Reaktorsicherheit (GRS) mbH, GRS-A-3358, Köln, 2007.

/BEC 03/ Becker, D.-A.; Buhmann, D.; Storck, R.; Alonso, J.; Cormenzana, J.-L.; Hugi, M.; van Gemert, F.; O'Sullivan, P.; Laciok, A.; Marivoet, J.; Sillen, X.; Nordman, H.; Vieno, T.; Niemeyer, M.: Testing of Safety and Performance Indicators (SPIN), EUR 19965 EN, European Commission, Brussels, 2003.

/BMU 03/ Bundesministerium für Umwelt, Naturschutz und Radioaktivität: Umweltradioaktivität und Strahlenbelastung. Jahresbericht 2002, Bonn, 2003.

/BMU 07/ Bundesministerium für Umwelt, Naturschutz und Radioaktivität: Umweltradioaktivität und Strahlenbelastung. Jahresbericht 2006, Bonn, 2007.

/BUE 88/ Bütow, E.; Brühl, G.; Gülker, M.; Heredia, L.; Lütkemeier-Hosseinipour, S.; Naff, R.; Struck, S.: PSE-Abschlussbericht, Fachband 18 - Modellrechnungen zur Ausbreitung von Radionukliden im Deckgebirge. Projektleitung HMI, Berlin, 1985.

/BUH 91/ Buhmann, D.; Nies, A.; Storck, R.: Analyse der Langzeitsicherheit von Endlagerkonzepten für wärmeerzeugende radioaktive Abfälle. GSF-Bericht 27/91. GSF – Forschungszentrum für Umwelt und Gesundheit GmbH, Braunschweig, 1991.

/BUH 99/ Buhmann, D.: Das Programmpaket EMOS. Ein Instrumentarium zur Analyse der Langzeitsicherheit von Endlagern. Gesellschaft für Anlagen- und Reaktorsicherheit (GRS) mbH, GRS-159, Braunschweig, 1999.

/BUH 08a/ Buhmann, D.; Mönig, J.; Wolf, J.; Heusermann, S.; Keller, S.; Weber, J. R.; Bollingerfehr, W.; Filbert, W.; Kreienmeyer, M.; Krone, J.; Tholen, M.: Überprüfung und Bewertung des Instrumentariums für eine sicherheitliche Bewertung von Endlagern für HAW – ISIBEL. Gemeinsamer Bericht von DBE TECHNOLOGY GmbH, BGR und GRS. DBE TECHNOLOGY GmbH Peine, 2008.

/BUH 08b/ Buhmann, D.; Mönig, J.; Wolf, J.: Untersuchungen zur Ermittlung und Bewertung von Freisetzungsszenarien. Gesellschaft für Anlagen- und Reaktorsicherheit (GRS) mbH, GRS-233, Braunschweig, 2008.

/GEL 97/ Gellerman, R.: Uran in Wässern – Untersuchungen in ostdeutschen Flüssen und Grundwässern. Z. Umweltchem. Ökotox. 9, 1997.

/HIS 99/ Hirsekorn, R.-P.; Boese, B.; Buhmann, D.: LOPOS: Programm zur Berechnung der Schadstofffreisetzung aus netzwerkartigen Grubengebäuden. Gesellschaft für Anlagen- und Reaktorsicherheit (GRS) mbH, GRS-157, Braunschweig, 1999.

/IAE 94/ IAEA: Safety indicators in different time frames for the safety assessment of underground radioactive waste repositories. IAEA-TECDOC-767, Vienna 1994.

/IAE 03/ IAEA: Safety indicators for the safety assessment of radioactive waste disposal. Sixth report of the Working Group on Principles and Criteria for Radioactive Waste Disposal. IAEA-TECDOC-1372, Vienna, 2003.

/ICR 96/ International Commission on Radiological Protection: Age-dependent doses to members of the public from intake of radionuclides: Part 5 Compilation of ingestion and inhalation dose coefficients. ICRP 72. Pergamon Press. Oxford, 1996.

/JOB 07/ Jobmann, M.; Amelung, P.; Billaux, D.; Polster, M.; Schmidt, H.; Uhlig, L.: Untersuchungen zur sicherheitstechnischen Auslegung eines generischen Endlagers im Tonstein in Deutschland. GENESIS Abschlussbericht, DBE Technology, 2007. Anlagenband: Geologie der Referenzregionen im Tonstein.

/KEN 02/ Kendall, G.M.; Smith, T.J.: Doses to organs and tissues from radon and its decay products. Journal of Radiol. Prot. 22: 389-406, 2002.

/KES 05/ Keesmann, S.; Noseck, U.; Buhmann, D.; Fein, E.; Schneider, A.: Modellrechnungen zur Langzeitsicherheit von Endlagern in Salz- und Granitformationen. Gesellschaft für Anlagen- und Reaktorsicherheit (GRS) mbH, GRS-206, Braunschweig, 2005.

/KLI 07/ Klinge, H.; Persönliche Mitteilung vom 26.11.2007.

/KUE 96/ Kühle, T.; Zude, F.; Lührmann, L.: Das eindimensionale Transportprogramm CHET1 unter Berücksichtigung der Sorption nach dem Kd-Konzept. Gesellschaft für Anlagen- und Reaktorsicherheit (GRS) mbH, GRS-124, Braunschweig, 1996.

/NAG 02/ Nagra: Projekt Opalinus Clay: The long-term safety of a repository for spent fuel, vitrified high-level waste and long-lived intermediate-level waste sited in the Opalinus Clay of the Züricher Weinland. Nagra, NTB 02-05, Wettingen, 2002.

/NEA 04/ NEA-OECD: Post-closure Safety Case for Geological Repositories. Nature and Purpose. Nuclear Energy Agency, 2004.

/PAG 88/ Cadelli, N.; Cottone, G., Orlowski, S.; Bertozzi, G.; Girardi, F.; Saltelli, A.: PAGIS: Performance Assessment of Geological Isolation Systems for Radioactive Waste – Summary Report. EUR Report 11775 EN, Luxemburg, 1988.

/RUE 07/ Rübel, A.; Becker, D.-A.; Fein, E.: Radionuclide transport modelling to assess the safety of repositories in clays. GRS-228, Gesellschaft für Anlagen und Reaktorsicherheit (GRS) mbH, Braunschweig, 2007.

/SSK 95/ Strahlenschutzkommission (SSK): Bewertung der Strahlenexposition durch Radon im Trinkwasser. Veröffentlichungen der Strahlenschutzkommission, Bd. 39, 1995.

/SUT 98/ Suter, D.; Biehler, D.; Blaser, P.; Hollmann, A.: Derivation of a Sorption Data Set for the Gorleben Overburden. Proc. DisTec ‘98 International Conference on Radioactive Waste Disposal, S. 581-584, Hamburg, September 9-11,1998.

List of Figures

List of Tables

Gesellschaft für Anlagen- und Reaktorsicherheit (GRS) mbH

Schwertnergasse 1
50667 Köln
Telefon +49 221 2068-0
Telefax +49 221 2068-888

Forschungszentrum
85748 Garching b. München
Telefon +49 89 32004-0
Telefax +49 89 32004-300

Kurfürstendamm 200
10719 Berlin
Telefon +49 30 88589-0
Telefax +49 30 88589-111

Theodor-Heuss-Straße 4
38122 Braunschweig
Telefon +49 531 8012-0
Telefax +49 531 8012-200

www.grs.de

ISBN 978-3-939355-14-4